# CARBON DIOXIDE TRANSPORT AND UPTAKE IN CONCRETE DURING ACCELERATED CARBONATION CURING

by

Sormeh Kashef Haghighi

Department of Civil Engineering and Applied Mechanics McGill University

A THESIS SUBMITTED TO MCGILL UNIVERSITY
IN PARTIAL FULFILLMENT OF THE REQUIREMENTS FOR THE
DEGREE OF
DOCTOR OF PHILOSOPHY

April 2012

© Sormeh Kashef Haghighi, 2012

#### **Abstract**

Carbon dioxide (CO<sub>2</sub>) is the dominant greenhouse gas resulting from many anthropogenic activities, mainly combustion of fossil fuels. One of the strategies to mitigate CO<sub>2</sub> emissions is considered to be carbon dioxide capture and storage (CCS). The current storage methods focus on enhanced oil recovery, underground geological storage, disposal in deep oceans, and *ex situ* mineral carbonation of abundant metal oxide minerals such as olivine, serpentinite and wollastonite.

During mineral carbonation, a gas stream rich in  $CO_2$  is reacted with mineral metal oxides to form thermodynamically stable carbonates. These carbonated minerals, however, store  $CO_2$  but do not produce any materials that are of value.

Accelerated carbonation curing of concrete can be used as a mineral sequestration method with the advantage of producing a value-added concrete product. During accelerated carbonation curing of concrete, CO<sub>2</sub> is reacted with cement and stored as a solid calcium carbonate in concrete construction products. Among the concrete products, non-reinforced precast concrete, such as blocks and bricks, can be used for carbonation curing. In previous studies, pressurized chambers have been used for accelerated CO<sub>2</sub> curing of concrete, where a high pressure of CO<sub>2</sub> is required for sufficient gas diffusion in concrete and homogeneous carbonation. In this research, a flow-through carbonation reactor was used for concrete curing and the rate and extent of CO<sub>2</sub> uptake by concrete was studied. One of the advantages of the carbonation reactor applied in this study is that significantly less energy for gas mixture compression is required compared to a CO<sub>2</sub> pressure chamber.

The overall objective of this thesis was to develop and assess the performance of an accelerated carbonation curing reactor for concrete using an advective flow of flue gas. The rate and extent of CO<sub>2</sub> uptake by concrete in a 1-D flow-through carbonation reactor were studied and compared with the published results on CO<sub>2</sub> uptake in pressurized chambers using diffusive flow of CO<sub>2</sub>. The factors limiting the CO<sub>2</sub> uptake were studied through experimental observation as well as mathematical modeling of CO<sub>2</sub> transport and reaction in concrete during accelerated carbonation curing.

Carbonation efficiencies of 16-20% attained in the flow-through reactor were comparable to those obtained for static CO<sub>2</sub> pressure chambers. The extent of CO<sub>2</sub> uptake was limited by formation of solid calcium carbonate in micro-scale pores. Intermittent carbonation experiments showed that the carbonation efficiency was limited in part by slow dissolution and/or diffusion of dissolved reactive components in the concrete matrix. The electron microprobe imaging technique used in this study also confirmed formation of solid calcium carbonate which filled up the narrow pores (<4 µm). The uptake efficiency reached 67% when cement was carbonated in an aqueous suspension in a completely mixed flow-through reactor where the effect of pore blockage was eliminated and a higher percentage of reacting surface area was exposed to dissolved CO<sub>2</sub>. However, formation of a calcium carbonate layer still inhibited diffusion of dissolved calcium and CO<sub>2</sub> through this layer. In the presence of the calcium carbonate layer and other carbonation products like silica (SiO<sub>2</sub> gel), and at partial pressure of CO<sub>2</sub> used for carbonation, the aqueous solution reached a chemical equilibrium and carbonation ceased before the maximum theoretical uptake could be achieved.

The effect of physico-chemical processes on CO<sub>2</sub> uptake during carbonation curing was also studied using a mathematical model. Equations describing the CO<sub>2</sub> transport by advection and dispersion in concrete pore space, dissolution in pore water and reaction with reactive cement species were solved numerically. The initial concentration of cement species were calculated based on a hydration model which was developed to simulate the 4 hours of hydration time before carbonation starts. The competition of various processes affecting the carbon uptake was investigated by dimensional analysis. The results show that the carbonation efficiency during the rapid uptake period (first 30 minutes) was not limited by the rate of CO<sub>2</sub> gas-liquid mass transfer. The carbonation reaction rates of unhydrated cement phases were the rate controlling processes during this period (i.e. higher uptake can be achieved in shorter time by improving the carbonation rates, for instance, by increasing the exposed surface area of these species).

#### Résumé

Le dioxyde de carbone (CO<sub>2</sub>) est le gaz d'effet de serre dominant, résultat des plusieurs activités anthropogènes, dont le plus important est la combustion des combustibles fossiles. Une des stratégies qui a pour but d'atténuer des émissions de CO<sub>2</sub> est le captage et le stockage du dioxyde de carbone (CCS en anglais). Les méthodes courantes de stockages incluent la récupération assistée du pétrole, le stockage géologique souterrain, la disposition sous les océans profonds, et la carbonatation minérale *ex situ* des gisements abondants des oxydes métalliques, comme l'olivine, la serpentinite et la wollastonite.

Pendant la carbonatation minérale, un jet de gaz riche en CO<sub>2</sub> est mis à réagir avec les oxydes des métaux minéraux pour former des carbonates thermodynamiquement stables. L'élimination des minerais carbonatés, cependant, stocke le CO<sub>2</sub> mais ne produit pas des matériaux de valeurs ajoutées.

La carbonatation accélérée pour murir du béton peut être employée comme une méthode de la séquestration minérale avec l'avantage de produire un produit de béton à valeur ajoutée. Pendant la carbonatation accélérée pour murir du béton, le CO<sub>2</sub> est mis à réagir avec le ciment et stocké comme carbonate de calcium solide dans les produits de béton utilisés en construction. Les produits en béton non-armés et préfabriqués tel que les blocs et les briques sont ceux qui peuvent être faits avec la méthode carbonatation pour murir le béton. Lors des études précédentes, des chambres sous pression ont été employées pour accélérer le durcissement du CO<sub>2</sub> au béton, où une haute pression de CO<sub>2</sub> est exigée pour une diffusion suffisante de gaz et une carbonatation homogène. Dans cette recherche,

un écoulement à travers le réacteur de carbonatation a été utilisé pour le durcissement du béton; le taux et l'ampleur de la prise de CO<sub>2</sub> par le béton ont été également étudiés. Un des avantages du réacteur de carbonatation appliqué dans cette étude est que l'énergie exigée est nettement inférieure, comparé à une chambre sous pression de CO<sub>2</sub>.

L'objectif global de cette thèse est de développer et d'évaluer la performance de l'exécution d'une carbonation accélérée traitant le réacteur pour le béton en utilisant un flux advectif des émissions gazeuses. Le taux et l'ampleur de la prise de CO<sub>2</sub> par le béton dans un écoulement unidimensionnel (1-D) à travers le réacteur de carbonation ont été étudiés et comparés aux résultats publiés sur la prise de CO<sub>2</sub> dans les chambres pressurisées en utilisant l'écoulement diffusif du CO<sub>2</sub>. Les facteurs limitant la prise de CO<sub>2</sub> ont été étudiés à travers l'observation expérimentale ainsi que la modélisation mathématique du transport et de la réaction du CO<sub>2</sub> dans le béton durant le traitement accéléré de la carbonation.

Les efficacités de carbonatation de 16-20% atteintes dans l'écoulement à travers le réacteur sont comparables à celles obtenues pour les chambres de pression statiques de CO<sub>2</sub>. L'ampleur de la prise de CO<sub>2</sub> a été limitée par la formation du carbonate de calcium solide dans des micro et macro-pores. Les expériences intermittentes de carbonatation ont prouvé que l'efficacité de carbonatation a été limitée en partie par la dissolution et/ou la diffusion lente des composants réactifs dissous dans la matrice de béton. La technique d'imagerie du micro-probe d'électron utilisé dans cette étude a également confirmé la formation du carbonate de calcium pendant la carbonatation, qui a rempli les micropores. L'efficacité de prise a atteint 67% quand le ciment a été carbonaté sous la forme de

boue dans un réacteur qui contienne un mélange de suspension aqueux (à travers du quel écoule le CO<sub>2</sub>), où l'effet du colmatage des pores a été éliminé et un pourcentage plus élevé de la superficie de surface de réaction a été exposé au CO<sub>2</sub> dissous. Cependant, la formation d'une couche de carbonate de calcium empêchait encore la diffusion du calcium dissous et du CO<sub>2</sub> à travers cette couche. En présence de la couche du carbonate de calcium et de toutes autres produit des carbonatations, comme la silice (gel SiO<sub>2</sub>), et à la pression partielle du CO<sub>2</sub> utilisée pour la carbonatation, la solution de ciment de boue a atteint un équilibre chimique et la carbonatation a cessé avant que la prise théorique maximum soit réalisée.

L'effet des processus physico-chimiques sur la prise de CO<sub>2</sub> durant le durcissement par carbonatation a été également étudié en utilisant un modèle mathématique. Des équations décrivant le transport du CO<sub>2</sub> par l'advection et la dispersion dans l'espace des pores du béton et la dissolution en eau qui se trouve dans les pores et la réaction avec des espèces réactives du ciment ont été résolues numériquement. La concentration initiale des espèces de ciment ont été calculées basée sur un modèle d'hydratation qui a été développé pour simuler les quatre heures d'hydratation avant que la carbonatation commence. La compétition entre divers processus affectant la prise de carbone a été étudiée par l'analyse dimensionnelle en utilisant des nombres sans dimensions. Les résultats montrent que l'efficacité de carbonatation pendant la période rapide de prise (30 premières minutes) n'a pas été limitée par le taux de transfert de masse gazeux liquide de CO<sub>2</sub>. Les taux des réactions de carbonatation des composés de ciment non hydraté étaient les facteurs contrôlant le taux pendant cette période (c.-à-d. une prise plus

élevée peut être réalisée dans un temps plus court en améliorant les taux de carbonatation, par exemple, en augmentant la superficie exposée de ces espèces).

#### Acknowledgements

I would like to dedicate my greatest gratitude to my thesis supervisor, Prof. Subhasis Ghoshal, for his continuous guidance and support during my studies at McGill. He provided encouragement, sound advice and brilliant ideas in every stage of this research as well as valuable comments in writing the journal publications. Completion of my Ph.D. was impossible without his patience and inspiration in all stages of this research project.

I would like to thank Prof. M. Nokken (Concordia University) for kindly providing me access to their Mercury Intrusion Porosimetry (MIP) facility and Prof. Vali (Faculty of Dentistry at McGill) for the very helpful discussion on electron microscope imaging techniques. Thanks to Rob Niven and summer students Kia and Cheryl for construction of the flow-through carbonation reactor, John Bartczak for his assistance in constructing the experimental apparatus, Lang Shi and George Panagiotidis for their help with scanning electron microscope (SEM) and electron microprobe analyses, Glenna Keating for her assistant in X-ray diffraction analyses (XRD), Ranjan Roy, Andrew Golsztajn and Daina Brumelis for their continuous guidance and assistant during the carbonation experiments, Dr. William Cook and Jorge Sayat for their technical advices whenever I had computer problems.

I would also like to acknowledge Natural Sciences and Engineering Research Council of Canada (NSERC), St. Lawrence Cement, CJS Technology for providing funding for this project, the Global Environmental and Climate Change Centre (GEC3) and le fonds québécois de la recherche sur la nature et les technologies (FQRNT) for their student grants and doctorate scholarship.

During my graduate studies at McGill, I was lucky to work with supporting people in the environmental research group who made this journey more enjoyable for me. I'd like to thank Wonjae for his guidance in the environmental lab and his always encouraging words, Trishikhi for her genuine support whenever I sought her help and Stoyan for always instilling positive vibe in the lab and thanks to David and Hagire for the French translation of the abstract.

I can not find the words to thank my parents and my sisters: Semira and Dorna. They have always encouraged me and supported me in every stage of my life. I owe whatever I have achieved to their unconditional love. Thank you.

## **Table of Contents**

ABSTI	RACT	i
RÉSUI	MÉ	iv
ACKN	OWLEDGMENTS	viii
TABL	E OF CONTENTS	X
LIST (	OF FIGURES	xiv
LIST (	OF TABLES	xvii
СНАР	TER 1:	
INTRO	DUCTION	1
1.1	Background	1
1	.1.1. Carbon capture and storage (CCS) methods	1
1	.1.2. Concrete as a candidate for mineral CO <sub>2</sub> sequestration	2
1.2	Motivation for this study	3
1.3	Objectives and approach	5
1.4	Scope and structure of the thesis	7
1	.4.1. Contribution of authors	8
1.5	References	9
СНАР	TER 2:	
LITER	ATURE REVIEW	12
2.1	Carbon dioxide mitigation by carbon capture and storage	
	technologies	12
2.2	Chemical composition of concrete and its potential for mineral CO <sub>2</sub>	
	sequestration during accelerated CO <sub>2</sub> curing	14
2	.2.1. Cement hydration.	15
2	.2.2. Current accelerated curing methods for precast concrete	16

4.	2.3. Carbonation curing of concrete
2.	2.4. Maximum theoretical CO <sub>2</sub> uptake by cement
2.	2.5. Carbon dioxide uptake by cement products
2.3.	Mathematical modeling of accelerated CO <sub>2</sub> curing of concrete in the
	1-D flow-through reactor.
2.4.	References
СНАР	ΓER 3:
CO <sub>2</sub> SE	QUESTRATION IN CONCRETE THROUGH ACCELERATED
CARBO	ONATION CURING IN A FLOW-THROUGH REACTOR
3.1	Introduction
3.2	Cement carbonation chemistry
3.3	Experimental section
3.	3.1. Materials and sample preparation
3.	3.2. Experimental set-up.
3.	3.3. Analytical instruments
3.4.	Results and discussion
3.	4.1.CO <sub>2</sub> uptake efficiency
3.	4.2. Dynamics of CO <sub>2</sub> uptake in 1-D flow-through reactor
3.	4.3. Effect of intermittent carbonation on CO <sub>2</sub> uptake efficiency
3.	4.4. Effect of carbonation on the porosity of compacted concrete
	samples
3.	4.5. CO <sub>2</sub> uptake with different gas flow-rates
3.5.	Conclusion
3.6.	Acknowledgments
3 7	References

#### **CHAPTER 4:**

PHYSICO-CHEMICAL PROCESSES LIMITING CO<sub>2</sub> UPTAKE IN

CONCR	ETE DURING ACCELERATED CARBONATION CURING
4.1. I	ntroduction
4.2. N	Materials and methods
4.2	2.1. Materials
4.2	2.2. Compact concrete experiment
4.2	2.3. Cement slurry experiment
4.2	2.4. Analytical methods
4.2	2.5. Microstructure imaging and analysis.
4.2	2.6. Chemical equilibrium model
4.3. 0	CO <sub>2</sub> uptake and carbonation efficiency
4.4. I	Results and discussion
4.4	4.1. Characterization of cement before carbonation
4.4	4.2. The extent of CO <sub>2</sub> uptake in compact concrete
4.4	4.3. Changes in the concrete matrix during carbonation and hydration
4.4	4.4. CO <sub>2</sub> uptake by aqueous cement suspension
4.4	4.5. Changes in chemistry of aqueous cement suspension and
	relationship to CO <sub>2</sub> uptake
4.5. (	Conclusions
4.6. A	Acknowledgments
4.7. I	References
4.8. \$	Supporting Information
CONNI	ECTING TEXT: CHAPTER 4&5
СНАРТ	TER 5:
MATHE	CMATICAL MODELING OF ACCELERATED CO <sub>2</sub> CURING OF
CONCR	ETE IN A FLOW-THROUGH REACTOR
5.1. I	ntroduction
5.2. I	Experimental materials and methods.
5.3.	The mathematical model framework
5 3	3.1. Boundary conditions and initial concentrations for the above

	Es
5.4. Pr	oduction and consumption rate of reactive compounds during
hyd	ration and carbonation curing
5.4.	Chemical reactions during hydration period prior to
	accelerated carbonation curing
5.4.	2. Chemical reactions during accelerated carbonation curing
5.4.	3. Rate of formation of hydration products
5.4.	4. Rate of CO <sub>2</sub> dissolution
5.4.	5. Rate of formation of carbonation products
5.4.	6. Changes in porosity and specific surface area of concrete
	during carbonation
5.5. Re	esults and Discussion
5.5.	1. Changes in concrete composition during hydration period
5.5.	2. Carbonation uptake calculated from the mathematical model
	for various water/cement ratios and gas flow-rates
5.5.	3. Prediction of carbonation uptake efficiency with changes in
	concrete parameters
5.6. Di	mensional Analysis
5.7. Co	onclusions
5.8. Ac	cknowledgments
5.9. No	otation
	References

## **List of Figures**

Figure.3.1. Carbonation apparatus set-up	38
Figure 3.2. Dynamics of carbonation reaction in compacted concrete samples using 1.17 Lpm gas flow-rate: measured N <sub>2</sub> gas (%) in the outlet for a pure N <sub>2</sub> injection (Δ), measured CO <sub>2</sub> gas (%) in outlet, and calculated cumulative CO <sub>2</sub> mass sequestered for 80% N <sub>2</sub> and 20% CO <sub>2</sub> mixture injection: (•[#117_1], □[#117_2], ×[#117_4], ○[#117_5], ▼[#117_6]). Numbers in brackets after each symbol refer to experiment runs explained in Table 3.1	38
Figure 3.3. Spatial and temporal distribution of carbonation efficiency during carbonation in 1-D flow-through reactor	39
Figure 3.4. Measured outlet CO <sub>2</sub> concentration profile in the 1-D flow-through reactor during intermittent carbonation (Δ), shut off times were 15 min, 325 min and 450 min. Shaded areas above the curve are proportional to the mass of CO <sub>2</sub> sequestered	40
Figure 3.5. Cumulative intrusion volume for an intrusion-extrusion cycle in non-carbonated sample (▼), 1-hour carbonated sample, for inlet middle (IM) (Δ), 1-hour carbonated sample, for inlet edge (IE) (□), and 1-hour carbonated sample, for outlet middle (OM) (▲)	41
Figure 3.6. Measured outlet CO <sub>2</sub> gas (%) using different gas flow-rates: 0.08 Lpm (−[#8_1], Δ[#8_2]), 1.17 Lpm (●[#117_1], ×[#117_4], ○[#117_5]) and 2 Lpm (▼[#200_1], □[#200_2]). Numbers in brackets after each symbol refer to experiment runs explained in Table 3.1	42
Figure 3.7. Measured cumulative mass of $CO_2$ uptake versus cumulative mass of inlet $CO_2$ at different flow-rates: 0.08 Lpm ( $-[\#8\_1]$ , $\Delta[\#8\_2]$ ), 1.17 Lpm ( $\bullet[\#117\_1]$ , $\times[\#117\_4]$ , $\circ[\#117\_5]$ ) and 2 Lpm ( $\blacktriangledown[\#200\_1]$ , $\Box[\#200\_2]$ ). Numbers in brackets after each symbol refer to experiment runs explained in Table 3.1	42
Figure 4.1. Schematic showing reaction products formed during accelerated CO <sub>2</sub> curing from various reactive cement phases	76
Figure 4.2. (A) Carbonation experiment set up which includes either of the following carbonation reactors (B) completely mixed flow-through (CMFT) carbonation reactor (C) 1-dimensional flow-through reactor	77

Figure	4.3. (A) Carbonation efficiency in compacted concrete with 20% and 40% CO <sub>2</sub> in nitrogen balance and water/cement ratios of 0.26 and 0.32 (B) measured ratio of outlet to inlet CO <sub>2</sub> gas concentration and carbonation efficiency in 1-D flow-through reactor with compacted concrete prepared with water/cement ratio of 0.32 and carbonated with 20% CO <sub>2</sub>
Figure	4.4. Scanning electron microprobe imaging with X-ray microanalysis (A) Backscattered Electron (BSE) image (B) Reconstructed image of pores (black), aggregate (grey), calcium carbonate (green), and remaining solid phase (white) in 24-hour hydrated (and non-carbonated) concrete
Figure	4.5. Scanning electron microprobe imaging with X-ray microanalysis (A) Backscattered Electron (BSE) image (B) reconstructed images of pores (black), aggregate (grey), calcium carbonate (green), and remaining solid phase (white) (C) reconstructed color map of Ca and distribution of calcium carbonate (white) in accelerated CO <sub>2</sub> cured concrete
Figure	4.6. (A) Measured ratio of outlet to inlet CO <sub>2</sub> gas concentration in CMFT reactor, calculated carbonation efficiency from inline CO <sub>2</sub> measurements and measured carbonation efficiency from combustion IR analyzer, (B) measured pH and concentrations of dissolved C and Ca in CMFT reactor during carbonation of aqueous cement suspension.
Figure 4	4.7. XRD results of (A) 4-hour hydrated and 1-hour carbonated Portland cement, (B) 4-hour hydrated Portland cement (Δ) C <sub>3</sub> S (Ca <sub>3</sub> SiO <sub>5</sub> ), (×) C <sub>2</sub> S (Ca <sub>2</sub> SiO <sub>4</sub> ), (■) calcite (CaCO <sub>3</sub> ), (•) C <sub>3</sub> A (3CaO.Al <sub>2</sub> O <sub>3</sub> ), (+) quartz (SiO <sub>2</sub> ) and (-) magnesite (MgCO <sub>3</sub> )
Figure 4	4S.1. XRD results of (A) 4-hour hydrated Portland cement, (B) unhydrated Portland cement ( $\Delta$ ) tricalcium silicate (Ca <sub>2</sub> SiO <sub>5</sub> ), (×) dicalcium silicate (Ca <sub>2</sub> SiO <sub>4</sub> ), ( $\square$ ) portlandite (Ca(OH) <sub>2</sub> ), and ( $\bullet$ ) tricalcium aluminate (3CaO.Al <sub>2</sub> O <sub>3</sub> )
Figure	5.1. Schematic view of concrete carbonation in the 1-D flow-through reactor
Figure	5.2. Changes in cement composition during hydration and carbonation, the numbers on arrows are related to equation numbers in Table 5.1
Figure	5.3. Concentration of cement phases during 4 hours of hydration calculated from the hydration model developed in this study
Figure	5.4. Ratio of outlet CO <sub>2</sub> concentration to inlet CO <sub>2</sub> concentration vs.

lines refer to the mathematical model (A) flow-rate: 1.17 Lpm, w/c: 0.26 (B) flow-rates: 0.08 and 2 Lpm, w/c: 0.26 and flow-rate: 1.17 Lpm, w/c: 0.32 (experimental results have been published in an earlier publication [23])	120
Figure 5.5. (A) Ratio of CO <sub>2</sub> (g) concentration in pores to inlet CO <sub>2</sub> (g) concentration along the length of concrete specimen during carbonation, the measured values at the outlet are shown by symbols (B) production of solid CaCO <sub>3</sub> along the length of the compact concrete with carbonation time, experimental measurements are shown by symbols	121
	121
Figure 5.6. Prediction of 30-minute carbonation efficiency by the mathematical model with changes in (A) percentage of CO <sub>2</sub> in the gas mixture, the experimental results for 20% and 40% CO <sub>2</sub> in N <sub>2</sub> balance are shown by symbols and (B) the specific surface area of concrete.	100
concrete	122
Figure 5.7. Sensitivity analysis with respect to (A) Damköhler number and	
(B) Stanton number	123

### **List of Tables**

Table 2.1. Cement hydration.	16
Table 2.2. Cement carbonation	19
Table 3.1. List of experiments and the carbonation efficiencies (water to cement ratio = 0.26; aggregate to cement ratio = 4)	52
Table 4.1. Composition and particle size of cement	83
Table 4S.1. Characteristics of water used in cement slurry	85
Table 4S.2. Calibration standards and detection limits for each element analyzed with electron microprobe for carbonated and hydrated concrete.	85
Table 4S.3. Selected electron microprobe analysis for crystals in Figures 4.4 and 4.5. Values are elemental oxide contents (wt%)	86
Table 5.1. Chemical reactions during hydration and carbonation of cement.	124
Table 5.2. Coefficients and constants for the cement hydration model	125
Table 5.3. Constants used in the carbonation model	126
Table 5.4. Dimensionless parameters used in this study. In these equations, $[i]$ is the concentration of cement phase $i$ in concrete	127
Table 5.5. Dimensionless parameters for gas flow-rate=1.17 Lpm and w/c=0.26	128

#### Chapter 1

#### Introduction

#### 1.1. Background

#### 1.1.1. Carbon capture and storage (CCS) methods

The total amount of carbon dioxide annually released due to human activities is 7.0 billion tons, out of which 5.4 billion tons is due to combustion of fossil fuels [1]. Since the beginning of the industrial age, the concentration of CO<sub>2</sub> in atmosphere has increased from 280 to 393 ppm [2]. The potential impacts of increased CO<sub>2</sub> concentrations are acidification of ocean surfaces [3], acid rain and the greenhouse effects. In order to manage climate change, the Intergovernmental Panel on Climate Change (IPCC) has set an upper limit of 550 ppm on atmospheric CO<sub>2</sub> concentration [4]. However, although the projections are for a doubling in the next 50 years, CO<sub>2</sub> emissions will have to be stabilized at current levels [5]. Carbon dioxide capture and storage (CCS) is considered to be one of the major strategies for limiting CO<sub>2</sub> emissions. Current ongoing studies on CCS technologies are focused on sequestration through enhanced oil recovery [6], underground geological storage [7, 8], enhanced biological sinks, deep oceans [9], and ex situ mineral carbonation [4]. The reactive mineral selected for carbonation should react with carbonic acid and provide alkalinity. There are naturally abundant mineral rocks containing calcium and magnesium which have the potential for mineral sequestration including olivine, serpentinite and wollastonite [10, 11]. Alkaline waste materials have also been proposed for carbon sequestration, because they are available in large amounts, low price, and generally rich in calcium. Among these waste materials are iron and steel slag, asbestos waste, and coal fly ash [12-15]. Slag is suitable for mineral carbonation because of calcium oxide and high alkalinity; it is rich in Fe<sub>2</sub>O<sub>3</sub> from processed iron ore and CaO from the addition of limestone for removal of impurities. The disposal of these carbonated minerals, however, stores CO<sub>2</sub> but does not provide materials that are of value.

#### 1.1.2. Concrete as a candidate for mineral CO<sub>2</sub> sequestration

Concrete is a mixture of aggregates, a binder, such as cement, and water. Cement components in concrete, such as calcium silicates and calcium hydroxide (a cement hydration product), can react with dissolved CO<sub>2</sub> in the presence of moisture. Among the various concrete products that can be used for CO<sub>2</sub> curing are non-reinforced concrete masonry units, concrete paving stones or fibreglass mesh reinforced cement board or cellulose fibre board [16].

Current methods for off-site precast concrete production include steam curing in which concrete is exposed to low or high pressure steam in autoclave and the heat from the steam causes faster hydration reactions [17]. In this accelerated curing method, a high amount of energy is used to produce steam, and the overall cost is relatively high compared to the ordinary curing methods. Carbon dioxide can be used to cure these precast and non-reinforced concrete products.

Carbonation reactions are faster than hydration reactions and form solid products which result in concrete setting.

#### 1.2. Motivation for this study

Previous studies showed that accelerated CO<sub>2</sub> curing of concrete causes rapid carbonation reactions and is expected to enhance the concrete properties such as compressive strength, durability and dimensional stability because of the depletion of calcium hydroxide as a result of carbonation [18-20]. Therefore, such a technology can reduce total CO<sub>2</sub> emissions from major point sources while developing a value-added product at the same time.

Among the CO<sub>2</sub> emitting industries, cement manufacturing contributes to 3.2% of global greenhouse gas (GHG) emissions [21]. The flue gases from cement plants can be used for accelerated CO<sub>2</sub> curing of concrete. Production lines for cement-based products can be installed next to the cement kilns, in order to achieve the economical and environmental advantages of this technology. For instance, from the 97.4 million tonnes of cement produced in the United States, over 16.4 million metric tonnes (approximately 17%) was delivered to concrete product manufacturers, 40% of which was used in production of concrete bricks and blocks [22]. Assuming the maximum theoretical uptake of 50% by weight of cement, the CO<sub>2</sub> uptake in these products can reach up to 3.2 million metric tons compared to the 45.7 million metric tons of CO<sub>2</sub> emissions from cement manufacture in the United States [23].

The previous studies on accelerated carbonation curing of concrete only focus on one type of carbonation reactor in which concrete blocks are exposed to pressurized CO<sub>2</sub> in a curing chamber [18, 19]. A high pressure of CO<sub>2</sub> is required in order to diffuse through the concrete matrix and might result in a non-homogeneous carbonated concrete. The energy for gas mixture compression can be saved, if concrete is cured in a flow-through reactor using a low pressure. In this study, a flow-through carbonation reactor was used for concrete curing and the rate and extent of CO<sub>2</sub> uptake by concrete was studied and compared with the published results on CO<sub>2</sub> uptake in pressurized chambers using diffusive flow of CO<sub>2</sub>.

In order to produce a better understanding of the chemical and physical phenomena affecting carbonation and CO<sub>2</sub> uptake efficiency of concrete, cement was also carbonated in an aqueous suspension form to eliminate the effect of inter-particle pores on carbonation and the concentration of some chemicals (such as dissolved carbon, calcium and pH) during carbonation was also monitored.

The mathematical approach to accelerated carbonation curing of concrete was also applied in this study in order to study the effect of physico-chemical processes on CO<sub>2</sub> uptake by concrete. Mathematical models have been developed in previous studies to study the passive carbonation of concrete by atmospheric CO<sub>2</sub> [24-31]. These theoretical models have been developed in order to study the penetration of CO<sub>2</sub> in concrete structures under different conditions. The CO<sub>2</sub> gas transport in the carbonation reactor in this study was by advection and dispersion while during weathering carbonation is only by diffusion through the porous media. Moreover, weathering carbonation happens in mature concrete during its

service life while accelerated carbonation curing is applied on freshly-made concrete with mainly unhydrated cement phases: calcium silicates (tricalcium silicate and dicalcium silicate) instead of hydration products (calcium hydroxide and calcium silicate hydrate gel).

#### 1.3. Objectives and approach

The overall objective of this thesis was to develop and assess the performance of an accelerated carbonation curing reactor for concrete in which  $CO_2$  gas flows through the concrete porous media instead of only diffusing through the pores, and also, to study the physico-chemical processes which limit the  $CO_2$  uptake by concrete during carbonation curing. In this research, application of a flow-through curing reactor was studied in which a lower  $CO_2$  pressure is required and the gas flows through the concrete matrix with an initial flow-rate instead of only diffusing through the pores. The accelerated carbonation curing experiments were conducted to measure the total  $CO_2$  uptake by concrete in the flow-through reactor. A model, synthetic flue gas of cement industry with 20%  $CO_2$  in nitrogen balance was used in this study for carbonation curing of concrete.

The specific objectives of this study are to:

a. Compare the extent and rate of CO<sub>2</sub> uptake by concrete during accelerated carbonation curing in a flow-through reactor and conventional pressure chambers. In order to determine whether using an advective CO<sub>2</sub> flow with

- lower partial pressure would improve the carbonation efficiency compared to diffusive flow and higher partial pressure of CO<sub>2</sub>.
- b. Investigate the spatial distribution of solid carbonation products (calcium carbonate) in the concrete matrix to provide insight on the role of calcium carbonate formation in limiting CO<sub>2</sub> uptake by concrete. Calcium carbonate might form in narrow pores and cause pore clogging or deposit on cement surface and inhibit further carbonation.
- c. Improve the understanding of maximum CO<sub>2</sub> uptake by cement. For this purpose the effect of interparticle pores was eliminated and cement was carbonated in an aqueous suspension with high water content in order to achieve the maximum possible CO<sub>2</sub> uptake.
- d. Study the effect of carbonation processes (such as gas transport, gas-liquid mass transfer and chemical reactions) on CO<sub>2</sub> uptake using a mathematical model of carbonation curing.

The following tasks were undertaken to address the objectives:

- 1. Carbon uptake by concrete during accelerated carbonation curing was measured in a 1-D flow through reactor using two different methods:
- CO<sub>2</sub> online measurement by IR gas analyzer in the gas outlet
- Carbon combustion IR analyzer on core samples taken from carbonated concrete
- 2. An electron microprobe imaging technique was used for samples taken from non-carbonated, 24-hour hydrated or 1-hour carbonated concrete and

an image analysis model was developed (using MATLAB) to remove noise and define the distribution of calcium carbonate in carbonated concrete.

- 3. Cement was carbonated in an aqueous suspension in a completely mixed reactor (CMFT) and CO<sub>2</sub> uptake by cement was measured. Samples were taken during carbonation and pH and concentration of dissolved calcium, carbon and other elements were measured using the atomic absorption method (AA).
- 4. A mathematical model for CO<sub>2</sub> advection and dispersion in concrete and carbonation chemical reactions in the 1-D flow-through reactor was developed in order to study the effect of operating conditions and physicochemical processes on CO<sub>2</sub> uptake by concrete.

#### 1.4. Scope and structure of the thesis

This is a manuscript-based thesis. Chapter 2 is a critical review of previous studies on topics related to this research. Chapter 3 presents the results of study on accelerated carbonation curing of concrete in a 1-D flow-through reactor. The carbon dioxide uptake by compact concrete during carbonation was assessed and the effect of carbonation on porosity of concrete was also studied using the mercury intrusion porosimetry (MIP) method. Chapter 4 presents the results of the completely mixed flow-through (CMFT) reactor used for carbonation of an

aqueous cement suspension and measurements of the CO<sub>2</sub> uptake, pH and concentration of different elements in the solution during carbonation. These measurements provided a better insight on the physico-chemical phenomena during carbonation. A mathematical simulation of accelerated CO<sub>2</sub> curing of concrete in the flow-through reactor was also developed. The results of mathematical model are discussed in Chapter 5. A summary of results and intellectual contributions are provided in Chapter 6.

#### 1.4.1. Contribution of authors

The contribution of authors of manuscripts in chapters 3, 4 and 5 are stated below.

#### Chapter 3.

CO<sub>2</sub> Sequestration in Concrete through Accelerated Carbonation Curing in a Flow-through Reactor. **S. Kashef-Haghighi and S. Ghoshal.** Industrial & Engineering Chemistry Research, 2010, 49 (3), pp 1143–1149.

The experiments of accelerated CO<sub>2</sub> curing in the flow-through reactor were performed by the author. Drafts of the chapter were prepared by the author and Prof. Ghoshal supervised the research, advised in writing and editing of the manuscript.

#### Chapter 4.

Physico-Chemical Processes Limiting CO<sub>2</sub> Uptake in Concrete during Accelerated CO<sub>2</sub> Curing. **S. Kashef-Haghighi and S. Ghoshal.** To be submitted to Industrial & Engineering Chemistry Research. April 2012.

The experimental design of completely mixed flow-through reactor, execution, analysis of results, concentration measurements, microprobe imaging and PHREEQC equilibrium model were carried out by the author. Drafts of the chapter were prepared by the author. Prof. Ghoshal supervised the experimental design and research and edited the manuscript.

#### Chapter 5.

Mathematical Modeling of Accelerated CO<sub>2</sub> Curing of Concrete in a Flow-Through Reactor. **S. Kashef-Haghighi and S. Ghoshal.** To be submitted to Cement & Concrete Research. April 2012.

The mathematical modeling of concrete carbonation in the flow-through reactor was developed by the author. Drafts of the chapter were prepared by the author. Prof. Ghoshal supervised the research and edited the manuscript.

#### 1.5. References

- [1] Liu, Z. and J. Zhao, Contribution of carbonate rock weathering to the atmospheric CO<sub>2</sub> sink. *Environ. Geol.*, **2000**, 39 (9), 1053.
- [2] Conway, T. and P. Tans. Trends in atmospheric carbon dioxide. [Retrieved 2012-04-09]; Available from: <a href="www.esrl.noaa.gov/gmd/ccgg/trends/">www.esrl.noaa.gov/gmd/ccgg/trends/</a>.
- [3] Doney, S.C., V.J. Fabry, R.A. Feely, and J.A. Kleypas, Ocean acidification: the other CO<sub>2</sub> problem. *Ann. Rev. Mar. Sci.*, **2009**, 1 (1), 169-192.
- [4] IPCC, Special report on carbon dioxide capture and storage. **2005**: Cambridge University Press.
- [5] Pacala, S. and R. Socolow, Stabilization wedges: solving the climate problem for the next 50 years with current technologies (Review). *Science*, **2004**, 305 (5686), 968.

- [6] Holt, T., J.I. Jensen, and E. Lindeberg, Underground storage of CO<sub>2</sub> in aquifers and oil reservoirs. *Energy Conversion and Management*, **1995**, 36 (6-9), 535.
- [7] Wilson, E.J., M.G. Morgan, J. Apt, M. Bonner, C. Bunting, J. Gode, R.S. Haszeldine, C.C. Jaeger, D.W. Keith, S.T. McCoy, M.F. Pollak, D.M. Reiner, E.S. Rubin, A. Torvanger, C. Ulardic, S.P. Vajjhala, D.G. Victor, and I.W. Wright, Regulating the Geological Sequestration of CO<sub>2</sub>. *Environ. Sci. Technol.*, **2008**, 42 (8), 2718-2722.
- [8] White, C.M., B.R. Strazisar, E.J. Granite, J.S. Hoffman, and H.W. Pennline, Separation and Capture of CO<sub>2</sub> from Large Stationary Sources and Sequestration in Geological Formations- Coalbeds and Deep Saline Aquifers (Critical Review). *J. Air & Waste Manage. Assoc.*, **2003**, 53, 645-715.
- [9] Riestenberg, D.E., C. Tsouris, P.G. Brewer, E.T. Peltzer, P. Walz, A.C. Chow, and E.E. Adams, Field studies on the formation of sinking CO<sub>2</sub> particles for ocean carbon sequestration: effects of injector geometry on particle density and dissolution rate and model simulation of plume behavior. *Environ. Sci. Technol.*, **2005**, 39 (18), 7287-7293.
- [10] Maroto-Valer, M.M., D.J. Fauth, M.E. Kuchta, Y. Zhang, and J.M. Andresen, Activation of magnesium rich minerals as carbonation feedstock materials for CO<sub>2</sub> sequestration. *Fuel Process. Technol.*, **2005**, 86 (14-15), 1627.
- [11] Huijgen, W.J.J., G.-J. Witkamp, and R.N.J. Comans, Mechanisms of aqueous wollastonite carbonation as a possible CO<sub>2</sub> sequestration process. *Chem. Eng. Sci.*, **2006**, 61 (13), 4242-4251.
- [12] Huijgen, W.J.J. and R.N.J. Comans, Carbonation of steel slag for CO<sub>2</sub> sequestration: leaching of products and reaction mechanisms. *Environ. Sci. Technol.*, **2006**, 40 (8), 2790-2796.
- [13] Huntzinger, D.N., J.S. Gierke, S.K. Kawatra, T.C. Eisele, and L.L. Sutter, Carbon dioxide sequestration in cement kiln dust through mineral carbonation. *Environ. Sci. Technol.*, **2009**, 43 (6), 1986-1992.
- [14] Iizuka, A., M. Fujii, A. Yamasaki, and Y. Yanagisawa, Development of a new CO<sub>2</sub> sequestration process utilizing the carbonation of waste cement. *Ind. Eng. Chem. Res.*, **2004**, 43, 7880-7887.
- [15] Montes-Hernandez, G., R. Perez-Lopez, F. Renard, J.M. Nieto, and L. Charlet, Mineral sequestration of CO<sub>2</sub> by aqueous carbonation of coal combustion fly-ash. *J. Hazard. Mater.*, **2009**, 161 (1347).
- [16] Monkman, S., Maximizing carbon uptake and performance gain in slagcontaining concretes through early carbonation. 2008, McGill University: Montreal, QC, Canada.
- [17] Kosmatka, S.H. and W.C. Panarese, Design and Control of Concrete Mixtures. 13th ed, ed. Association, P.C. **1988**, Skokie, IL.
- [18] Monkman, S. and Y. Shao, Assessing the carbonation behavior of cementitious materials. *J. Mater. Civ. Eng.*, **2006**, 18 (6), 768.
- [19] Shao, Y., M.S. Mirza, and X. Wu, CO<sub>2</sub> sequestration using calcium-silicate concrete. *Can. J. Civ. Eng.*, **2006**, 33 (6), 776-784.

- [20] Logan, C.O., Carbon dioxide absorption and durability of carbonation cured cement and concrete compacts. 2006, McGill University: Montreal, Canada.
- [21] Rehan, R. and M. Nehdi, Carbon dioxide emissions and climate change: policy implications for the cement industry. *Environ. Sci. Policy*, **2005**, 8 (2), 105.
- [22] Van Oss, H.G., Cement. U.S. Geological Survey Minerals Yearbook. **2004**.
- [23] EIA, Emissions of greenhouse gases in the United States 2006. **2007**, Washington, DC.: Energy Information Administration, U.S. Department of Energy.
- [24] Meier, S.A., M.A. Peter, A. Muntean, and M. Böhm, Dynamics of the internal reaction layer arising during carbonation of concrete. *Chem. Eng. Sci.*, **2007**, 62 (4), 1125-1137.
- [25] Saetta, A.V., B.A. Schrefler, and R.V. Vitaliani, The carbonation of concrete and the mechanism of moisture, heat and carbon dioxide flow through porous materials. *Cem. Concr. Res.*, **1993**, 23 (4), 761.
- [26] Saetta, A.V., B.A. Schrefler, and R.V. Vitaliani, 2-D model for carbonation and moisture/heat flow in porous materials. *Cem. Concr. Res.*, **1995**, 25 (8), 1703.
- [27] Papadakis, V.G., C.G. Vayenas, and M.N. Fardis, A reaction engineering approach to the problem of concrete carbonation. *AlChE J.*, **1989**, 35 (10), 1639-1650.
- [28] Papadakis, V.G., C.G. Vayenas, and M.N. Fardis, Physical and chemical characteristics affecting the durability of concrete. *ACI Mater. J.*, **1991a**, 8 (2), 186-196.
- [29] Papadakis, V.G., C.G. Vayenas, and M.N. Fardis, Fundamental modeling and experimental investigation of concrete carbonation. *ACI Mater. J.*, **1991b**, 88 (4), 363-373.
- [30] Papadakis, V.G., C.G. Vayenas, and M.N. Fardis, Experimental investigation and mathematical modeling of the concrete carbonation problem. *Chem. Eng. Sci.*, **1991c**, 46 (5-6), 1333.
- [31] Peter, M.A., A. Muntean, S.A. Meier, and M. Böhm, Competition of several carbonation reactions in concrete: a parametric study. *Cem. Concr. Res.*, **2008**, 38 (12), 1385-1393.

#### Chapter 2

#### **Literature Review**

# 2.1. Carbon dioxide mitigation by carbon capture and storage technologies

Carbon dioxide capture and storage (CCS) technologies are considered as the main solution for stabilization of atmospheric CO<sub>2</sub> concentrations. In these technologies, carbon dioxide is first separated from any industry source, transported to an appropriate location with potential of long-term storage and then stored and isolated from the atmosphere [1]. Prior to storage, a concentrated CO<sub>2</sub> stream is produced from point source emissions, such as fossil fuel power plants, using CO<sub>2</sub> capture processes. The common capture technologies include post-combustion capture, pre-combustion capture and oxy-combustion [2, 3]. Zeman et al. [4] also studied a CO<sub>2</sub> capture technology from ambient air using a NaOH-based alkaline liquid as a solvent.

In mineral sequestration, one of the CCS methods, a gas stream rich in CO<sub>2</sub> (e.g. from a capture step) is reacted with mineral metal oxides to form thermodynamically stable carbonates. Storage and disposal of CO<sub>2</sub> in the form of carbonates was first suggested by Seifritz [5]. One of the advantages of this technology is that the products formed are thermodynamically stable and, therefore, the sequestration of CO<sub>2</sub> in the form of a carbonate ensures long term storage of CO<sub>2</sub> and minimizes the expensive monitoring costs for the possibility

of CO<sub>2</sub> leakage back into the atmosphere [6]. Moreover, the suitable feedstock deposits for carbonation, for example steel slag or fly ash, are available in large scales around the world. Also, these carbonation reactions are exothermic and spontaneous [7]. One of the main factors hindering the use of this technology on a large scale is that the natural carbonation reaction is so slow that a pre-treatment, generally very energy intensive, is needed to enhance the rate of reaction [1].

Among the magnesium or calcium rich, naturally abundant silicate minerals candidate sequestration for  $CO_2$ are olivine  $(Mg_2SiO_4)$ , (Mg<sub>3</sub>Si<sub>2</sub>O<sub>5</sub>(OH)<sub>4</sub>) and wollastonite (CaSiO<sub>3</sub>) [6, 8]. The carbonate product will be stable over a geologic time frame as the energy state of a mineral carbonate is 60 to 180 kJ/mol lower than CO<sub>2</sub> [6]. Alkaline waste materials can also be good candidates for carbon sequestration, because they are available in large amounts and low price, and are generally rich in calcium [9]. The potential of waste material in soil for CO<sub>2</sub> storage was studied by Renforth [10]. These soils are also rich in calcium in the form of Portlandite (Ca(OH)<sub>2</sub>), resulting in CaCO<sub>3</sub> precipitation because of weathering of portlandite. The carbonation potential of steel slag was studied by Huijgen et al. [9, 11]. They explained the carbonation process in two subsequent steps. In the first step, calcium leaches from the steel slag particles into the solution; in the second step the calcium carbonate product precipitates on the particles. The first step, which includes the diffusion of calcium, is hindered by the precipitation of solid products formed from the carbonation reaction in solution. Thus, it is apparent that mass transport processes in addition to the CO<sub>2</sub> reaction rate can influence the rate and extent of carbonation. The enhancement of the overall carbonation rate is essential for the application of this mechanism as a CCS technology.

# 2.2. Chemical composition of concrete and its potential for mineral CO<sub>2</sub> sequestration during accelerated CO<sub>2</sub> curing

Concrete is a product of mixing water, cement and aggregate and sometimes other additives for specific applications and it should be cured in order to obtain strength [12]. Based on recent studies, carbon dioxide can be used for curing of some concrete products [13-16]. Cement components in concrete, such as calcium hydroxide can react with dissolved CO<sub>2</sub> in the presence of moisture while the silica aggregates are inert to the carbonation reaction and only affect the physical parameters of the porous media such as porosity, permeability and effective diffusivity of the gas. However, aggregates with high percentages of CaO, for instance ladle slag with approximately 58% CaO, have been proposed for carbonation and can improve the total uptake by concrete [17].

The cement phases are usually expressed as a combination of oxides. The four main oxides are SiO<sub>2</sub>, CaO, Al<sub>2</sub>O<sub>3</sub>, Fe<sub>2</sub>O<sub>3</sub>. For example, the most abundant phase in Portland cement is tricalcium silicate (3CaO.SiO<sub>2</sub>) which is composed of three units of calcium oxide and one unit silicon oxide. Within the cement industry, the oxides are typically abbreviated as a single letter: C<sub>3</sub>S standing for tricalcium silicate. The major cement phases are 3CaO.SiO<sub>2</sub> (C<sub>3</sub>S), 2CaO.SiO<sub>2</sub> (C<sub>2</sub>S), 3CaO.Al<sub>2</sub>O<sub>3</sub> (C<sub>3</sub>A) and 4CaO.Al<sub>2</sub>O<sub>3</sub>.Fe<sub>2</sub>O<sub>3</sub> (C<sub>4</sub>AF). There may also be 1% free lime (CaO) which is not combined during the clinkering process and around 2%

CaO in calcium sulfate (gypsum) added during the grinding process. The cement chemistry is explained in more detail in several references [18-20].

#### 2.2.1. Cement hydration

In order to attain an initial hardening required for accelerated carbonation curing in the 1-D flow-through reactor, the concrete matrix was hydrated for 4 hours prior to carbonation. When anhydrous cement is mixed with water, hydration reactions occur. The main hydration reactions of cement compounds are shown in Table 2.1. Calcium silicates (C<sub>3</sub>S and C<sub>2</sub>S) react with water and form calcium hydroxide (CH) and amorphous calcium silicate hydrate (C-S-H) gel (Eqs. 2.1-2.2). Calcium silicate hydrate gel formed from hydration of C<sub>3</sub>S and C<sub>2</sub>S is referred to as C-S-H in order to imply that no particular composition is implied. The X-ray diffraction (XRD) studies on Portland cement shows that about 70% of the C<sub>3</sub>S reacts in 28 days of hydration, and virtually all in 1 year. Dicalcium silicate (C<sub>2</sub>S) also hydrates but at a much slower rate, about 30% reacts in 28 days and 90% in 1 year [19]. Calcium aluminoferrite (C<sub>4</sub>AF) and tricalcium aluminate (C<sub>3</sub>A) also react with water, CH and gypsum to form hydration products (Eqs. 2.3-2.4) [18]. Ettringite (3CaO.Al<sub>2</sub>O<sub>3</sub>.3CaSO<sub>4</sub>.32H<sub>2</sub>O) is an intermediate product of the reaction of calcium aluminate with gypsum (Eq. 2.4), which is also called trisulfate or AFt. Reactions 2.5 and 2.6 dominate once all gypsum is consumed.

**TABLE 2.1.** Cement hydration

Hydration of 3CaO.SiO <sub>2</sub> and 2CaO.SiO <sub>2</sub> :	Eq.
$2(3\text{CaO.SiO}_2) + 6\text{H}_2\text{O} \rightarrow (3\text{CaO.2SiO}_2.3\text{H}_2\text{O}) + 3\text{Ca(OH)}_2$	(2.1)
$2(2\text{CaO.SiO}_2) + 4\text{H}_2\text{O} \rightarrow (3\text{CaO.2SiO}_2.3\text{H}_2\text{O}) + \text{Ca(OH)}_2$	(2.2)

Hydration of 4CaO.Al<sub>2</sub>O<sub>3</sub>.Fe<sub>2</sub>O<sub>3</sub> and 3CaO.Al<sub>2</sub>O<sub>3</sub> in the presence of gypsum:

$$(4\text{CaO.Al}_2\text{O}_3.\text{Fe}_2\text{O}_3) + 2\text{Ca}(\text{OH})_2 + 2(\text{CaSO}_4.2\text{H}_2\text{O}) + 18\text{H}_2\text{O} \rightarrow$$
 (2.3)  
 $(6\text{CaO.Al}_2\text{O}_3.\text{Fe}_2\text{O}_3.2\text{CaSO}_4.24\text{H}_2\text{O})$ 

$$(3CaO.Al_2O_3) + CaSO_4.2H_2O + 10H_2O \rightarrow (3CaO.Al_2O_3.CaSO_4.12H_2O)$$
 (2.4)

In the absence of gypsum:

$$(4CaO.Al_2O_3.Fe_2O_3) + 4Ca(OH)_2 + 22H_2O \to$$

$$(6CaO.Al_2O_3.Fe_2O_3.2Ca(OH)_2.24H_2O)$$
(2.5)

$$(3CaO.Al_2O_3) + Ca(OH)_2 + 12H_2O \rightarrow (3CaO.Al_2O_3.Ca(OH)_2.12H_2O)$$
 (2.6)

#### 2.2.2. Current accelerated curing methods for precast concrete

One of the accelerated curing methods currently employed by commercial precast manufactures is the implementation of elevated temperature. The rate of hydration increases with increased temperature and, therefore, high early compressive strengths can be achieved. The temperature can be increased through the employment of conduction/convection techniques or through electrical resistance [21, 22]. Providing sufficient humidity to prevent drying of concrete and proper insulation for energy efficiency is essential when this curing technology is used. Steam curing is another accelerated curing method in which elevated curing temperature and the addition of moisture are both used. Steam curing can be at both low-pressure (close to atmospheric pressure) and high

pressure. In high pressure steam curing, also known as autoclaving, the increase in temperature and humidity is combined with an increase in pressure. High pressure steam curing is employed in a pressure chamber also called an autoclave. In this method, the heat from the steam causes faster hydration reactions and cement setting. In this accelerated curing method a high amount of energy is used to produce steam, and the overall cost is relatively high compared to ordinary curing methods.

Concrete curing using CO<sub>2</sub> has been suggested as an accelerated curing method as carbonation reactions are faster than hydration reactions. In this method, concrete products are cured in a pressure chamber exposed to high pressure CO<sub>2</sub>. Pure CO<sub>2</sub> has been used for carbonation curing in several previous studies [14, 16, 23]. However, the use of low-pressure flue gas directly from the industry will eliminate the separation step and reduce the energy required for gas compression and transport and will, therefore, enhance the CO<sub>2</sub> mitigation potential of this process.

#### 2.2.3. Carbonation curing of concrete

During carbonation, calcium dioxide dissolves in water and forms carbonate and bicarbonate.

$$CO_2(g) \to CO_2(aq)$$
 (2.7)

$$CO_2(aq) + OH^-(aq) \rightarrow HCO_3^-(aq)$$
 (2.8)

$$HCO_3^-(aq) + OH^-(aq) \rightarrow CO_3^{2-}(aq) + H_2O$$
 (2.9)

Cement compounds dissolve in pore water and react with dissolved CO<sub>2</sub> to form calcium carbonate. The overall carbonation reactions for cement compounds are listed in Table 2.2.

One of the first studies which used carbon dioxide for accelerated curing of calcium silicate mortars was done by Young et al. [24]. They studied the compressive strength of compacted mortar samples of C<sub>3</sub>S and C<sub>2</sub>S after a few minutes exposed to CO<sub>2</sub>. Strength developed rapidly in compacted samples after 81 minutes of exposure. Goodbrake et al. [25] and Young et al. [24] explained carbonation of C<sub>3</sub>S and β-C<sub>2</sub>S (a polymorph of C<sub>2</sub>S) as accelerated hydration, forming C-S-H and calcite, C-S-H is also carbonated and eventually silica gel is formed. Groves et al. [26] also reported changes in Ca/Si ratio of C-S-H gel during carbonation before formation of silica gel in hardened C<sub>3</sub>S carbonated by pure CO<sub>2</sub>. In carbonation of  $\gamma$ -C<sub>2</sub>S (a stable polymorph of C<sub>2</sub>S) and C<sub>3</sub>S powder in carbonation chamber with 5% CO<sub>2</sub> (100% RH), Goto et al. [27] reported that calcite was formed more than aragonite and vaterite. However, in β-C<sub>2</sub>S, aragonite was more prevalent, with some traces of calcite and vaterite. Klemm and Berger [28] also reported calcite as the main calcium carbonate crystallite formed during carbonation as detected by X-ray diffraction (XRD). Formation and decay of different phases of hydrated cement during carbonation was also confirmed by Neutron diffraction analysis by Castellote et al. [29]. Due to the initial lime content in cement, calcite was not zero initially but increased progressively during carbonation. They also reported the rate of carbonation of hydration cement compounds (C-S-H, ettringite and portlandite) as exponential of the first order. Ettringite was reported to have the fastest rate and portlandite the slowest rate of disappearance in the sample during carbonation.

**TABLE 2.2.** Cement compound and hydration product carbonation

Carbonation of C <sub>3</sub> S and C <sub>2</sub> S:	Eq.
$3\text{CaO.SiO}_2 + 3\text{CO}_2(\text{aq}) + \mu\text{H}_2\text{O} \rightarrow \text{SiO}_2. \mu \text{H}_2\text{O} + 3\text{CaCO}_3(\text{s})$	(2.10)
$2\text{CaO.SiO}_2 + 2\text{CO}_2(\text{aq}) + \mu\text{H}_2\text{O} \rightarrow \text{SiO}_2. \mu \text{H}_2\text{O} + 2\text{CaCO}_3(\text{s})$	(2.11)
Carbonation of CH and C-S-H:	
$Ca(OH)_2 + CO_2(aq) \rightarrow CaCO_3 + H_2O$	(2.12)
$3\text{CaO.2SiO}_2.3\text{H}_2\text{O} + 3\text{CO}_2(\text{aq}) \rightarrow 3\text{CaCO}_3.2\text{SiO}_2.3\text{H}_2\text{O}$	(2.13)
Carbonation of ettringite:	
$Ca_6.Al_2O_6(SO_4)_3.32H_2O(s) + 6CO_2(aq) \rightarrow$ $6CaCO_3(s) + 2Al(OH)_3(s) + 26H_2O + 3SO_4^{2-} + 6H^+$	(2.14)

#### 2.2.4. Maximum theoretical CO<sub>2</sub> uptake by cement

The maximum theoretical  $CO_2$  uptake by cement is a function of the relative masses of oxides present in the cement and can be estimated with the Steinour formula (Eq. 2.15) [30].

$$CO_{2}(\%) = 0.785(X_{CaO} - 0.560X_{CaCO_{3}} - 0.700X_{SO_{3}}) + 1.091X_{MgO} + 1.420X_{Na,O} + 0.935X_{K,O}$$
(2.15)

The  $(X_i)$  represents the percent dry mass of phase i in cement. In this equation, the stoichiometric factors assume that all CaO (except the percentage bound in CaCO<sub>3</sub> and CaSO<sub>4</sub>) forms calcium carbonate, all MgO forms MgCO<sub>3</sub>, and Na<sub>2</sub>O and K<sub>2</sub>O form Na<sub>2</sub>CO<sub>3</sub> and K<sub>2</sub>CO<sub>3</sub>. The maximum uptake for a typical Type 10 cement composition is calculated as approximately 50% [31]. Therefore,

assuming 100% carbonation efficiency, one metric ton of cement has the sequestration potential of a half metric ton of carbon dioxide.

#### 2.2.5. Carbon dioxide uptake by cement products

The carbonation efficiency by compact concrete in pressure chambers was measured by Shao et al. [16]. The efficiency reached 17-28% in Type 10 Portland cement-containing concrete with pure CO<sub>2</sub> at 0.5 MPa pressure. The CO<sub>2</sub> uptake in a waste cement product, cement kiln dust (CKD), was studied by Huntzinger et al. [32] in packed columns as well as in a batch reactor. The carbon uptake by CKD in a batch reactor reached approximately 80% while in packed columns was in the range of 58.7-75.6% for different types of CKD with different compositions and dimensions. Carbon dioxide uptake by cement waste was also approximately 67% measured by Iizuka et al. [33]. They applied high CO<sub>2</sub> pressure (several megapascals) in a completely mixed reactor in order to extract calcium from the cement and then subsequently carbonate under a lower pressure of CO<sub>2</sub>. The efficiency did not reach the theoretical value even with the enhancement in calcium dissolution. Formation of solid calcium carbonate product has been mentioned as a reason for limiting CO<sub>2</sub> uptake by several researchers. Dennis and Pacciani [34] reported the carbonation process of a synthetic mixture of calcium oxide in two phases: a rapid carbonation phase followed by a slower rate phase. The first phase ceased when the volume available in small pores (pore diameter <150 nm) filled with solid calcium carbonate. In the second phase, most of the pores internal to the grain are filled and a layer of product is being deposited on the grain.

## 2.3. Mathematical modeling of accelerated CO<sub>2</sub> curing of concrete in the1-D flow-through reactor

The mathematical modeling of concrete carbonation gained much attention since carbonation was considered as a detrimental process to the durability of reinforced concrete. The numerical simulation of the carbonation process, including the diffusion of CO<sub>2</sub> gas into the concrete pores and the resulting chemical reactions, has been developed by several researchers [35-40].

Papadakis et al. [35, 37, 41] modeled the carbonation process using the differential mass balance equations for CO2 in gas and liquid phase, solid and dissolved Ca(OH)<sub>2</sub> and other cement phases such as C-S-H, C<sub>3</sub>S and C<sub>2</sub>S accounting for their transport, production and consumption. Applying the carbonation chemistry, Burkan-Isgor et al. [42] also developed a two-dimensional finite element model of concrete carbonation. Their carbonation model, unlike that of Papadakis et al. [35], coupled heat, moisture and carbon dioxide diffusion in order to account for the heat and moisture produced during carbonation. Saetta et al. [36, 43] also numerically solved the coupled differential equations governing the moisture, heat and carbon dioxide flow, in both one and two dimensions, to study the effect of temperature and relative humidity on the progress of carbonation in reinforced concrete. The objective of the above mentioned studies was to evaluate the effect of concrete parameters and ambient CO<sub>2</sub> concentration, humidity and pressure on the progress of the carbonation front in reinforced concrete rather than the amount of CO<sub>2</sub> uptake by concrete. Moreover, all the above studies were aimed at monitoring the weathering process

of reinforced concrete due to carbonation where the CO<sub>2</sub> transport in concrete is through diffusion only. Since the weathering of concrete by carbonation occurs in mature and hydrated concrete structures, the composition of the hydrated cement paste is different from the freshly-made concrete used in this study.

The carbonation model in this study, however, monitors the amount of CO<sub>2</sub> uptake, the concentration of all cement constituents that are subject to carbonation and concrete porosity during CO<sub>2</sub> accelerated curing. The accelerated curing in this study takes place in a 1-D flow-through reactor where CO<sub>2</sub> is transported by an initial flow-rate through the sample in order to achieve a more homogeneous carbonated concrete compared to an accelerated carbonation curing in a pressure chamber, therefore, the transport of CO<sub>2</sub> is through advection and dispersion rather than only diffusion. The CO<sub>2</sub> transport and uptake by concrete during carbonation curing was modeled in order to develop a tool for identifying the optimal conditions for maximizing the uptake and further predictions of CO<sub>2</sub> uptake under different operating conditions such as gas flow-rate, water/cement ratio or total surface area.

#### 2.4. References

- [1] IPCC, Special report on carbon dioxide capture and storage. **2005**: Cambridge University Press.
- [2] Figueroa, J.D., T. Fout, S. Plasynski, H. McIlvried, and R.D. Srivastava, Advances in CO<sub>2</sub> capture technology--the U.S. Department of Energy's carbon sequestration program. *Int. J. Greenhouse Gas Control*, **2008**, 2 (1), 9.
- [3] Riemer, P., Greenhouse gas mitigation technologies, an overview of the CO<sub>2</sub> capture, storage and future activities of the IEA Greenhouse Gas R&D programme. *Energy Convers. Mgmt.*, **1996**, 37 (6-8), 665.

- [4] Zeman, F., Energy and material balance of CO<sub>2</sub> capture from ambient air. *Environ. Sci. Technol.*, **2007**, 41 (21), 7558-7563.
- [5] Seifritz, W., CO<sub>2</sub> disposal by means of silicates. *Nature*, **1990**, 345, 486.
- [6] Maroto-Valer, M.M., D.J. Fauth, M.E. Kuchta, Y. Zhang, and J.M. Andresen, Activation of magnesium rich minerals as carbonation feedstock materials for CO<sub>2</sub> sequestration. *Fuel Process. Technol.*, **2005**, 86 (14-15), 1627.
- [7] Huijgen, W.J.J. and R.N.J. Comans, Carbon dioxide storage by mineral carbonation. IEA GHG report 2005/11. **2005**, Cheltenham, UK: Energy Research Centre of the Netherlands.
- [8] Huijgen, W.J.J., G.-J. Witkamp, and R.N.J. Comans, Mechanisms of aqueous wollastonite carbonation as a possible CO<sub>2</sub> sequestration process. *Chem. Eng. Sci.*, **2006**, 61 (13), 4242-4251.
- [9] Huijgen, W.J.J. and R.N.J. Comans, Carbonation of steel slag for CO<sub>2</sub> sequestration: leaching of products and reaction mechanisms. *Environ. Sci. Technol.*, **2006**, 40 (8), 2790-2796.
- [10] Renforth, P., D.A.C. Manning, and E. Lopez-Capel, Carbonate precipitation in artificial soils as a sink for atmospheric carbon dioxide. *Applied Geochemistry*, **2009**, 24, 1757–1764.
- [11] Huijgen, W.J.J., G.J. Witkamp, and R.N.J. Comans, Mineral CO<sub>2</sub> sequestration by steel slag carbonation. *Environ. Sci. Technol.*, **2005**, 39 (24), 9676-9682.
- [12] Kosmatka, S.H. and W.C. Panarese, Design and Control of Concrete Mixtures. 13th ed, ed. Association, P.C. **1988**, Skokie, IL.
- [13] Shao, Y., X. Zhou, and S. Monkman, A new CO<sub>2</sub> sequestration process via concrete products production. 2006b: Ottawa, ON, Canada. p. 216-221.
- [14] Shi, C. and Y. Wu, Studies on some factors affecting CO<sub>2</sub> curing of lightweight concrete products. *Resour. Conserv. Recy.*, **2008**, 52 (8-9), 1087-1092.
- [15] Rostami, V., Y. Shao, and A.J. Boyd, Durability of concrete pipes subjected to combined steam and carbonation curing. *Constr. Build. Mater.*, 25 (8), 3345-3355.
- [16] Shao, Y., M.S. Mirza, and X. Wu, CO<sub>2</sub> sequestration using calcium-silicate concrete. *Can. J. Civ. Eng.*, **2006**, 33 (6), 776-784.
- [17] Monkman, S., Y. Shao, and C. Shi, Carbonated ladle slag fines for carbon uptake and sand substitute. *J. Mater. Civ. Eng.*, **2009**, 21 (11), 657-665.
- [18] Lea, F.M., The Chemistry of Cement and Concrete. **1970**, London: Edward Arnold.
- [19] Taylor, H.F., Cement Chemistry 2ed. 1997: Telford.
- [20] Hewlett, P., ed. *Lea's Chemistry of Cement and Concrete*. 4th ed. **1998**, Butterworth-Heinemann.
- [21] Heritage, I., F.M. Khalaf, and J.G. Wilson, Thermal acceleration of Portland cement concretes using direct electronic curing. *ACI Mater. J.*, **2000**, January-February, 37-40.
- [22] Ben C. Gerwick, J., Construction of Prestressed Concrete Structures. 2nd ed. 1993, New York, NY: John Wiley & Sons, Inc.,.

- [23] Reardon, E.J., B.R. James, and J. Abouchar, High pressure carbonation of cementitious grout. *Cem. Concr. Res.*, **1989**, 19 (3), 385.
- [24] Young, J.F., R.L. Berger, and J. Breese, Accelerated curing of compacted calcium silicate mortars on exposure to CO<sub>2</sub>. *J. Am. Ceram. Soc.*, **1974**, 57 (9), 394-397.
- [25] Goodbrake, C.J., J.F. Young, and R.L. Berger, Reaction of hydraulic calcium silicates with carbon dioxide and water. *J. Am. Ceram. Soc.*, **1979**, 62 (9-10), 488-491.
- [26] Groves, G.W., A. Brough, I.G. Richardson, and C.M. Dobson, Progressive changes in the structure of hardened C<sub>3</sub>S cement pastes due to carbonation. *J. Am. Ceram. Soc.*, **1991**, 74 (11), 2891-2896.
- [27] Goto, S., K. Suenaga, and T. Kado, Calcium silicate carbonation products. J. Am. Ceram. Soc., 1995, 78 (11), 2867-72.
- [28] Klemm, W.A. and R.L. Berger, Accelerated curing of cementitious systems by carbon dioxide: Part I. Portland cement. *Cem. Concr. Res.*, **1972**, 2 (5), 567.
- [29] Castellote, M., C. Andrade, X. Turrillas, J. Campo, and G.J. Cuello, Accelerated carbonation of cement pastes in situ monitored by neutron diffraction. *Cem. Concr. Res.*, **2008**, 38 (12), 1365-1373.
- [30] Steinour, H.H., Some effects of carbon dioxide on mortars and concrete-discussion. *J. Am. Concr. Inst.*, **1959**, 30, 905-907.
- [31] Monkman, S. and Y. Shao, Assessing the carbonation behavior of cementitious materials. *J. Mater. Civ. Eng.*, **2006**, 18 (6), 768.
- [32] Huntzinger, D.N., J.S. Gierke, S.K. Kawatra, T.C. Eisele, and L.L. Sutter, Carbon dioxide sequestration in cement kiln dust through mineral carbonation. *Environ. Sci. Technol.*, **2009**, 43 (6), 1986-1992.
- [33] Iizuka, A., M. Fujii, A. Yamasaki, and Y. Yanagisawa, Development of a new CO<sub>2</sub> sequestration process utilizing the carbonation of waste cement. *Ind. Eng. Chem. Res.*, **2004**, 43, 7880-7887.
- [34] Dennis, J.S. and R. Pacciani, The rate and extent of uptake of CO<sub>2</sub> by a synthetic, CaO-containing sorbent. *Chem. Eng. Sci.*, **2009**, 64 (9), 2147-2157.
- [35] Papadakis, V.G., C.G. Vayenas, and M.N. Fardis, Fundamental modeling and experimental investigation of concrete carbonation. *ACI Mater. J.*, **1991a**, 88 (4), 363-373.
- [36] Saetta, A.V., B.A. Schrefler, and R.V. Vitaliani, The carbonation of concrete and the mechanism of moisture, heat and carbon dioxide flow through porous materials. *Cem. Concr. Res.*, **1993**, 23 (4), 761.
- [37] Papadakis, V.G., C.G. Vayenas, and M.N. Fardis, Experimental investigation and mathematical modeling of the concrete carbonation problem. *Chem. Eng. Sci.*, **1991b**, 46 (5-6), 1333.
- [38] Peter, M.A., A. Muntean, S.A. Meier, and M. Böhm, Competition of several carbonation reactions in concrete: a parametric study. *Cem. Concr. Res.*, **2008**, 38 (12), 1385-1393.
- [39] Meier, S.A., M.A. Peter, A. Muntean, and M. Böhm, Dynamics of the internal reaction layer arising during carbonation of concrete. *Chem. Eng. Sci.*, **2007**, 62 (4), 1125-1137.

- [40] Thiery, M., G. Villain, P. Dangla, and G. Platret, Investigation of the carbonation front shape on cementitious materials: effects of the chemical kinetics. *Cem. Concr. Res.*, **2007**, 37 (7), 1047-1058.
- [41] Papadakis, V.G., C.G. Vayenas, and M.N. Fardis, A reaction engineering approach to the problem of concrete carbonation. *AlChE J.*, **1989**, 35 (10), 1639-1650.
- [42] Burkan Isgor, O. and A.G. Razaqpur, Finite element modeling of coupled heat transfer, moisture transport and carbonation processes in concrete structures. *Cem. Concr. Compos.*, **2004**, 26 (1), 57.
- [43] Saetta, A.V., B.A. Schrefler, and R.V. Vitaliani, 2-D model for carbonation and moisture/heat flow in porous materials. *Cem. Concr. Res.*, **1995**, 25 (8), 1703.

### **Chapter 3**

# CO<sub>2</sub> SEQUESTRATION IN CONCRETE THROUGH ACCELERATED CARBONATION CURING IN A FLOW-THROUGH REACTOR

Sormeh Kashef-Haghighi, Subhasis Ghoshal

Department of Civil Engineering, McGill University, Montreal, QC, Canada

#### Published in

Industrial & Engineering Chemistry Research, 2010, 49 (3), pp 1143–1149

#### 3.1. Introduction

Carbon dioxide is the dominant greenhouse gas resulting from many anthropogenic activities, mainly the combustion of fossil fuels. Burning these fuels leads to emissions of about 22x10<sup>9</sup> tonne CO<sub>2</sub>/year [1]. To stabilize the atmospheric CO<sub>2</sub> levels at 500 ppm, CO<sub>2</sub> emissions will have to be stabilized at current levels [2], although the projections are for a doubling over the next 50 years. Carbon capture and storage is considered to be one of the major strategies for limiting CO<sub>2</sub> emissions [3]. A CO<sub>2</sub> capture process should precede the storage to produce a concentrated CO<sub>2</sub> stream from point source emissions such as fossil fuel power plants. Common capture technologies include separation with solvents or membranes. Many ongoing studies on carbon dioxide (CO<sub>2</sub>) sequestration scenarios focus on enhanced oil recovery and/or underground geological storage, disposal in deep oceans, and *ex-situ* mineral sequestration [3]. Storage and disposal of CO<sub>2</sub> in the form of thermodynamically stable carbonates was first suggested by Seifritz [4] and more recently by others [5, 6].

Storage of  $CO_2$  in reactive minerals involves the chemical reaction of  $CO_2$  with reactive metal oxide feedstocks. For example, olivine  $(Mg_2SiO_4)$ , serpentine  $(Mg_3Si_2O_5(OH)_4)$  and wollastonite  $(CaSiO_3)$  are naturally abundant minerals proposed for use in mineral sequestration. The general carbonation reaction is shown as [7]:

$$(Mg, Ca)_x Si_y O_{x+2y} + xCO_2 \rightarrow x(Mg, Ca)CO_3 + ySiO_2$$
(3.1)

Other than mineral rocks, alkaline Ca-rich waste materials can also be candidates for carbon dioxide sequestration. Carbon dioxide sequestration in waste iron and steel slag, coal fly ash, cement kiln dust and concrete debris has been demonstrated in recent studies [6, 8-10]. However, economic incentives for mineral sequestration of CO<sub>2</sub> would be greater if the carbonated products have beneficial uses. For example, Monkman [11] suggested that carbonated steel slag may be used as aggregates in concrete production. Accelerated curing of fresh concrete using CO<sub>2</sub> or CO<sub>2</sub>-rich flue gas has been suggested as a carbon dioxide sequestration process which provides a value-added product, CO<sub>2</sub>-cured concrete [12]. Carbonation of non-reinforced concrete is expected to enhance the compressive strength, durability and dimensional stability because of the depletion of calcium hydroxide as a result of carbonation. The effect of accelerated carbonation curing on these characteristics of concrete was studied in detail [11, 13, 14] and generally indicates higher strength and performance characteristics.

It should be noted, though, that cement, its derivatives and by-products and Ca-rich waste materials such as slag are often generated from processes involving calcination of CaCO<sub>3</sub>, and thus reacting CO<sub>2</sub> with such materials does not result in a net removal of CO<sub>2</sub> as in mineral sequestration processes identified by the Intergovernmental Panel on Climate Change (IPCC) [3]. Nonetheless, reaction of CO<sub>2</sub> with cement and cementitious waste materials provides an important means to sequester CO<sub>2</sub> that would have otherwise been discharged to the atmosphere.

Among the various concrete products that can be used for CO<sub>2</sub> uptake are non-reinforced concrete blocks and bricks, or concrete products with non-metallic

reinforcements [14]. In 2004, from the 97.4 million tonnes of cement produced in the United States, over 16.4 million metric tonnes (approximately 17%) was delivered to concrete product manufacturers [15]. Of this, 6.4 Mt was for brick and block production, 3.5 Mt for precast and prestressed concrete production, 2.1 Mt for pipe and 4.2 Mt for other concrete products.

Current methods for off-site block production include steam curing or autoclave curing in which the concrete is exposed to pressurized steam in a sealed chamber. In this method, the heat from the steam induces faster hydration reactions and cement setting, but a high amount of energy is needed to produce and pressurize steam. For one cubic meter of concrete, the energy consumption related to steam curing and autoclave curing are 0.59 and 0.71 GJ, respectively [16].

Carbonation of cement or calcium silicates has been reported by several studies [13, 14, 17], the carbonation was achieved in closed chambers where CO<sub>2</sub> is delivered at high pressures (i.e. 0.5 MPa by Shao et al. [14]), with the intent of creating a high diffusive gradient for CO<sub>2</sub> to be transported to the interior of the fresh concrete sample. This carbonation approach has a major shortcoming: pressurizing CO<sub>2</sub> or CO<sub>2</sub>-rich flue gases, for either storage or transport off site, entails energy investments and related GHG emissions. The total energy for compression and liquefaction of pure CO<sub>2</sub> to 2 MPa and -31°C is estimated to be 0.33 GJ per tonne of CO<sub>2</sub> [11, 18]. Therefore, the electrical energy required for compression of 1 tonne of CO<sub>2</sub> would generate 56 kg of CO<sub>2</sub> emissions on the basis of power sources used in electrical power production in the US [19], and thus represents a 5.6% loss in CO<sub>2</sub> sequestration efficiency. Additional losses in

sequestration efficiency would result from CO<sub>2</sub> separation from flue gases. The energy required for CO<sub>2</sub> capture from power plant flue gases with low CO<sub>2</sub> content might reach up to 1.27 GJ per tonne of CO<sub>2</sub> processed [20], which represents an additional loss of 21.3% in CO<sub>2</sub> sequestration efficiency.

The focus of this research is to compare the rate and extent of CO<sub>2</sub> uptake in fresh concrete and the uniformity of carbonation in a flow-through, ambient pressure carbonation reactor with those reported for pressurized CO<sub>2</sub> chambers. Furthermore, the research identifies some important processes that control CO<sub>2</sub> uptake in flow-through reactors. In this article, compacted fresh concrete or grout was carbonated with a model, synthetic flue gas composed of 20% CO<sub>2</sub> in N<sub>2</sub> balance. The synthetic flue gas was passed through the sample under low inlet pressure (0.11 MPa) at ambient temperature in a 1-D flow-through reactor and the CO<sub>2</sub> uptake was monitored during carbonation.

Although the use of CO<sub>2</sub> in concrete curing was suggested several decades ago, those studied only considered the use of pure CO<sub>2</sub> and did not envision the use of flue gas or the CO<sub>2</sub> mitigation potential of this process. On-site CO<sub>2</sub> accelerated concrete curing with low-pressure flue gas reduces the energy required for gas compression and transport and the associated CO<sub>2</sub> emissions. The energy required for carbonation curing of 1 m<sup>3</sup> of concrete with flue gas compressed to 0.11 MPa is less than 0.013 GJ [11] and is negligible compared to energy required for steam and autoclave curing (0.59 and 0.71 GJ) or the energy required for carbonation curing in a pressure chamber. The energy required for compression of flue gas containing 76% N<sub>2</sub>, 14% CO<sub>2</sub> and 10% O<sub>2</sub> was calculated using the thermodynamic data of gases [18].

#### 3.2. Cement carbonation chemistry

Cement is mainly composed of calcium silicates, which undergo carbonation reactions in the presence of CO<sub>2</sub>. Carbonation of calcium silicates has been the subject of several studies since the 1970s [21-24]. During carbonation, the CO<sub>2</sub> gas permeates through the solid, dissolves in water and hydrates to form H<sub>2</sub>CO<sub>3</sub> which then ionizes to H<sup>+</sup>, HCO<sub>3</sub><sup>-</sup> and CO<sub>3</sub><sup>2-</sup> ions. The cement phases, mainly the tricalcium silicates (3CaO.SiO<sub>2</sub> or C<sub>3</sub>S) and dicalcium silicates (2CaO.SiO<sub>2</sub> or C<sub>2</sub>S), also dissolve and release Ca<sup>2+</sup> and SiO<sub>4</sub><sup>4-</sup> ions [25]. The carbonation products are calcium carbonate and silica gel and the reactions can be described by Eqs. 3.2 and 3.3 [23].

$$3\text{CaO.SiO}_2 + 3\text{CO}_2 + \mu\text{H}_2\text{O} \rightarrow \text{SiO}_2.\mu\text{H}_2\text{O} + 3\text{CaCO}_3$$
(3.2)

$$2\text{CaO.SiO}_2 + 2\text{CO}_2 + \mu\text{H}_2\text{O} \rightarrow \text{SiO}_2.\mu\text{H}_2\text{O} + 2\text{CaCO}_3$$
(3.3)

The formation of different polymorphs of calcium carbonate from carbonation of calcium silicates was also reported by Goto et al. [24]. In the first 3 minutes of carbonation of C<sub>3</sub>S and C<sub>2</sub>S, Young et al. [21] reported the formation of C-S-H like gel as well as calcite which subsequently carbonated to silica gel and calcium carbonate.

It should be noted that carbonation reactions in hydration-cured concrete or other calcium rich products such as slag, exhibit a significant difference in the chemistry of carbonation than the carbonation of freshly prepared concrete in that the former products have significant amounts of calcium hydroxide that react with CO<sub>2</sub> to form calcium carbonate. In freshly prepared concrete (subject to hydration

for less than 3 hours) there is negligible calcium hydroxide present, and  $C_3S$  and  $C_2S$  are the primary reactants for carbonation [26].

#### 3.3. Experimental section

#### 3.3.1. Materials and sample preparation

Fresh concrete samples were prepared with Type 10 Portland cement (St. Lawrence Cement), kiln dried sand and tap water. Coarse aggregates were not used in the mixture in order to maintain sample homogeneity. The elemental oxide composition of cement was analyzed by X-Ray Fluorescence (XRF) spectroscopy. The major oxide was CaO with 63.1 wt%, followed by SiO<sub>2</sub>, Al<sub>2</sub>O<sub>3</sub>, SO<sub>3</sub>, MgO and Fe<sub>2</sub>O<sub>3</sub> at 19.8, 5, 3.8, 2 and 1.7 wt%, respectively. The abundance of oxides determines the maximum theoretical CO<sub>2</sub> uptake based on the Steinour formula [27].

Each batch of fresh concrete contained a homogenous mixture of approximately 151g of cement, 607 g of fine aggregate (sand) and 39 mL of water (shown in Table 3.1) representing an aggregate to cement ratio (a/c) of 4 and water to cement ratio (w/c) of 0.26, which are within the range of dry-mix concrete mixes [11]. The water to cement ratio was selected to be high enough to provide enough moisture for carbonation reactions and low enough to leave enough pore space for CO<sub>2</sub> permeation. The fresh mixture was compacted in a steel mould using a compaction force of 100 kN, corresponding to an even pressure of 8 MPa. The compacted concrete samples had dimensions of 127 mm diameter and 25 mm height. One hour after casting, they were mounted in a PVC

shell, sealed using 5-minute epoxy and stored in a sealed 100% humidity chamber at room temperature to prevent water evaporation. The samples were maintained for 3 hours in order to gain sufficient initial strength for gas flow. These compact, partially water saturated, concrete samples in a PVC-shell constituted the 'column' which was subjected to carbonation in the flow-through reactor.

#### 3.3.2. Experimental set-up

Accelerated carbonation of samples was conducted in a 1-D flow-through reactor (Figure 3.1) with constant inlet gas pressure, flow-rate and CO<sub>2</sub> partial pressure. The reactor consisted of two stainless steel flanges on the top and bottom of the compacted sample. The inlet and outlet gas was passed through the center of the flanges. The reactor was operated while submerged in a water bath to maintain constant temperature and to check for the leaks. A constant mixture of 20% CO<sub>2</sub> in nitrogen balance was used for carbonation.

#### 3.3.3. Analytical instruments

Two infrared gas absorption instruments were used to monitor the rate and extent of CO<sub>2</sub> uptake. A Quantek model 906 NDIR gas sensor was used to monitor the concentration of CO<sub>2</sub> in the effluent gas of the reactor during the carbonation process. The extent of the carbonation was also measured by an infrared-based CO<sub>2</sub> analyzer (Eltra CS-800). The analyzer quantifies the CO<sub>2</sub> in carbonates by measuring the CO<sub>2</sub> released by an infra-red sensor after the decomposition of carbonates at 1000°C. The pore volumes of non-carbonated and carbonated samples were also measured using a Micrometrics 9320 Mercury

porosimeter, with a pressure range of sum-ambient to 207 MPa. Concentration of  $O_2$  was measured by a gas sensor, ATX620 (Industrial Scientific, Oakdale, PA, USA), equipped with an electrochemical sensor. The concentration of  $O_2$  was used to compute the concentration of  $O_2$  (assumed to be the balance concentration), to characterize the approximate advection and dispersion pattern of gases in the fresh concrete sample.

#### 3.4. Results and discussion

#### 3.4.1. $CO_2$ uptake efficiency

The concentration of the effluent gas ( $[CO_2]_o$ ) was measured and recorded every five seconds ( $\Delta t = 5s$ ). The absolute mass of sequestered  $CO_2$  ( $M_{CO_2}$ ) for each time interval was calculated using Eq. 3.4. The sum of all time intervals for any time period provided the cumulative  $CO_2$  mass gain ( $M_{CO_2-Tot}$ ).

The CO<sub>2</sub> uptake potential of cement is a function of the relative mass of oxides present in the raw material ( $X_{CaO, MgO, SO_3, Na_2O, K_2O}$ ) and is estimated by the Steinour formula [27] (Eq. 3.5). Based on the relative mass of oxides within cement, its CO<sub>2</sub> uptake capacity ( $X_{CO_2, Tot}$ ) was found to be 49.62 wt%, i.e. CO<sub>2</sub> can be reacted up to half of the cement's weight. The carbonation efficiency ( $\xi$ ) was a function of the recorded cumulative CO<sub>2</sub> mass gain ( $M_{CO_2, Tot}$ ), the CO<sub>2</sub> uptake potential ( $X_{CO_2, Tot}$ ) and the dry mass of cement in the sample ( $M_C$ ) (Eq. 3.6).

$$M_{CO_{2}}(t) = ([CO_{2}]_{i} \times Q_{i} - [CO_{2}]_{o}(t) \times Q_{o}(t)) \times \Delta t \times \rho_{CO_{2}}$$
(3.4)

$$\begin{split} X_{\text{CO}_2,\text{Tot}} &= 0.785(X_{\text{CaO}} - 0.560X_{\text{CaCO}_3} - 0.700X_{\text{SO}_3}) + 1.091X_{\text{MgO}} + 1.420X_{\text{Na}_2\text{O}} \\ &+ 0.935X_{\text{K}_2\text{O}} \end{split}$$

$$\xi = \frac{M_{\text{CO}_2,\text{Tot}}}{X_{\text{CO}_2,\text{Tot}} \times M_{\text{C}}}$$
(3.6)

where  $\rho_{CO_2}$  is the density of  $CO_2$ ,  $[CO_2]_i$  and  $[CO_2]_o(t)$  are the concentration of  $CO_2$  in the inlet and outlet gas and  $Q_i$  and  $Q_o(t)$  are the flow-rate of inlet and outlet gas. The gas flow-rate has different values in the inlet and outlet surfaces because  $CO_2$  is being reacted in the sample.

The efficiencies calculated using the inline NDIR  $CO_2$  measurements compared well with the efficiency computed with the combustion infrared analysis results. Under standard carbonating gas flow conditions (1.17 litre per minute (Lpm), 20%  $CO_2$ , w/c = 0.26, 40% RH, 20°C) the carbonation efficiency ( $\xi$ ) was 18.5  $\pm$  1.4% measured by combustion IR compared to 17.7  $\pm$  1.5% calculated based on the inline  $CO_2$  measurements.

Recently, Huntzinger et al. [9] also demonstrated the use of column systems for CO<sub>2</sub> uptake in a waste cement product, cement kiln dust (CKD). They reported that carbonation efficiency in packed columns of cement kiln dust (CKD) was in the range of 58.7-75.6% in different types of CKD with various material composition and particle dimensions. However, there are significant differences in the chemical composition and particle characteristics of CKD and the cement/sand mixtures employed in our study. Furthermore, there is significant loss of reactive surface area of cement particles bonded to sand particles and this may contribute to the difference in observed carbonation efficiencies.

Enhancements in calcium dissolution have been shown to yield higher carbonation efficiencies but carbonation was still incomplete. Iizuka et al [10] applied a high CO<sub>2</sub> pressure (several megapascals) in a completely mixed batch reactor in order to extract Ca<sup>2+</sup> from the cement waste and then subsequently carbonated the solution at 0.1 MPa pressure. The carbonation efficiency attained in their study was approximately 67% with an extraction CO<sub>2</sub> pressure of 3 MPa. These conditions are not relevant to the manufacturing of concrete products by accelerated curing. The saturated concentration of Ca<sup>2+</sup> will be 3 times lower using pure CO<sub>2</sub> at atmospheric pressure and 6 times lower at 0.02 MPa partial pressure used in this study.

#### 3.4.2. Dynamics of CO<sub>2</sub> uptake in 1-D flow-through reactor

Several carbonation experiments were conducted in the 1-D flow-through reactor and the uptake efficiency was measured both inline and using IR combustion methods as shown in Table 3.1. A typical CO<sub>2</sub> uptake plot under standard conditions is shown in Figure 3.2. To enhance the clarity, only one data point in every 20 measurements is shown in the Figure. The plot shows that almost all the CO<sub>2</sub> supplied during approximately the first 16 minutes is retained or consumed by the carbonation reaction. Thereafter, the CO<sub>2</sub> concentration at the outlet rapidly approached the inlet concentration. The phenomena contributing to this breakthrough curve are CO<sub>2</sub> advection and dispersion through the partially-water saturated, porous, compacted fresh concrete and the reaction of CO<sub>2</sub> with calcium silicates. In order to assess the relative contributions of advection and dispersion versus the CO<sub>2</sub> uptake by reaction in the breakthrough curve, an inert

gas, pure  $N_2$ , was passed through an identically prepared fresh concrete sample in a parallel experiment with the same flow-rate of 1.17 Lpm. The  $N_2$  concentration profile provides the approximate breakthrough with advection and dispersion only, and comparing it with the outlet  $CO_2$  concentration profile, it is apparent that the  $CO_2$  is being completely reacted in the compacted concrete sample during the first 16 minutes.

The amount of CO<sub>2</sub> uptake was calculated based on Eq. 3.4 and is shown as the cumulative CO<sub>2</sub> mass sequestered in Figure 3.2. Following the initial high uptake stage, the CO<sub>2</sub> uptake gradually declined, without reaching the complete theoretical uptake in a 1-hour period.

To verify the spatial and temporal distribution of CO<sub>2</sub> uptake in the compacted sample, the CO<sub>2</sub> uptake was measured in the mid-length section, inlet and outlet surfaces of the compacted concrete subjected to carbonation for various periods of time ranging from 5 minutes to 60 minutes. The concrete samples carbonated for certain durations were sacrificed and sliced to expose the mid-length section. Solid samples of 2 mL volume were then extruded in triplicate from over a 5 mm depth at the inlet, outlet and mid-length section surfaces. These samples were analyzed with the combustion infrared analyzer. The CO<sub>2</sub> uptake during carbonation was calculated based on the total measured CO<sub>2</sub> content and the initial CO<sub>2</sub> content of 0.7% in non-carbonated concrete sample. Knowing the amount of CO<sub>2</sub> uptake, the carbonation efficiency was then calculated using Eq. 3.6.

Figure 3.3 shows the carbonation efficiencies in the samples taken at 3 locations (center and edges of the cross-section) of the compact concrete column

carbonated for various times. The error bars represent the standard deviations. The carbonation efficiency at the inlet was 8% at 5 minutes and thereafter reached a relatively constant value of approximately 17%. In contrast, at the mid-length section and the outlet, it took longer to approach the 17% carbonation efficiency. This suggests that a higher degree of carbonation occurs at the inlet at the early period, and a carbonation 'front' advances over time towards the outlet. The carbonation at all 3 locations of each cross-section was very similar, suggesting the carbonation front was generally homogenous in the transverse plane to the flow. The time of 30 minutes, when uniform carbonation efficiency was reached in the sample, corresponds to the time point in Figure 3.2 where the CO<sub>2</sub> concentration in the outlet approaches the inlet concentration and plateaus off.

#### 3.4.3. Effect of intermittent carbonation on CO<sub>2</sub> uptake efficiency.

The measured uptake efficiency of approximately 17% suggests that there are significant mass transport limitations for dissolved CO<sub>2</sub> or Ca<sup>2+</sup> during the carbonation process. The reaction of Ca<sup>2+</sup> with CO<sub>3</sub><sup>2-</sup> is rapid [28], and is thus unlikely to be a rate limiting factor. The extent of mass transport limitations was investigated by stopping CO<sub>2</sub> injection over periods of time, during the carbonation process.

As shown in Figure 3.4, after an hour of carbonation, when the CO<sub>2</sub> concentration in the outlet gas approached 19% CO<sub>2</sub> (i.e. 95% of the inlet concentration), CO<sub>2</sub> gas flow was switched to the bypass. The inlet and outlet port valves were closed to allow trapping of the CO<sub>2</sub> gas in the concrete for varying lengths of time. This operation was repeated 3 times: (i) for 25 minutes at the 60

minute time point, (ii) for 325 minutes at 100 minutes and (iii) for 450 minutes at 440 minutes. When flow was resumed following the shut off, CO<sub>2</sub> concentrations decreased significantly. This suggests that the CO<sub>2</sub> contained in the concrete sample was partly consumed by further carbonation. The CO<sub>2</sub> concentration following the shut off period in all cases was non-zero suggesting that availability of CO<sub>2</sub> gas is not limiting carbonation. The CO<sub>2</sub> concentrations rebounded rapidly approaching 20%, the inlet concentration of CO<sub>2</sub>, after each shut off period. The CO<sub>2</sub> concentration profiles were used to estimate the additional CO<sub>2</sub> uptake following each shut-off period. The CO<sub>2</sub> mass uptake following each shut off period varied only slightly (0.55 to 1 g), even though the shut off duration varied significantly. It is likely that during the shut off period, the Ca<sup>2+</sup> diffused into the pore waters from the unreacted cement. The amount of Ca<sup>2+</sup> released would be dependent on the Ca2+ dissolution kinetics from the C3S and C2S solids and the equilibrium solubility of Ca<sup>2+</sup> in the system. After the available Ca<sup>2+</sup> is consumed rapidly by the CO<sub>2</sub> from the resumed flow, the CO<sub>2</sub> concentrations increase rapidly approaching the inlet concentrations. Samples were taken from the inlet and outlet of the concrete after the entire carbonation period, the CO<sub>2</sub> uptake was measured by combustion IR and the efficiency was measured as 23.9±0.7%.

The calcium carbonate formed as a result of carbonation, as shown in Eqs. 3.2 and 3, has been reported to form a solidified layer on the reactive Ca-rich cement particles [25]. This hinders the transport of Ca<sup>2+</sup> and CO<sub>2</sub> for reaction because these species have to diffuse through the solid layer before reaction. Formation of solid calcite was also reported by Huijgen et al. [6] during carbonation of steel slag. They found that precipitation of calcite on the particles follows the leaching

of calcium from the steel slag particles into the solution. Those authors demonstrated that the diffusion of calcium is hindered by the precipitation of solid products formed from its reaction in solution. The rate limiting process in steel slag carbonation was found to be either the diffusion of Ca<sup>2+</sup> to the solution or the deficiency of dissolved CO<sub>2</sub> depending on the temperature and CO<sub>2</sub> pressure. The trends observed during intermittent carbonation are in agreement with the findings of these authors. In summary, intermittent carbonation suggests that carbonation efficiency may be limited by diffusion kinetics and Ca<sup>2+</sup> availability in the pore waters.

The formation of CaCO<sub>3</sub> is likely to reduce pore volume (1 mole of C<sub>3</sub>S produces 3 moles of CaCO<sub>3</sub>, which causes a 30% increase in the molar volume of the solid phase) and CaCO<sub>3</sub> deposits also possibly contribute to pore blockages at narrow pore throats. This may also contribute to CO<sub>2</sub> and Ca<sup>2+</sup> mass transport limitations, which contribute to less than ideal carbonation efficiencies. A detailed study of pore structure changes during carbonation is currently underway.

## 3.4.4. Effect of carbonation on the porosity of compacted concrete samples

Formation of solid calcium carbonate in the concrete matrix decreased the available pore volume. The effect of accelerated carbonation on the porosity of compact concrete was studied using Mercury Intrusion Porosimetry (MIP). Several samples were cored from different locations of the compact concrete column, dried and then used for porosity measurement. In this method, mercury (a

non-wetting fluid) is intruded with increasing pressures into the porous media and the pore radius is calculated based on the Washburn equation [29]:

$$P = \frac{2\gamma \cos(\theta_m)}{r} \tag{3.7}$$

where P is the applied pressure of mercury. The surface tension and contact angle of mercury at room temperature were assumed as  $\gamma$ =485 dyn/cm and  $\theta_m$ =130°. The tests were performed with a pressure range of sub-ambient to 207 MPa (2.07x10<sup>9</sup> dyn/cm<sup>2</sup>). Therefore, the range of pore diameter detected was 0.006 -237 µm. The cumulative intrusion volume of mercury in an intrusion-extrusion cycle for non-carbonated and 1-hour carbonated samples is shown in Figure 3.5. The non-carbonated sample was hydrated over a 24-hour period to allow the fresh concrete to stabilize as a solid porous media. This short hydration period does not produce significant amounts of solid hydration products [26], and thus serves as a surrogate for a non-carbonated but hardened porous media. The data in Figure 3.5 shows that the non-carbonated sample has a higher pore volume, compared to the carbonated sample, particularly for pore sizes smaller than 10 microns. This reduction in pore volume is attributable to the expansion of the solid matrix with the formation of CaCO<sub>3</sub> and any pore blockages. The hysteresis observed in the mercury volume entrapped in the porous media during the intrusion and extrusion cycles is attributable to the presence of narrow and 'ink-bottle' pores [29]. The extrusion curve shows an initial increase in the cumulative intruded mercury volume after lowering of pressure from the maximum. This increase is due to the commonly observed artefact related to compression of the entire concrete matrix at high pressure, and is discussed elsewhere [29].

#### 3.4.5. $CO_2$ uptake with different gas flow-rates.

The effect of gas transport on CO<sub>2</sub> uptake was studied through a series of column experiments with constant water content but different gas flow-rates. Flow-rates of 0.08, 1.17 and 2.00 Lpm were selected corresponding to residence times of 0.30-0.01 minutes while maintaining the constant CO<sub>2</sub> concentration of 20% and water to cement ratio of 0.26. The CO<sub>2</sub> concentration profiles at different flow-rates are shown in Figure 3.6. At a flow-rate of 0.08 Lpm, CO<sub>2</sub> uptake proceeded for up to 300 minutes, in part because of the relatively low amount of CO<sub>2</sub> supplied.

The  $CO_2$  efficiency measured by combustion IR  $CO_2$  analyzer were  $21.2 \pm 0.2$ ,  $18.5 \pm 1.4$  and  $10.7 \pm 0.1$  for concrete samples subjected to flow-rates of 0.08, 1.17 and 2.00 Lpm, respectively. The dramatically higher amount of  $CO_2$  uptake is due to the higher residence time of  $CO_2$  in the column, which allows a greater fraction to be reacted. As shown in Figure 3.7, for the first 13.0 g of  $CO_2$  introduced in the fresh concrete column, approximately 13.0 g of  $CO_2$  is taken up at a flow-rate of 0.08 Lpm versus only 6.5 g of  $CO_2$  at a flow-rate of 2 Lpm. In fact, the first 13.0 g of  $CO_2$  uptake at a flow-rate of 0.08 Lpm follows the maximum uptake line. However, it is important to note that the carbonation efficiency was not 100% in the column, because uptake slowed down dramatically after the first 13 g of  $CO_2$  uptake.

#### 3.5. Conclusion

The average carbonation efficiencies of approximately 18% obtained in our flow-through reactors with 20% CO<sub>2</sub>, compare very well with the carbonation efficiency of 17-28% measured by Shao et al. [14] in Type 10 Portland cement-containing concrete in CO<sub>2</sub> pressure chambers operated at 0.5 MPa pressure and supplied with 100% CO<sub>2</sub>. This suggests that flow-through reactors may be efficient for accelerated CO<sub>2</sub> curing of concrete, especially given that compression of gases is energy intensive as is the purification of CO<sub>2</sub> from waste flue gases [30].

The CO<sub>2</sub> residence time in the concrete column appears to have a dramatic effect on uptake efficiency, and operation conditions which allow for longer carbonation duration appear to provide more CO<sub>2</sub> uptake. The durability and the mechanical properties of finished carbonated concrete should be taken into consideration for identifying overall process conditions. Porosity of concrete decreased during carbonation because of the formation of solid calcium carbonate. Additional studies on the chemical and microstructure changes during carbonation may better explain the factors that control CO<sub>2</sub> uptake and that knowledge may lead to possible improvements in uptake efficiency.

Accelerated CO<sub>2</sub> curing of concrete may be considered as one of several CO<sub>2</sub> mitigation measures in the cement and concrete industries. Based on the average 18% carbonation efficiency in our 1-D flow-through reactor, and the annual 16.4 Mt of cement used in concrete products in the United States in 2004, the amount of CO<sub>2</sub> which can be sequestered in this process will be 1.5 Mt compared to the

that the theoretical maximum CO<sub>2</sub> uptake can only match the CO<sub>2</sub> that is generated during calcination of limestone. Given the measured CO<sub>2</sub> uptake efficiency of approximately 18%, and the significant emissions from fuel combustion in the cement and concrete industry, other CCS technologies and/or the use of alternative fuels will be required to manage carbon emissions in the industry.

#### 3.6. Acknowledgments

The study supported by the National Science and Engineering Research Council of Canada, St. Lawrence Cement and CJS Technology. Graduate student fellowship funding by Le Fonds québécois de la recherche sur la nature et les technologies to SKH, access to MIP facilities provided by Prof. M. Nokken at Concordia University, and assistance by R. Niven in the construction of the carbonation reactor are gratefully acknowledged.

#### 3.7. References

- 1. Holloway, S., Underground sequestration of carbon dioxide--a viable greenhouse gas mitigation option. *Energy* **2005**, *30*, (11-12), 2318.
- 2. Pacala, S.; Socolow, R., Stabilization wedges: solving the climate problem for the next 50 years with current technologies (Review). *Science* **2004**, *305*, (5686), 968.
- 3. IPCC, *Special report on carbon dioxide capture and storage*. Cambridge University Press: 2005.
- 4. Seifritz, W., CO<sub>2</sub> disposal by means of silicates. *Nature* **1990,** *345*, 486.

- 5. Lackner, K. S.; Wendt, C. H.; Butt, D. P.; Joyce, E. L.; Sharp, D. H., Carbon Dioxide Disposal in Carbonate Minerals. *Energy* **1995**, *20*, 1153.
- 6. Huijgen, W. J. J.; Witkamp, G. J.; Comans, R. N. J., Mineral CO<sub>2</sub> sequestration by steel slag carbonation. *Environ. Sci. Technol.* **2005**, *39*, (24), 9676-9682.
- 7. Maroto-Valer, M. M.; Fauth, D. J.; Kuchta, M. E.; Zhang, Y.; Andresen, J. M., Activation of magnesium rich minerals as carbonation feedstock materials for CO<sub>2</sub> sequestration. *Fuel Process. Technol.* **2005**, *86*, (14-15), 1627.
- 8. Montes-Hernandez, G.; Perez-Lopez, R.; Renard, F.; Nieto, J. M.; Charlet, L., Mineral Sequestration of CO<sub>2</sub> by Aqueous Carbonation of Coal Combustion Fly-Ash. *J. Hazard. Mater.* **2009**, *161*, (2-3), 1347.
- 9. Huntzinger, D. N.; Gierke, J. S.; Kawatra, S. K.; Eisele, T. C.; Sutter, L. L., Carbon dioxide sequestration in cement kiln dust through mineral carbonation. *Environ. Sci. Technol.* **2009**, *43*, (6), 1986-1992.
- 10. Iizuka, A.; Fujii, M.; Yamasaki, A.; Yanagisawa, Y., Development of a New CO<sub>2</sub> Sequestration Process Utilizing the Carbonation of Waste Cement. *Ind. Eng. Chem. Res.* **2004**, *43*, 7880.
- 11. Monkman, S. Maximizing carbon uptake and performance gain in slag-containing concretes through early carbonation. McGill University, Montreal, QC, Canada, 2008.
- 12. Monkman, S.; Shao, Y., Assessing the carbonation behavior of cementitious materials. *J. Mater. Civ. Eng.* **2006**, *18*, (6), 768.
- 13. Shi, C.; Wu, Y., Studies on some factors affecting CO<sub>2</sub> curing of lightweight concrete products. *Resour. Conserv. Recy.* **2008**, *52*, (8-9), 1087-1092.
- 14. Shao, Y.; Mirza, M. S.; Wu, X., CO<sub>2</sub> sequestration using calcium-silicate concrete. *Can. J. Civ. Eng.* **2006**, *33*, (6), 776-784.
- 15. Van Oss, H. G. Cement; 2004.
- 16. Kawai, K.; Sugiyama, T.; Kobayashi, K.; Sano, S., Inventory Data and Case Studies for Environmental Performance Evaluation of Concrete Structure Construction. *J. Adv. Concr. Technol.* **2005,** *3*, (3), 435-456.
- 17. Reardon, E. J.; James, B. R.; Abouchar, J., High pressure carbonation of cementitious grout. *Cem. Concr. Res.* **1989**, *19*, (3), 385.
- 18. NIST NIST Chemistry WebBook Thermophysical Properties of Fluid Systems [online]. <a href="http://webbook.nist.gov/chemistry/fluid/">http://webbook.nist.gov/chemistry/fluid/</a> (02/08/09),
- 19. EIA *Emissions of greenhouse gases in the United States 2006*; Energy Information Administration, U.S. Department of Energy: Washington, DC., 2007.
- 20. David, J.; Herzog, H. In *The Cost of Carbon Capture*, Workshop on Carbon Sequestration Science, May 22-24, 2001; NETL: 2001.
- 21. Young, J. F.; Berger, R. L.; Breese, J., Accelerated curing of compacted calcium silicate mortars on exposure to CO<sub>2</sub>. *J. Am. Ceram. Soc.* **1974,** *57*, (9), 394-397.
- 22. Bukowski, J. M.; Berger, R. L., Reactivity and Strength Development of CO<sub>2</sub> Activated Non-hydraulic Calcium Silicates. *Cem. Concr. Res.* **1979**, *9*, (1), 57-68.

- 23. Goodbrake, C. J.; Young, J. F.; Berger, R. L., Reaction of hydraulic calcium silicates with carbon dioxide and water. *J. Am. Ceram. Soc.* **1979**, *62*, (9-10), 488-491.
- 24. Seishi Goto, K. S. T. K. M. F., Calcium Silicate Carbonation Products. *Journal of the American Ceramic Society* **1995**, *78*, (11), 2867-2872.
- 25. Fernandez Bertos, M.; Simons, S. J. R.; Hills, C. D.; Carey, P. J., A review of accelerated carbonation technology in the treatment of cement-based materials and sequestration of CO<sub>2</sub>. *J. Hazard. Mater.* **2004**, *112*, (3), 193.
- 26. Chen, Y.; Odler, I., On the Kinetics of Portland Cement Hydration in the Presence of Selected Chemical Admixtures. *Adv. Cement Res.* **1993**, *5*, (17), 9-13.
- 27. Steinour, H. H., Some effects of carbon dioxide on mortars and concrete-discussion. *J. Am. Concr. Inst.* **1959**, *30*, 905-907.
- 28. Papadakis, V. G.; Vayenas, C. G.; Fardis, M. N., A reaction engineering approach to the problem of concrete carbonation. *AlChE J.* **1989**, *35*, (10), 1639-1650.
- 29. Moro, F.; Böhni, H., Ink-bottle effect in mercury intrusion porosimetry of cement-based materials. *Journal of Colloid and Interface Science* **2002**, *249*, (1), 262.
- 30. White, C. M.; Strazisar, B. R.; Granite, E. J.; Hoffman, J. S.; Pennline, H. W., Separation and Capture of CO<sub>2</sub> from Large Stationary Sources and Sequestration in Geological Formations- Coalbeds and Deep Saline Aquifers (Critical Review). *J. Air & Waste Manage. Assoc.* **2003**, *53*, 645-715.

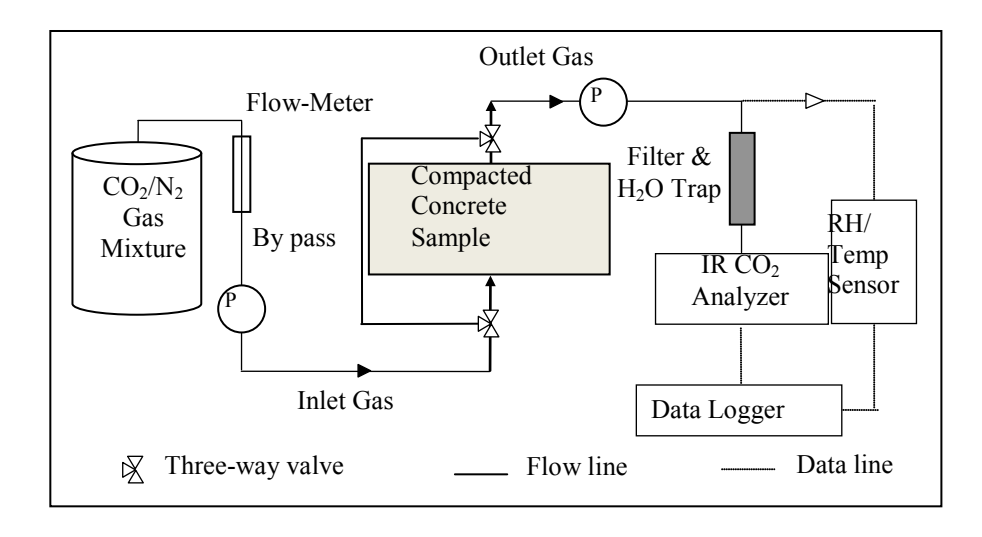
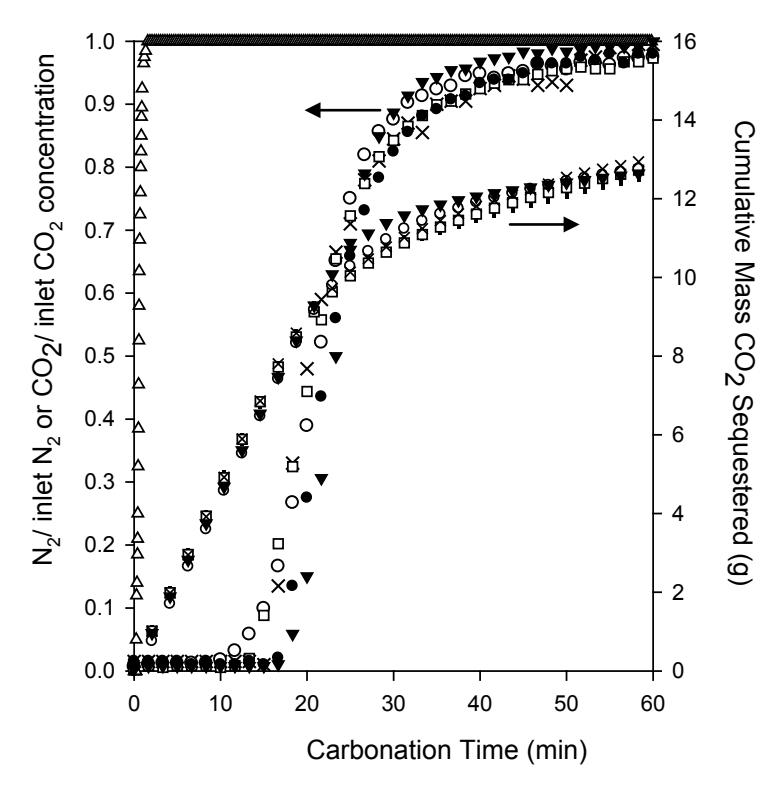
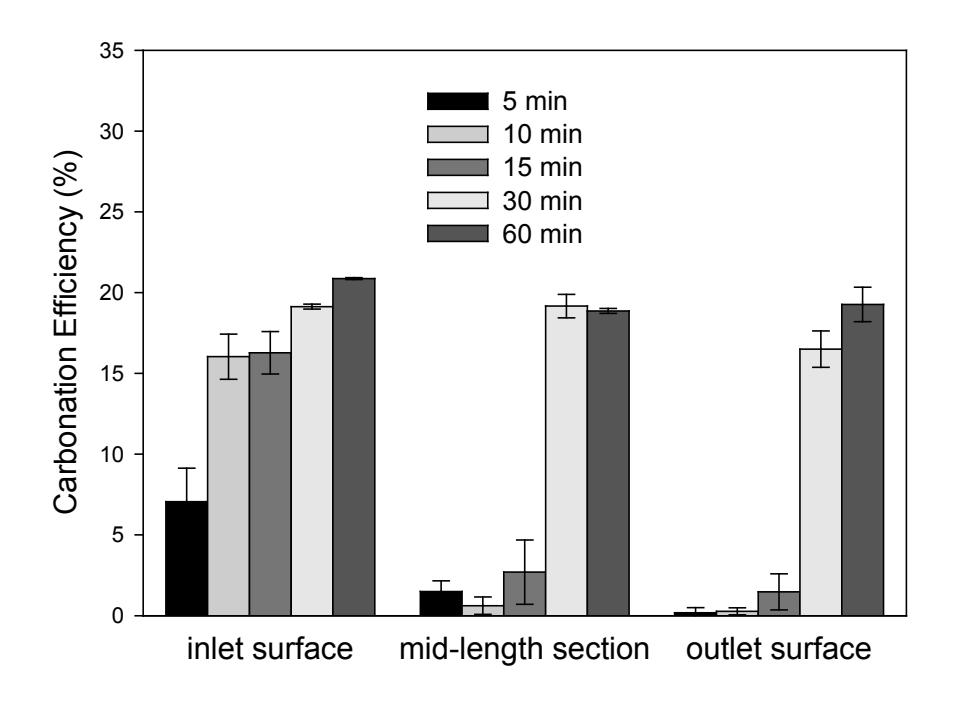


FIGURE 3.1. Carbonation apparatus set-up



**FIGURE 3.2.** Dynamics of carbonation reaction in compacted concrete samples using 1.17 Lpm gas flow-rate: measured  $N_2$  gas (%) in the outlet for a pure  $N_2$  injection (Δ), measured  $CO_2$  gas (%) in outlet, and calculated cumulative  $CO_2$  mass sequestered for 80%  $N_2$  and 20%  $CO_2$  mixture injection: ( $\bullet$ [#117\_1],  $\Box$ [#117\_2], ×[#117\_4],  $\odot$ [#117\_5],  $\blacktriangledown$ [#117\_6]). Numbers in brackets after each symbol refer to experiment runs explained in Table 3.1.



**FIGURE 3.3.** Spatial and temporal distribution of carbonation efficiency during carbonation in 1-D flow-through reactor.

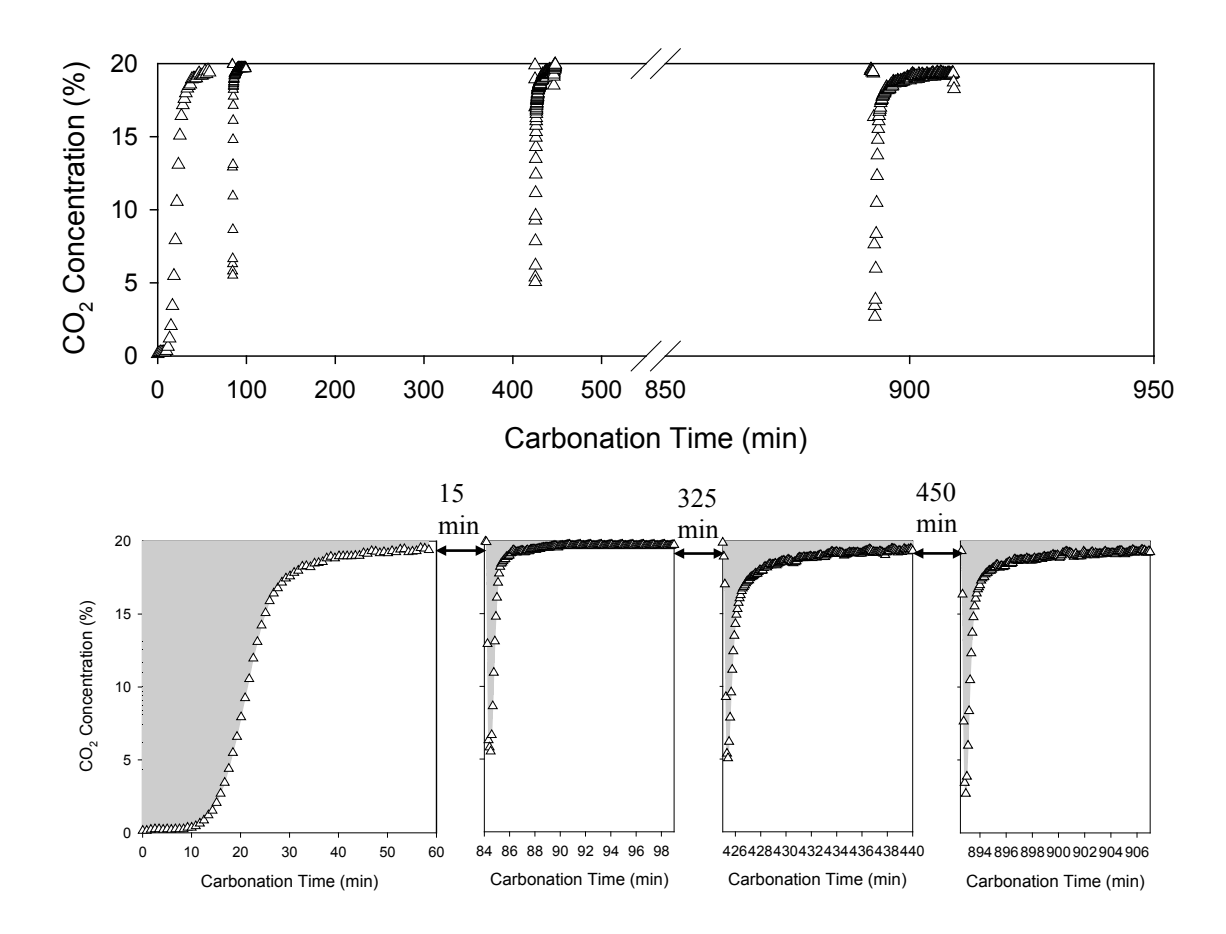


**FIGURE 3.4.** Measured outlet  $CO_2$  concentration profile in the 1-D flow-through reactor during intermittent carbonation ( $\Delta$ ), shut off times were 15 min, 325 min and 450 min. Shaded areas above the curve are proportional to the mass of  $CO_2$  sequestered.

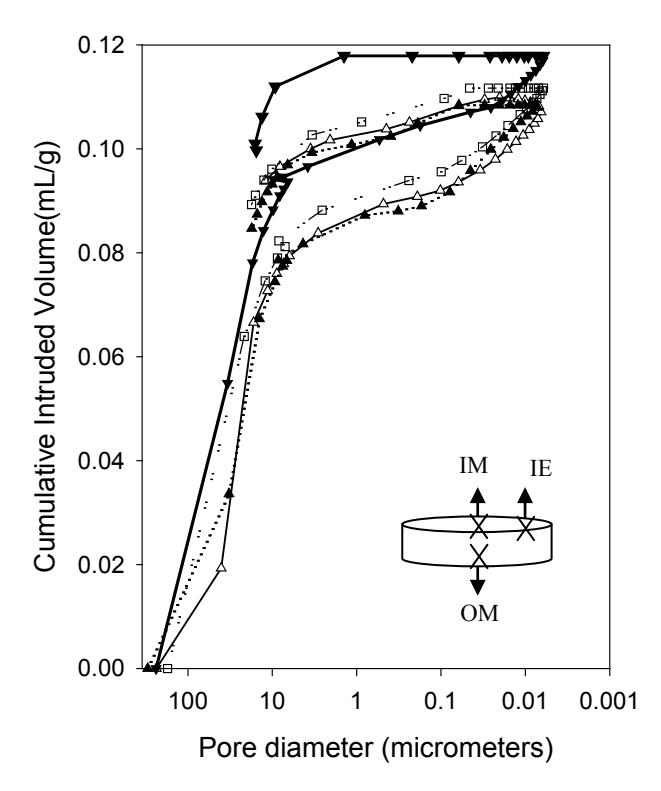


**FIGURE 3.5.** Cumulative intrusion volume for an intrusion-extrusion cycle in non-carbonated sample ( $\nabla$ ), 1-hour carbonated sample, for inlet middle (IM) ( $\Delta$ ), 1-hour carbonated sample, for inlet edge (IE) ( $\square$ ), and 1-hour carbonated sample, for outlet middle (OM) ( $\triangle$ )

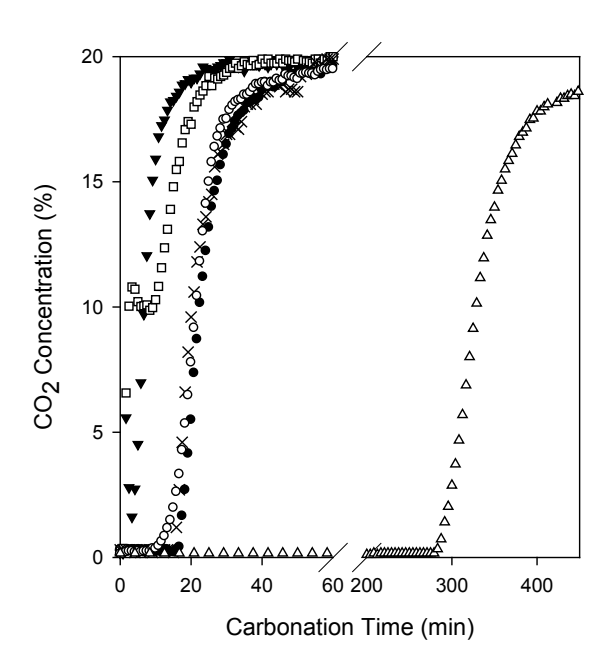


**FIGURE 3.6.** Measured outlet  $CO_2$  gas (%) using different gas flow-rates: 0.08 Lpm ( $-[\#8\_1]$ ,  $\Delta[\#8\_2]$ ), 1.17 Lpm ( $\bullet[\#117\_1]$ ,×[ $\#117\_4$ ], $\circ[\#117\_5]$ ) and 2 Lpm ( $\blacktriangledown[\#200\_1]$ , $\Box[\#200\_2]$ ). Numbers in brackets after each symbol refer to experiment runs explained in Table 3.1.

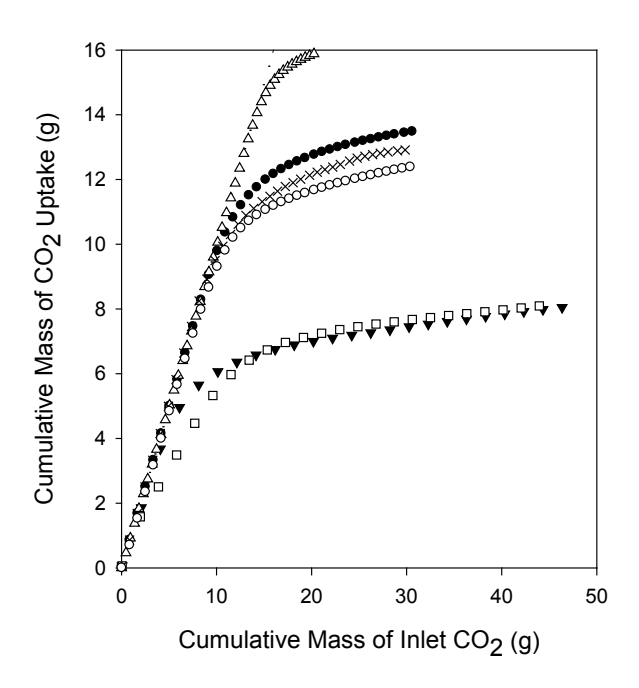


**FIGURE 3.7.** Measured cumulative mass of  $CO_2$  uptake versus cumulative mass of inlet  $CO_2$  at different flow-rates: 0.08 Lpm ( $-[\#8\_1]$ ,  $\Delta[\#8\_2]$ ), 1.17 Lpm ( $\bullet[\#117\_1]$ ,  $\times[\#117\_4]$ ,  $\circ$  [ $\#117\_5$ ]) and 2 Lpm ( $\blacktriangledown[\#200\_1]$ ,  $\square[\#200\_2]$ ). Numbers in brackets after each symbol refer to experiment runs explained in Table 3.1.

**TABLE 3.1.** List of experiments and the carbonation efficiencies (water to cement ratio = 0.26; aggregate to cement ratio = 4)

Run#	Cement mass (g)	Mass of CO <sub>2</sub> Sequestered (g)	Efficiency (inline measurement)	Efficiency (IR combustion)	Gas flow-rate (Lpm)
117_1	151.6	13.5	17.8%	20.0%±0.7	
117_2	151.7	15.4	20.3%	17.1%±4.1	1.17
117_3	151.2	14.0	18.5%	20.2%±1.6	
117_4	151.6	12.9	17.0%	17.4%±1.0	
117_5	151.5	12.4	16.4%		
117_6	150.0	12.5	16.7%	17.7%±0.3	
200_1	151.5	8.1	10.7%	12.3%±4.8	2.00
200_2	151.9	8.1	10.7%	11.6%±3.5	2.00
8_1	151.5	15.9	21.0%	21.5%±4.9	0.00
8_2	151.5	16.1	21.3%	20.8%±3.7	0.08

In Chapter 3, the CO<sub>2</sub> uptake rate and extent during accelerated carbonation curing of concrete was studied in a 1-D flow-through reactor. The CO<sub>2</sub> uptake efficiency achieved was approximately 17% of the maximum theoretical value calculated from Steinour formula based on the composition of cement. The physico-chemical processes limiting the carbonation efficiency were assessed by further study on carbonation of cement in an aqueous suspension in a completely mixed flow-through reactor and also using imaging techniques. The results are presented in Chapter 4.

### **Chapter 4**

# PHYSICO-CHEMICAL PROCESSES LIMITING CO<sub>2</sub> UPTAKE IN CONCRETE DURING ACCELERATED CARBONATION CURING

Sormeh Kashef-Haghighi, Subhasis Ghoshal

Department of Civil Engineering, McGill University, Montreal, QC, Canada

To be submitted in

Industrial & Engineering Chemistry Research, April 2012

### 4.1. Introduction

Carbon dioxide capture and storage (CCS) technologies are being developed for stabilization of atmospheric CO<sub>2</sub> concentrations. Potential CO<sub>2</sub> storage methods include storage of CO<sub>2</sub> in geological formations such as oil and gas fields, unminable coal beds, deep saline formations [1, 2], on the deep seafloor [3-5], or on land as inorganic carbonates through chemical reactions with abundant metal oxide minerals such as olivine or wollastonite [6-9] or industrial waste products such as cement kiln dust (CKD) [10]. With the exception of injection of CO<sub>2</sub> in oil fields for enhaced oil recovery or into coal beds for enhanced methane extraction [11, 12], the above CO<sub>2</sub> storage procedures do not lead to value-added products.

Accelerated concrete curing using CO<sub>2</sub> is an alternative process to the conventional hydration curing of cement, and has the potential for creation of value-added commercial concrete products such as masonry units, while providing mineral sequesteration of CO<sub>2</sub>. Compared to conventional accelerated curing methods using water vapour and steam, accelerated carbonation is based on CO<sub>2</sub> reactions with cement minerals and results in rapid hardening of concrete and a stronger and more durable concrete when used without steel reinforcement [13-15].

Cement has potential for mineral sequesteration of CO<sub>2</sub> because it is rich in calcium, mainly tricalcium silicate (3CaO.SiO<sub>2</sub> or C<sub>3</sub>S) and dicalcium silicate (2CaO.SiO<sub>2</sub> or C<sub>2</sub>S), which can react with CO<sub>2</sub> under ambient conditions to form thermodynamically stable calcium carbonate. Carbonation of pure calcium silicate

mortars (C<sub>3</sub>S and C<sub>2</sub>S) with CO<sub>2</sub> gas and water vapour results in exothermic carbonation reactions leading to the formation of calcium carbonate (CaCO<sub>3</sub>(s)) and silica gel (SiO<sub>2</sub>(s)) [16, 17]. Accelerated carbonation of calcium silicates is a sequential mechanism [18]. The overall carbonation reactions of C<sub>3</sub>S and C<sub>2</sub>S, the dominant cement phases, are as Eqs. 4.1-4.2. A schematic of carbonation of cement phases is presented in Figure 4.1.

$$3\text{CaO.SiO}_2(s) + 3\text{CO}_2(aq) \rightarrow \text{SiO}_2(s) + 3\text{CaCO}_3(s)$$
(4.1)

$$2\text{CaO.SiO}_2(s) + 2\text{CO}_2(aq) \rightarrow \text{SiO}_2(s) + 2\text{CaCO}_3(s)$$
(4.2)

Cement can store CO<sub>2</sub> up to 50% of its weight based on reactions with the oxides present in its composition according to the Steinour formula [13, 19, 20], assuming all the metal oxides in cement are available for carbonation reaction. The CO<sub>2</sub> uptake in concrete during accelared carbonation curing has been reported in recent studies [13, 21]. The average carbonation efficiency of 17.7%±1.5 obtained in the flow-through reactor with 20% CO<sub>2</sub> in our previous study [21] was comparable with the carbonation efficiency of 17-28% measured by Shao et al. [13] in CO<sub>2</sub> pressure chambers supplied with pure CO<sub>2</sub>. None of the carbonation reactors was able to produce a CO<sub>2</sub> uptake efficiency comparable with the theoretical maximum.

Possible reasons for limited CO<sub>2</sub> uptake could be that the dissolution of these metal oxides might be hindered, for instance, by the formation of a CaCO<sub>3</sub>(s) product layer which may prevent complete carbonation and thus lower CO<sub>2</sub> uptake than predicted [22]. The formation of CaCO<sub>3</sub>(s) has been confirmed in previous studies [13, 23]. However, its spatial distribution in the concrete matrix

determines whether precipitation of CaCO<sub>3</sub>(s) causes diminished exposed surface area of cement or leads to concrete pore clogging and thus limited transport of CO<sub>2</sub>. There are no systematic studies identifying the exact causes for limited CO<sub>2</sub> uptake in concrete. In this study, we compared the carbonation efficiency in compacted concrete and an aqueous suspension of cement. In addition, we investigated the spatial distribution of precipitated CaCO<sub>3</sub>(s) in the compacted concrete matrix and its relationship to the pore structure which provided insight on the role of pore blockage in limiting CO<sub>2</sub> uptake by concrete. The distribution of solid products in the microstructure of compacted concrete after carbonation was examined by a scanning electron microprobe imaging technique. The CO<sub>2</sub> uptake efficiency was evaluated by carbonating an aqueous suspension of cement in a completely mixed flow-through reactor. Because interparticle pores were no longer present in the aqueous suspension, the possible CO<sub>2</sub> uptake in the absence of pore blockage was indirectly assessed from these experiments.

### 4.2. Materials and methods

#### 4.2.1. Materials

The concrete specimen and aqueous suspension of cement were prepared with Type 10 Portland cement (St. Lawrence Cement), kiln dried sand (Bomix) and tap water as used in standard concrete manufacturing [24]. The composition of the water is reported in Table 4S.1. The starting material, cement, was characterized for its elemental composition using X-Ray Fluorescence (XRF) spectroscopy to determine the relative abundance of cement phases. Particle size distribution of

cement was measured using the LAS-W laser diffraction technique by suspending cement in isopropyl alcohol. The gas mixture was 20% high purity CO<sub>2</sub> in nitrogen balance (Praxair Inc) to simulate as-captured flue gas from the cement industry. A 40% CO<sub>2</sub> gas mixture (Praxair Inc) was also used to study the effect of CO<sub>2</sub> partial pressure on carbonation efficiency.

### 4.2.2. Compact concrete experiment

Compact concrete specimens were prepared with a mixture of either 0.32 or 0.26 water/cement and 4 aggregate/cement weight/weight ratios. Each sample contained 151 g of cement, 607 g of fine aggregate and 39 or 48 mL of water. The fresh mixture was compacted in a steel mold (125×40 mm dia.×height) by 8 MPa pressure (corresponding to a compaction force of 100 kN) in order to gain a concrete density of 2103 kg/m<sup>3</sup> acceptable for precast concrete products [25]. An hour after casting, the samples were mounted in a PVC shell (125×35 mm internal dia.×height) and sealed using 5-minute epoxy (McMaster-Carr). Prior to carbonation, the mounted samples were stored in a sealed 100% humidity chamber at room temperature for hydration for 3 hours, in order to gain an initial strength for handling in the carbonation curing reactor. The compaction and subsequent hydration produces a compact, solid, concrete matrix from the paste like mixture of cement, water and sand. More details on sample preparation can be found elsewhere [21]. The compacted concrete in the PVC shell was carbonated in a 1-D flow-through, stainless steel reactor at constant temperature, inlet gas pressure, gas flow-rate, CO<sub>2</sub> partial pressure and relative humidity. The gas flow-rate was 1.17 sLpm. The effluent CO<sub>2</sub> concentration was monitored

inline during carbonation using a Quantek model 906 NDIR gas sensor. The CO<sub>2</sub> uptake was calculated based on the inline measurement of effluent CO<sub>2</sub> concentration and the known influent concentration [21]. The carbonation efficiency was also calculated based on measurements of the total carbon content of carbonated solids carried out with an Eltra CS-800 carbon combustion infrared analyzer.

### 4.2.3. Aqueous suspension of cement

Cement suspension samples were prepared with 3.8 g of Type 10 Portland cement and water/cement ratio of 30. The aqueous cement suspension was carbonated in a three-port completely mixed flow-through (CMFT) reactor with the same gas mixture as used for the compacted concrete. The reactor was made of glass with an approximate volume of 250 mL. The gas flow-rate was 0.5 sLpm. The reactor was kept on a shaker operating at 300 rpm during carbonation in order to maintain a homogeneous suspension. The effluent CO<sub>2</sub> concentrations were measured online as described above.

The overall experimental set up (Figure 4.2) was designed to accommodate either reactor, depending on whether the experiment involved carbonating a compacted concrete or an aqueous suspension of cement and includes the analytical instrumentation, control systems and gas supply.

### 4.2.4. Analytical methods

The concentrations of total Ca and Si in the carbonated and non-carbonated aqueous cement suspension were measured using a Perkin Elmer AAnalyst 100

atomic absorption spectrometer. The samples were prepared from filtering 10 mL of the solution through a 0.45 micron filter. Total dissolved inorganic carbon (DIC) was also measured by a carbon analyzer (Folio DC-80 Instruments Inc.). A Mettler DL25 autotitrator was used to measure the alkalinity in the sample with two solutions of HCl and NaOH both at 0.01 N concentrations. Alkalinity was measured to the endpoint pH of 4.3. Raw cement particles, hydrated cement and carbonated cement solids were characterized by X-ray Diffraction (XRD). The XRD facility used in this study was a Rigaku D/MAX 2400 (12 kW) with a rotating anode diffractometer. In all situations, the solution was dried in the oven and the powder was compacted in the specific mold.

### 4.2.5. Microstructure imaging and analysis

The microprobe analysis instrument was JXA JEOL-8900L, operated with an accelerating voltage of 15 kV and the current of 20 nA for high resolution digital X-ray mapping with both electron dispersive spectroscopy (EDS) and wavelength dispersive spectroscopy (WDS). Solid core samples with dimensions of 27 mm diameter and approximately 7 mm depth were taken from compacted concrete specimens subjected to carbonation as described above or to hydration only. In order to image the non-carbonated (hydrated) concrete matrix, the compact concrete was hydrated for 24 hours to gain an initial strength sufficient for coring. For both samples, pores were filled with an epoxy resin and the surface was sawed and polished using the same procedure as Stutzman [26]. The surface was coated with chrome to provide a conductive surface for electron microscopy. The imaging technique applied in this study was similar to Stutzman [26] and

Scrivener [27] who applied scanning electron microscopy (SEM) with X-ray microanalysis for studying the composition of cement and clinker. The backscattered electron images as well as the X-ray images for Ca, C, Mg, Na, K, Si, Fe and Al were collected at the same location. Knowledge of the different elements at the same location allowed determination of the mineral phase at each pixel. The analysis was based on segmentation [26]. In this method, threshold values of X-ray intensity for each element were assigned based on the frequency of intensity levels [28]. The solid cement phases were identified based on the elements at each pixel which have intensities higher than the threshold value. For instance, calcium carbonate was defined as the pixels containing both calcium and carbon with intensities more than the threshold values. The digitized images were post-processed to reduce noise and to clearly define the boundaries of different solid cement phases. Image analysis was done by MATLAB in order to define the materials in each pixel and to reduce the noise. Calibration was performed on standard materials such as wollastonite and calcite as listed in Table 4S.2 in the SI section.

### 4.2.6. Chemical equilibrium model

A chemical equilibrium model for the aqueous cement suspension in contact with CO<sub>2</sub> gas mixture was developed using PHREEQC, an ion association model [29]. This model can be used with the Pitzer ion interaction model for the calculation of ion activity coefficients for solutions with high solute concentrations and high activity coefficients. The Pitzer model was previously used by Reardon and Dewaele [30] for simulation of reactions in a cement/water

system. The equilibrium constants for reactions at 25°C were obtained from Reardon [31] and Bullard et al. [32] and the ion interaction data were obtained from Reardon [33].

### 4.3. CO<sub>2</sub> uptake and carbonation efficiency

The mass of sequestered  $CO_2$  in carbonation experiments was calculated based on its concentration in the effluent gas which was measured and recorded every five seconds and the inlet and outlet gas flow-rates. The carbonation efficiency ( $\xi$ ) is defined as the ratio of  $CO_2$  stored within the sample to the Steinour-derived theoretical mass uptake [21]. The carbonation efficiency was corrected for the pre-existing  $CO_2$  content of 0.7 wt% contained within the unreacted concrete as carbonate minerals.

The potential theoretical  $CO_2$  uptake is a function of the elemental composition of the raw material and was estimated to be 49.62 wt% by the Steinour formula (Eq. 4.3) [19]:

$$\begin{split} X_{\text{CO}_2,\text{Tot}} &= 0.785 (X_{\text{CaO}} - 0.560 X_{\text{CaCO}_3} - 0.700 X_{\text{SO}_3}) + 1.091 X_{\text{MgO}} + 1.420 X_{\text{Na}_2\text{O}} \\ &+ 0.935 X_{\text{K}_2\text{O}} \end{split} \tag{4.3}$$

where  $X_{CO_2,Tot}$  is the  $CO_2$  uptake potential (wt%) and is a function of the relative mass of oxides present in raw material ( $X_i$ ) listed in Table 4.1.

### 4.4. Results and discussion

### 4.4.1. Characterization of cement before carbonation

The grout material constituents were characterized using X-ray fluorescence (XRF) shown in Table 4.1. The amount of cement phases such as C<sub>3</sub>S and C<sub>2</sub>S was estimated using modified Bogue calculation [34].

During 4-hours of hydration, cement undergoes hydration recations and forms solid products. The products formed during the first 4 hours are calcium silicate hydrate gel (3CaO.2SiO<sub>2</sub>.3H<sub>2</sub>O(s)), calcium hydroxide (Ca(OH)<sub>2</sub>(s)) and ettringite (3CaO.Al<sub>2</sub>O<sub>3</sub>.3CaSO<sub>4</sub>.32H<sub>2</sub>O(s)) as a result of the following reactions [35].

$$2(3CaO.SiO_2(s)) + 6H_2O(1) \rightarrow 3CaO.2SiO_2.3H_2O(s) + 3Ca(OH)_2(s)$$
 (4.4)

$$2(2\text{CaO.SiO}_2(s)) + 4\text{H}_2\text{O}(l) \rightarrow 3\text{CaO.2SiO}_2.3\text{H}_2\text{O}(s) + \text{Ca(OH)}_2(s)$$
 (4.5)

$$(3\text{CaO.Al}_2\text{O}_3 (s)) + 3(\text{CaSO}_4.2\text{H}_2\text{O}(s)) + 26\text{H}_2\text{O}(l) \rightarrow 3\text{CaO.Al}_2\text{O}_3.3\text{CaSO}_4.32\text{H}_2\text{O}(s)$$
 (4.6)

C<sub>3</sub>S and C<sub>2</sub>S remained the most abundant cement phases, after the 4-hour hydration period, as confirmed by the X-ray diffraction (XRD) analysis of the raw and 4-hour hydrated cement (Figure 4S.1). The amount of hydration products produced in the 4-hour hydrated sample is approximately only 3% of cement weight [35].

### 4.4.2. The extent of CO<sub>2</sub> uptake in compact concrete

The carbonation of compacted concrete was performed in a 1-D flow-through reactor. The CO<sub>2</sub> uptake efficiency achieved within an hour of carbonation was

 $17.7\% \pm 1.5$  using 20% CO<sub>2</sub> and flow-rate of 1.17 Lpm [21]. Using the same inlet gas pressure but a higher CO<sub>2</sub> percentage of 40% in the mixture, the maximum CO<sub>2</sub> uptake did not improve and the 1-hour carbonation efficiency remained at  $17.8\% \pm 1.3$  (Figure 4.3-A). Changing the water/cement ratio from 0.26 to 0.32, i.e., water saturation from 0.43 to 0.53 (volume/volume), decreased the 1-hour uptake efficiency of carbonation to  $14.5 \pm 1\%$  which is likely because higher water content fills up some of the pores and inhibits the CO<sub>2</sub> gas from flowing through the pores. The typical time profile of CO<sub>2</sub> uptake, Figure 4.3-B, shows fast uptake of CO<sub>2</sub> by concrete in the first 10 minutes where almost all CO<sub>2</sub> was consumed by concrete. Following the rapid CO<sub>2</sub> uptake, the CO<sub>2</sub> concentration in the outlet approached the inlet concentration and the CO<sub>2</sub> uptake decreased.

### 4.4.3. Changes in the concrete matrix during carbonation and hydration

Formation of solid products in the pores during carbonation (mainly CaCO<sub>3</sub>(s)) decreased the porosity of compact concrete during accelerated CO<sub>2</sub> curing [21]. To determine the spatial distribution of the solid carbonation products in the porous concrete matrix, core samples were taken from non-carbonated and carbonated concrete specimens used in CO<sub>2</sub> flow-though experiments (with w/c=0.26 and flow-rate=1.17 Lpm). Scanning electron microscopy and X-ray imaging analysis of representative small areas of the non-carbonated and carbonated concrete in order to determine how the CaCO<sub>3</sub>(s) formed during carbonation altered the pore spaces and solid matrix. In Figure 4.4, the backscattered electron (BSE) images for the noncarbonated samples are shown in

two different locations (A1 and A2). Overall, the image shows the cement between two silica aggregates and a large pore or air void (in A1).  $CO_2$  advection would occur through the pores and connected voids and dissolved  $CO_2$  would react with the dissolved Ca in the pore waters. The distribution of  $CaCO_3(s)$  after image processing of X-ray maps is shown in B1 and B2. The pores are shown in black, aggregate in grey,  $CaCO_3(s)$  in green, and other solid phases ( $C_3S$ ,  $C_2S$ , etc) in white. The pore space map from the BSE image was overlapped with the solid cement phase map. The narrow pores in non-carbonated concrete, Figures 4.4-B1 and B2, had pore diameters smaller than 4  $\mu$ m. The purpose of this image reconstruction was to clearly show the presence of a network of narrow pores in the cement matrix, as well as the presence of some background  $CaCO_3(s)$  which is the unreacted limestone in cement clinker.

The BSE images for carbonated concrete are shown in Figures 4.5-A3 and A4. The reconstructed images for carbonated concrete and  $CaCO_3(s)$  distribution are shown in Figures 4.5-B3 and B4. These figures show that  $CaCO_3(s)$  deposited as veins, presumably from filling of the abundant narrow pores that were visible in Figure 4.4, as well as in the form of larger irregular deposits particularly close to the large pores. Deposition of  $CaCO_3(s)$  was also observed as a layer along the walls of the large pores or voids (>10  $\mu$ m). Some of these larger deposits may also be unreacted limestone in the cement clinker.

In contrast to the non-carbonated samples shown in Figure 4.4, the carbonated samples shown in Figure 4.5 have virtually no narrow pores that are visible at the image resolution, clearly indicating that the pores of 4  $\mu$ m and smaller become

clogged with CaCO<sub>3</sub>(s) during the 1-hr carbonation period. The decrease in pore volume due to CaCO<sub>3</sub>(s) deposition is easily observed from the images. For a quantitative analysis, porosity was calculated based on the number of pixels containing pores and the total number of pixels in each image. The porosity in non-carbonated concrete images was calculated as  $0.30 \pm 0.03$  (number of images=7) decreasing to  $0.18 \pm 0.04$  (number of images=8) after carbonation which correlates with the reduction in porosity determined by mercury intrusion porosimetry (MIP) reported in our previous study [21]. Mercury intrusion porosimetry analyses showed that pores smaller than 4  $\mu$ m of diameter accounted for 27% of the total pore volume [21].

Some crystals were selected in the BSE images for mineral analysis. The weight percentage of different oxides was measured and the mineral was defined as listed in Table 4S.3 in the SI section. These minerals were used to verify the results from image analysis of X-ray maps.

In Figure 4.5, the panels C3 and C4 show the X-ray maps of calcium combined with the calcium carbonate maps derived from image analysis of carbonated concrete samples. The colors in the map from blue to pink indicate increasing concentration of Ca. The reconstructed map of  $CaCO_3(s)$  is overlapped on the Ca map. The  $CaCO_3(s)$  in Figures 4.5-C3 and C4 are shown in white. These images confirmed the existence of calcium in solid phases (other than  $CaCO_3(s)$ ) even though the  $CO_2$  uptake ceased in concrete. The calcium-containing minerals, in most cases are surrounded by the formed  $CaCO_3(s)$  in narrow pores. These unreactive Ca minerals can only be carbonated if  $Ca^{2+}$  and

carbonate ions diffuse into the water in the remaining pore space, and the deposits of CaCO<sub>3</sub>(s) would inhibit mass transport of these ions.

### 4.4.4. CO<sub>2</sub> uptake by aqueous cement suspension

The effect of inter-particle pore structure was eliminated by carbonation of cement in aqueous suspension form in order to study the other factors that limit the CO<sub>2</sub> uptake by cement. The dynamics of carbon uptake is depicted in Figure 4.6-A. The CO<sub>2</sub> concentration in the outlet gas increased rapidly during the first 20 minutes and CO<sub>2</sub> uptake ceased around 68% efficiency. The error bars represent the standard deviation of CO<sub>2</sub> measurements in three sets of experiments with identical conditions.

The maximum theoretical CO<sub>2</sub> uptake potential was not achieved in any carbonation study to date. The maximum carbonation efficiency reported to date is for CKD, and is approximately 80%. The carbonation was conducted in flow-through columns and batch reactors with 80% CO<sub>2</sub> [10]. The carbonation efficiencies in various calcium-rich products and minerals such as steel slag, wetted powders of C<sub>3</sub>S and C<sub>2</sub>S and Ca(OH)<sub>2</sub> have also been reported in the range of 40%-80% [6, 16, 34, 36]. The ultimate carbonation efficiency achieved in CaO with CO<sub>2</sub> gas (direct gas-solid carbonation) in a fluidized bed reactor was 70-80% [22]. The diffusion of ions through the pores in the deposited product layer becomes more rate controlling towards the final stage of carbonation, after which the rate of carbonation becomes too slow to be detected. An average thickness of 50 nm for the CaCO<sub>3</sub> layer was determined by Alvarez and Abanades [22] as the start of the slow reaction period.

## 4.4.5. Changes in chemistry of aqueous cement suspension and relationship to $CO_2$ uptake

We tested the hypotheses that if all reactive surfaces are covered with CaCO<sub>3</sub>(s) deposits, the aqueous concentration of various ions will be equal to that predicted from the chemical equilibrium of a system containing calcium as CaCO<sub>3</sub>(s) only. To study the aqueous chemistry during carbonation, the amount of different elements as well as the pH of the aqueous cement suspension was monitored during carbonation (Figure 4.6-B). The concentration of calcium and pH in the 4-hour hydrated aqueous cement suspension were measured as 28.5±0.3 mmol/L and  $13.2 \pm 0.1$ , respectively. The CO<sub>2</sub> uptake by cement ceased within 30 minutes and the concentrations of calcium, dissolved carbon and pH in the aqueous cement suspension reached steady-state values. The steady-state values for pH, carbon, calcium and silica were 6.84, 26.4 mmol/L, 9.5 mmol/L and 2.9 mmol/L, respectively. The alkalinity of cement solution decreased from an initial value of 64.96 meg/L to 21.57 meg/L after 30 minutes of carbonation. A chemical equilibrium model was developed using PHREEQC. The system modeled for chemical equilibrium composition was a pure aqueous phase in contact with excess calcite and silica, the two carbonation products given by Eqs. 4.1 and 4.2, in the presence of CO<sub>2</sub> gas with partial pressure of 0.21 atm. The model results show that at equilibrium, the solution pH is 6.5 and the concentration of carbon, calcium and silica are 24.2 mmol/L, 5.4 mmol/L, and 2.0 mmol/L, respectively. Thus there was a good agreement between the predicted and measured equilibrium concentrations. The equilibrium model showed that in the presence of reactive phases, such as C<sub>3</sub>S or Ca(OH)<sub>2</sub>(s), the equilibrium pH is 8.4 and 11.6,

respectively, and much higher than the measured value of 6.8. Therefore, in the absence of exposed C<sub>3</sub>S and Ca(OH)<sub>2</sub>(s), the aqueous cement suspension reached a chemical equilibrium with the CaCO<sub>3</sub>(s) product layer and CO<sub>2</sub> uptake ceased before a theoretical maximum uptake could be achieved.

The changes in concentrations of dissolved Ca<sup>2+</sup>, H<sup>+</sup> and carbonate species during the 90-minute carbonation period, shown in Figure 4.6-B, can be explained on the basis of the various carbonation reactions. Earlier studies on C<sub>3</sub>S hydration showed that dissolution starts immediately upon addition of water to cement [37]. The pH of a C<sub>3</sub>S solution rises very rapidly because of the formation of OH<sup>-</sup> from dissolusion of C<sub>3</sub>S (Eq. 4.7). The solution pH increases to approximately 12.5 and the concentration of calcium ions increases to 10-20 mmol/L in the fist 30 seconds. Dicalcium silicate (C<sub>2</sub>S), the second most abundant phase in OPC, also dissolves in water but more slowly compared to C<sub>3</sub>S. The Ca(OH)<sub>2</sub>(s) formed during the hydration period, also dissolves to calcium and hydroxide ions.

$$C_3S + 3H_2O \rightarrow 3Ca^{2+} + H_2SiO_4^{-2} + 4OH^{-}$$
 (4.7)

When carbonation starts, each mole of CO<sub>2</sub> gas dissolves in the aqueous cement suspension and forms one mole of CO<sub>3</sub><sup>2-</sup> and two moles of H<sup>+</sup> (Eq. 4.8) which decreases the pH. The pH is initially buffered because of the presence of alkalies (calcium silicates and a small amount of Ca(OH)<sub>2</sub>(s)) and thus decreases gradually during Stage 1. Formation of a carbonate and bicarbonate system is another source of buffering as they consume H<sup>+</sup> ions. The rate of decrease in solution pH was minimum as pH reached 9.8 which indicates the solution is at maximum buffering capacity which is very close to the carbonic acid dissociation

constant (pK<sub>2</sub>=10.3) where the buffering capacity of a carbonate system is at a maximum. The concentration of calcium decreased rapidly in the aqueous cement suspension (Figure 4.6-B) because of reaction with carbonate and formation of solid calcium carbonate (Eq. 4.9).

$$CO_2(g) + H_2O \rightarrow H_2CO_3 \rightarrow 2H^+ + CO_3^{2-}$$
 (4.8)

$$Ca^{2+} + CO_3^{2-} \rightarrow CaCO_3(s)$$

$$(4.9)$$

During carbonation, the concentration of dissolved calcium and pH both decreased as CO<sub>2</sub> dissolved in the aqueous solution but the rate of decrease were not similar. The carbonation process happened in three distinct stages in terms of carbon uptake. In the first stage, rapid uptake of CO<sub>2</sub> was observed. CO<sub>2</sub> dissolved in water and dropped the pH from an initial value of 13 to 9.8. Calcium ion concentration decreased from 28.5 mmol/L to 2.8 mmol/L due to carbonation to CaCO<sub>3</sub>(s) during this phase and the carbonation efficiency in this period was approximately 47%. In this stage, the pH dropped from an initial value of 13 to 9.8 and in this pH range, which is mostly higher than the second dissociation constant of carbonic acid (pK<sub>2</sub>=10.3), dissolved CO<sub>2</sub> is converted more abundantly to the carbonate form than bicarbonate and, therefore, CaCO<sub>3</sub>(s) is formed rapidly.

Following the rapid uptake of  $CO_2$  in Stage 1 during which the outlet  $CO_2$  concentration remained unchanged, there was further  $CO_2$  uptake but at a slower rate and a corresponding increase in the outlet  $CO_2$  concentration. This slow  $CO_2$  uptake phase is referred to as Stage 2. In this stage, the suspension pH dropped from 9.8 to 7.1. In this pH range (pK<sub>1</sub>=6.4<pH<pK<sub>2</sub>=10.3), carbonate

concentration would decrease as bicarbonate, HCO<sub>3</sub>, would start to dominate and thus the rate of formation of CaCO<sub>3</sub>(s) (Eq. 4.9) decreased as shown in Figure 4.6-A.

In Stage 3, pH dropped further to 6.8 and reached a plateau. At this pH (close to pK<sub>1</sub>), dissolved carbon is primarily present as bicarbonate and undissociated carbonic acid (H<sub>2</sub>CO<sub>3</sub>). Carbon uptake stopped and CO<sub>2</sub> concentration measured in the outlet gas reached the inlet value. The total dissolved carbon and calcium increased to 26.4 mmol/L and 9.5 mmol/L, respectively. In Stage 3, some decalcification of the CaCO<sub>3</sub>(s) and formation of water soluble calcium bicarbonate, Ca(HCO<sub>3</sub>)<sub>2</sub>, is likely to occur at the pH levels reached [38]. Dissolved calcium increased from 2.9 (mmol/L) to 7.5 (mmol/L) and dissolved carbon concentration started to increase from 1.3 (mmol/L) to 13.6 (mmol/L).

The presence of calcite in the carbonated cement suspension as the main carbonation product was confirmed by XRD analysis on 1-hour carbonated cement in the CMFT reactor. The diffraction peaks of calcite  $(2\theta(\text{CuK}\alpha)=29.4^{\circ}\text{ and }39.4^{\circ})$  in the carbonated cement as well as raw cement are shown in Figure 4.7. The formation of calcite as the main crystalline product of carbonation was also confirmed by Goto et al. [39] from carbonation of calcium silicate  $(C_3S)$  with 5%  $CO_2$  in  $N_2$  balance at room temperature. No aragonite peaks were detected in the XRD results, i.e. calcite was the only form of calcium carbonate detected. Aragonite forms when the specimen is dried during carbonation [16]. Therefore, in the presence of liquid water, calcite forms as the main product and aragonite forms only after the specimen dries.

### 4.5. Conclusions

The CO<sub>2</sub> uptake by compact concrete was rapid and the carbonation efficiency of 16-20% was achieved within an hour of carbonation with a gas flow-rate of 1.17 Lpm and CO<sub>2</sub> partial pressure of 0.021 or 0.042 MPa related to 20% or 40% CO<sub>2</sub> in gas mixture, respectively. A critical phenomenon inhibiting CO<sub>2</sub> uptake is CaCO<sub>3</sub>(s) filling of narrow pores and deposition of a CaCO<sub>3</sub>(s) product layer. In compacted concrete, pore blockage leads to mass transfer limitations of CO<sub>2</sub> gas to reactive cement materials. The lack of availability of reactive surfaces in cement exposed to dissolved CO<sub>2</sub> both due to pore blockages and formation of product layers imposes limitations on the total CO<sub>2</sub> uptake by concrete.

The carbonation efficiency increased when the mass transfer limitation imposed by pore bockages was removed by carbonating cement in aqueous suspension form. The CO<sub>2</sub> uptake by cement in aqueous suspension was approximately 68% of the theoretical uptake calculated from Steinour formula. The concentration of calcium and dissolved carbon decreased rapidly in the solution because of the carbonation reaction and formation of CaCO<sub>3</sub>(s). The CO<sub>2</sub> uptake, however, ceased in approximately 20 minutes and the aqueous phase concentrations of calcium, dissolved carbon and pH reached equilibrium concentrations for an aqueous system saturated with CaCO<sub>3</sub>(s) and SiO<sub>2</sub>(s), indicating that all cement surfaces were saturated with these products.

### 4.6. Acknowledgements

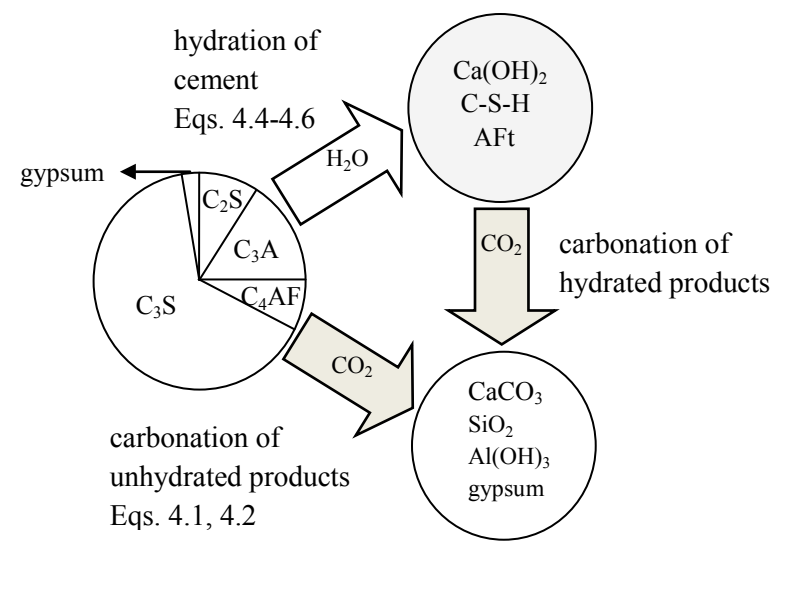
The authors would like to acknowledge the Natural Sciences and Engineering Research Council of Canada (NSERC), St. Lawrence Cement, CJS Technology for providing funding for this project, the Global Environmental and Climate Change Centre (GEC3) and le fonds québécois de la recherche sur la nature et les technologies (FQRNT) for providing scholarships to SKH, and Robert Niven for his assistance in conducting the XRF analysis.

### 4.7. References

- [1] White, C.M., B.R. Strazisar, E.J. Granite, J.S. Hoffman, and H.W. Pennline, Separation and Capture of CO<sub>2</sub> from Large Stationary Sources and Sequestration in Geological Formations- Coalbeds and Deep Saline Aquifers (Critical Review). *J. Air & Waste Manage. Assoc.*, **2003**, 53, 645-715.
- [2] Wilson, E.J., M.G. Morgan, J. Apt, M. Bonner, C. Bunting, J. Gode, R.S. Haszeldine, C.C. Jaeger, D.W. Keith, S.T. McCoy, M.F. Pollak, D.M. Reiner, E.S. Rubin, A. Torvanger, C. Ulardic, S.P. Vajjhala, D.G. Victor, and I.W. Wright, Regulating the Geological Sequestration of CO<sub>2</sub>. *Environ. Sci. Technol.*, **2008**, 42 (8), 2718-2722.
- [3] Hoffert, M.I., K. Caldeira, G. Benford, D.R. Criswell, C. Green, H. Herzog, A.K. Jain, H.S. Kheshgi, K.S. Lackner, J.S. Lewis, H.D. Lightfoot, W. Manheimer, J.C. Mankins, M.E. Mauel, L.J. Perkins, M.E. Schlesinger, T. Volk, and T.M.L. Wigley, Advanced Technology Paths to Global Climate Stability: Energy for a Greenhouse Planet. *Science*, 2002, 298 (5595), 981-987.
- [4] Tsouris, C., P. Brewer, E. Peltzer, P. Walz, D. Riestenberg, L. Liang, and O.R. West, Hydrate Composite Particles for Ocean Carbon Sequestration: Field Verification. *Environ. Sci. Technol.*, **2004**, 38 (8), 2470-2475.
- [5] IPCC, Special report on carbon dioxide capture and storage. **2005**: Cambridge University Press.
- [6] Huijgen, W.J.J., G.J. Witkamp, and R.N.J. Comans, Mineral CO<sub>2</sub> sequestration by steel slag carbonation. *Environ. Sci. Technol.*, **2005**, 39 (24), 9676-9682.

- [7] Lackner, K.S., C.H. Wendt, D.P. Butt, E.L. Joyce, and D.H. Sharp, Carbon Dioxide Disposal in Carbonate Minerals. *Energy*, **1995**, 20, 1153.
- [8] Jarvis, K., R.W. Carpenter, T. Windman, Y. Kim, R. Nunez, and F. Alawneh, Reaction Mechanisms for Enhancing Mineral Sequestration of CO<sub>2</sub>. *Environ. Sci. Technol.*, **2009**, 43 (16), 6314-6319.
- [9] Huijgen, W.J.J., G.-J. Witkamp, and R.N.J. Comans, Mechanisms of aqueous wollastonite carbonation as a possible CO<sub>2</sub> sequestration process. *Chem. Eng. Sci.*, **2006**, 61 (13), 4242-4251.
- [10] Huntzinger, D.N., J.S. Gierke, S.K. Kawatra, T.C. Eisele, and L.L. Sutter, Carbon dioxide sequestration in cement kiln dust through mineral carbonation. *Environ. Sci. Technol.*, **2009**, 43 (6), 1986-1992.
- [11] van Bergen, F., H. Pagnier, and P. Krzystolik, Field experiment of enhanced coalbed methane-CO<sub>2</sub> in the upper Silesian basin in Poland. *Environ. Geosci.*, **2006**, 13 (3), 201-224.
- [12] Gentzis, T., Subsurface sequestration of carbon dioxide--an overview from an Alberta (Canada) perspective. *Int. J. Coal Geol.*, **2000**, 43 (1-4), 287-305.
- [13] Shao, Y., M.S. Mirza, and X. Wu, CO<sub>2</sub> sequestration using calcium-silicate concrete. *Can. J. Civ. Eng.*, **2006**, 33 (6), 776-784.
- [14] Shi, C. and Y. Wu, Studies on some factors affecting CO<sub>2</sub> curing of lightweight concrete products. *Resour. Conserv. Recy.*, **2008**, 52 (8-9), 1087-1092.
- [15] Watanabe, K., K. Yokozeki, R. Ashizawa, N. Sakata, M. Morioka, E. Sakai, and M. Daimon, High durability cementitious material with mineral admixtures and carbonation curing. *Waste Management*, **2006**, 26 (7), 752.
- [16] Goodbrake, C.J., J.F. Young, and R.L. Berger, Reaction of hydraulic calcium silicates with carbon dioxide and water. *J. Am. Ceram. Soc.*, **1979**, 62 (9-10), 488-491.
- [17] Young, J.F., R.L. Berger, and J. Breese, Accelerated curing of compacted calcium silicate mortars on exposure to CO<sub>2</sub>. *J. Am. Ceram. Soc.*, **1974**, 57 (9), 394-397.
- [18] Fernandez Bertos, M., S.J.R. Simons, C.D. Hills, and P.J. Carey, A review of accelerated carbonation technology in the treatment of cement-based materials and sequestration of CO<sub>2</sub>. *J. Hazard. Mater.*, **2004**, 112 (3), 193.
- [19] Steinour, H.H., Some effects of carbon dioxide on mortars and concrete-discussion. *J. Am. Concr. Inst.*, **1959**, 30, 905-907.
- [20] Shi, C., F. He, and Y. Wu, Effect of pre-conditioning on CO2 curing of lightweight concrete blocks mixtures., In Press, Corrected Proof. *Constr. Build. Mater.*, **2012**, 26 (1), 257-267.
- [21] Kashef-Haghighi, S. and S. Ghoshal., CO<sub>2</sub> sequestration in concrete through accelerated carbonation curing in a flow-through reactor. *Ind. Eng. Chem. Res.*, **2010**, 49, 1143-1149.
- [22] Alvarez, D. and J.C. Abanades, Determination of the critical product layer thickness in the reaction of CaO with CO<sub>2</sub>. *Ind. Eng. Chem. Res.*, **2005**, 44, 5608-5615.
- [23] Monkman, S. and Y. Shao, Assessing the carbonation behavior of cementitious materials. *J. Mater. Civ. Eng.*, **2006**, 18 (6), 768.

- [24] Lamond;, J. and J. Pielert, Significance of tests and properties of concrete and concrete-making materials. **2006**: ASTM International. 645.
- [25] Warszawski, A., Industrialized and automated building systems. 2nd ed. 1999: Taylor & Francis.
- [26] Stutzman, P., Scanning electron microscopy imaging of hydraulic cement microstructure. *Cem. Concr. Compos.*, **2004**, 26 (8), 957.
- [27] Scrivener, K.L., Backscattered electron imaging of cementitious microstructures: understanding and quantification. *Cem. Concr. Compos.*, **2004**, 26 (8), 935.
- [28] Bentz, D.P. and P.E. Stutzman. SEM/X-Ray imaging of cement-based materials. in 7th euroseminar on microscopy applied to building materials. 1999.
- [29] Parkhurst, D.L. and C.A.J. Appelo, User's guide to PHREEQC (Version 2)— A computer program for speciation, batch-reaction, one-dimensional transport, and inverse geochemical calculations. Water-Resources Investigations Report 99-4259. **1999**, Denver, Colorado: U.S. Department of the Interior, U.S. Geological Survey, 310
- [30] Reardon, E.J. and P. Dewaele, Chemical model for the carbonation of a grout/water slurry. *J. Am. Ceram. Soc.*, **1990**, 73 (6), 1681-1690.
- [31] Reardon, E.J., Problems and approaches to the prediction of the chemical composition in cement/water systems. *Waste Manage.*, **1992**, 12, 221-239.
- [32] Bullard, J.W., E. Enjolras, W.L. George, S.G. Satterfield, and J.E. Terrill, A parallel reaction-transport model applied to cement hydration and microstructure development. *Model. Simul. Mater. Sci. Eng.*, **2010**, 18, 711–738.
- [33] Reardon, E.J., An ion interaction model for the determination of chemical equilibria in cement/water systems. *Cem. Concr. Res.*, **1990**, 20 (2), 175-192.
- [34] Taylor, H.F., Cement Chemistry 2ed. 1997: Telford.
- [35] Lea, F.M., The Chemistry of Cement and Concrete. **1970**, London: Edward Arnold.
- [36] Shih, S.M., C.S. Ho, Y.S. Song, and J.P. Lin, Kinetics of the reaction of Ca(OH)<sub>2</sub> with CO<sub>2</sub> at low temperature. *Ind. Eng. Chem. Res.*, **1999**, 38 (4), 1316-1322.
- [37] Bullard, J.W., A determination of hydration mechanisms for tricalcium silicate using a kinetic cellular automaton model. *J. Am. Ceram. Soc.*, **2008**, 91 (7), 2088-2097.
- [38] Kutchko, B.G., B.R. Strazisar, D.A. Dzombak, G.V. Lowry, and N. Thaulow, Degradation of well cement by CO<sub>2</sub> under geologic sequestration conditions. *Environ. Sci. Technol.*, **2007**, 41 (13), 4787-4792.
- [39] Goto, S., K. Suenaga, and T. Kado, Calcium silicate carbonation products. J. Am. Ceram. Soc., 1995, 78 (11), 2867-72.



C<sub>3</sub>S: 3CaO.SiO<sub>2</sub>(s)
C<sub>2</sub>S: 2CaO.SiO<sub>2</sub>(s)
C<sub>3</sub>A: 3CaO.Al<sub>2</sub>O<sub>3</sub>(s)
C<sub>4</sub>AF: 4CaO.Al<sub>2</sub>O<sub>3</sub>.Fe<sub>2</sub>O<sub>3</sub>(s)
gypsum: CaSO<sub>4</sub>.2H<sub>2</sub>O (s)
C-S-H: 3CaO.2SiO<sub>2</sub>.3H<sub>2</sub>O (s)
AFt: 3CaO.Al<sub>2</sub>O<sub>3</sub>.3CaSO<sub>4</sub>.32H<sub>2</sub>O (s)

**FIGURE 4.1.** Schematic showing reaction products formed during accelerated CO<sub>2</sub> curing from various reactive cement phases.

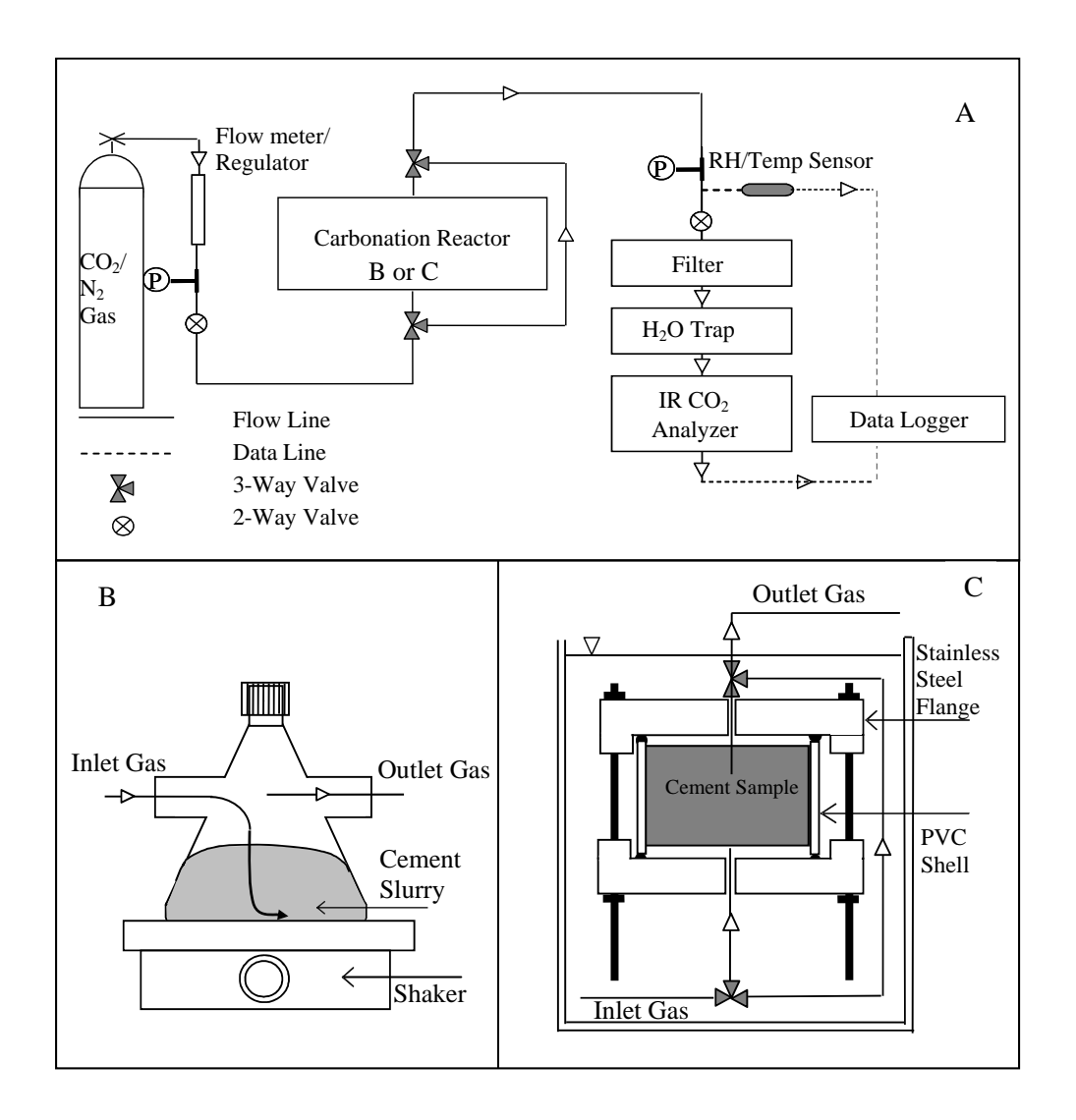


**FIGURE 4.2.** (A) Carbonation experiment set up which includes either of the following carbonation reactors (B) completely mixed flow-through (CMFT) carbonation reactor (C) 1-dimensional flow-through reactor

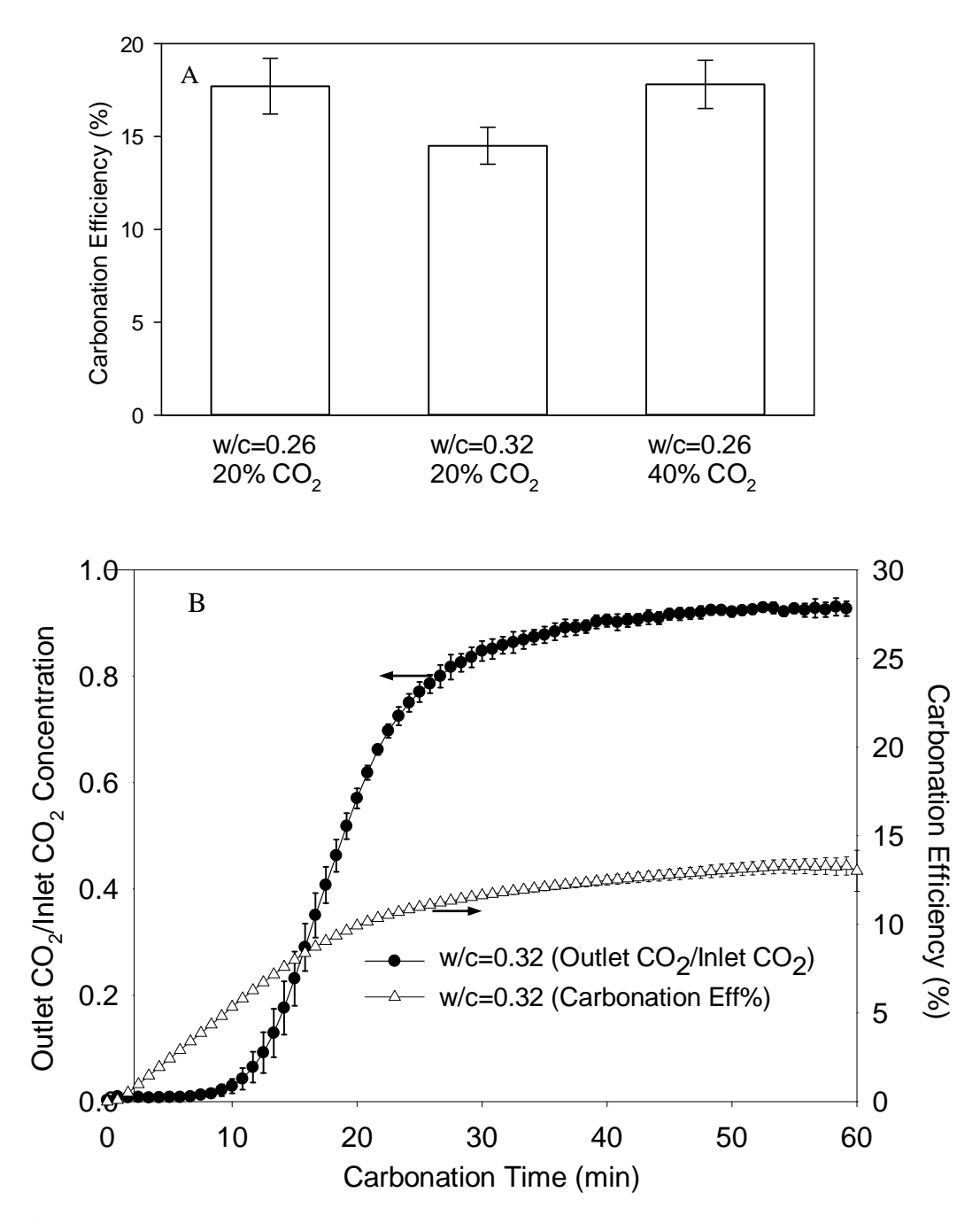


**FIGURE 4.3.** (A) Carbonation efficiency in compacted concrete with 20% and 40% CO<sub>2</sub> in nitrogen balance and water/cement ratios of 0.26 and 0.32 (B) measured ratio of outlet to inlet CO<sub>2</sub> gas concentration and carbonation efficiency in 1-D flow-through reactor with compacted concrete prepared with water/cement ratio of 0.32 and carbonated with 20% CO<sub>2</sub>.

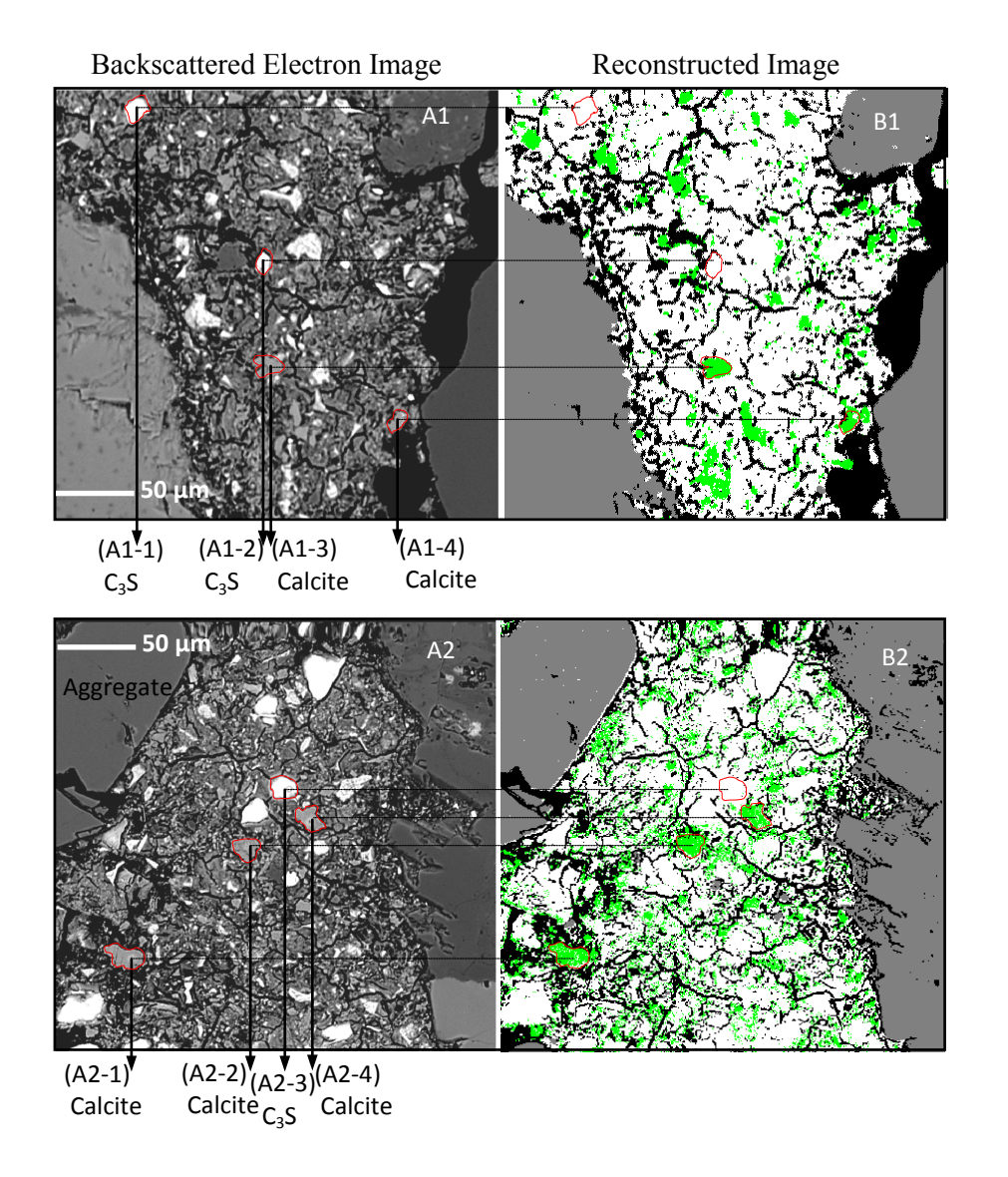


**FIGURE 4.4.** Scanning electron microprobe imaging with X-ray microanalysis (A) Backscattered Electron (BSE) image (B) reconstructed image of pores (black), aggregate (grey), calcium carbonate (green), and remaining solid phase (white) in 24-hour hydrated (and non-carbonated) concrete

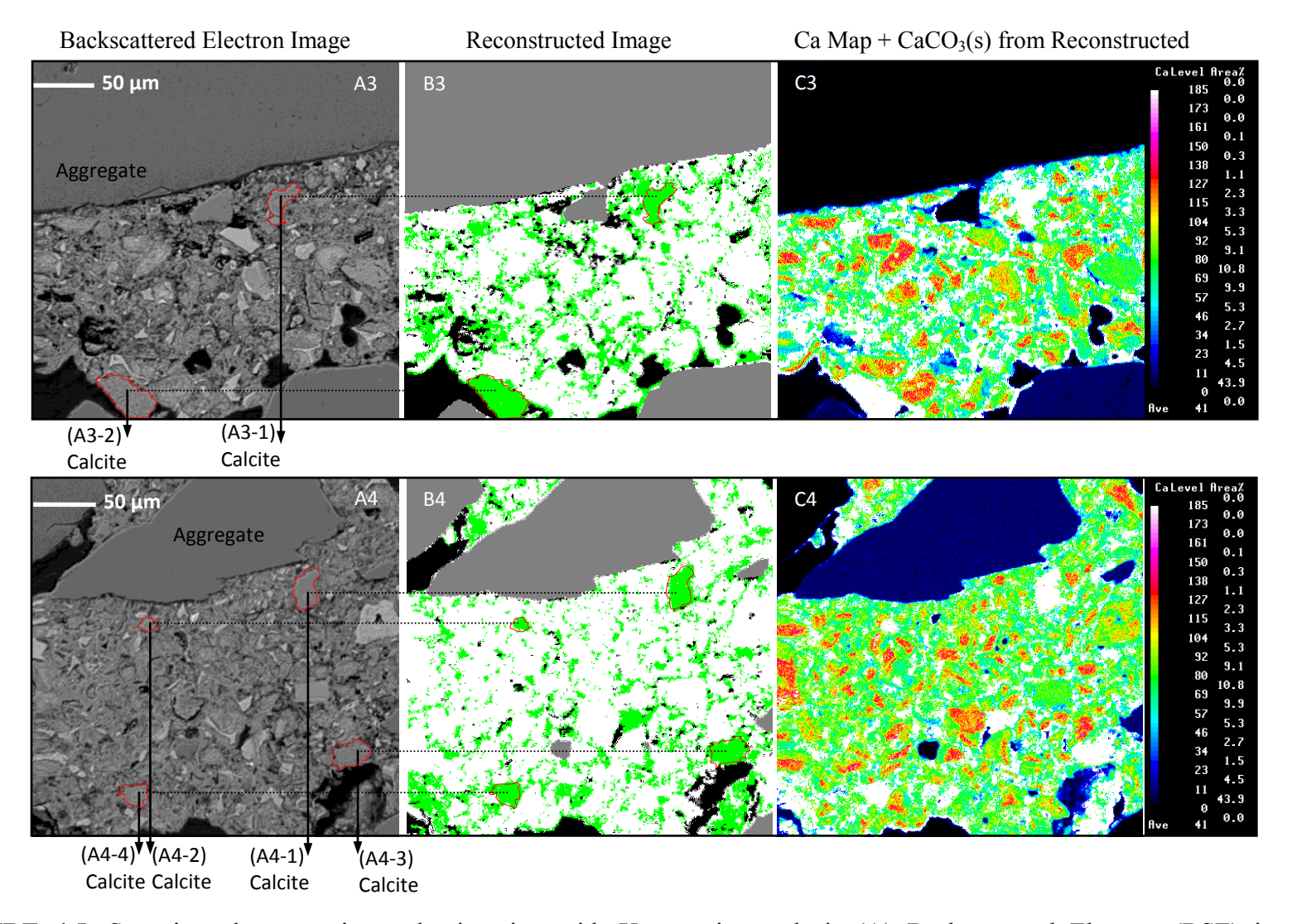


**FIGURE 4.5.** Scanning electron microprobe imaging with X-ray microanalysis (A) Backscattered Electron (BSE) image (B) reconstructed images of pores (black), aggregate (grey), calcium carbonate (green), and remaining solid phase (white) (C) reconstructed color map of Ca and distribution of calcium carbonate (white) in accelerated CO<sub>2</sub> cured concrete.

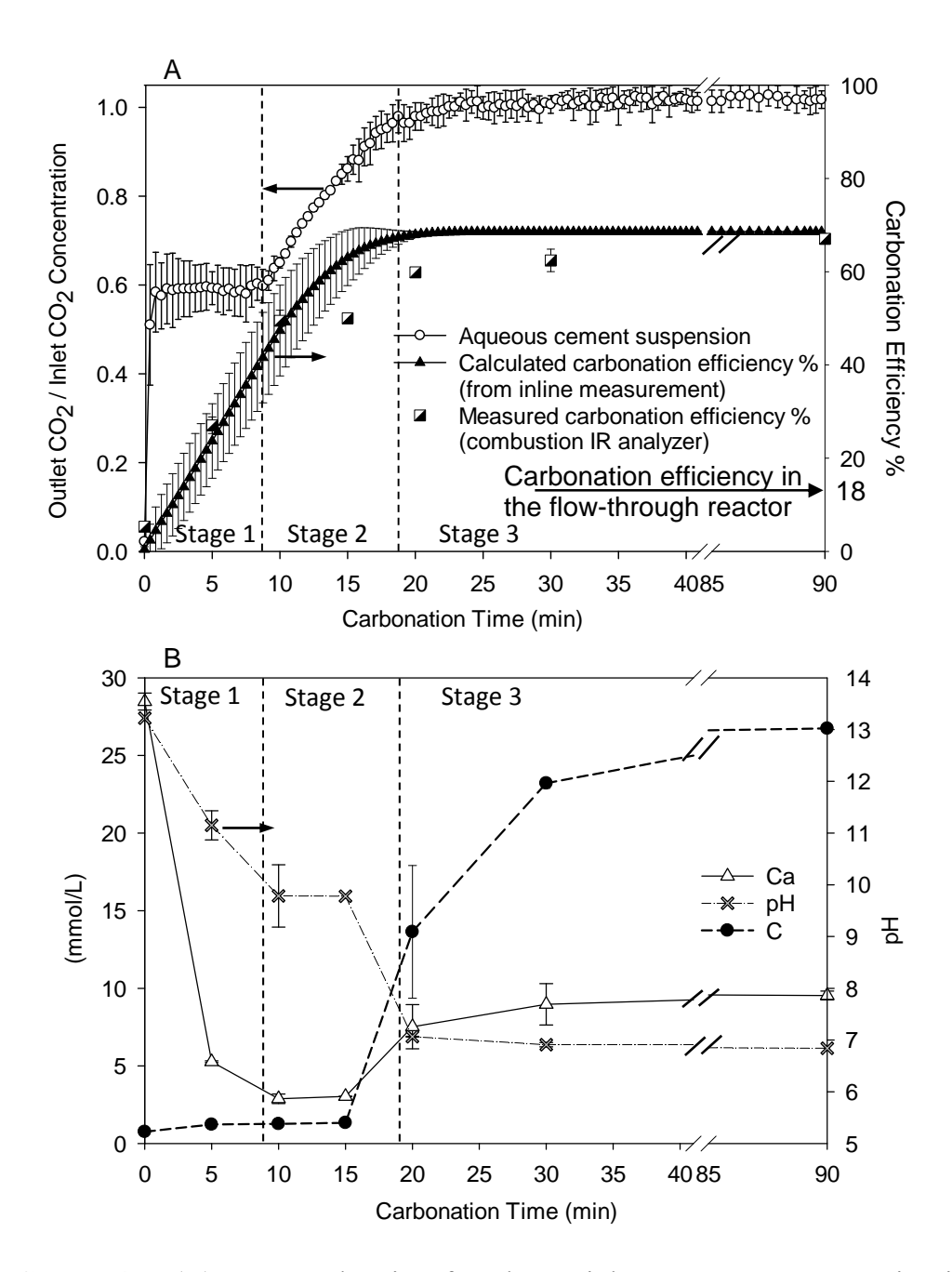


**FIGURE 4.6.** (A) Measured ratio of outlet to inlet CO<sub>2</sub> gas concentration in CMFT reactor, calculated carbonation efficiency from inline CO<sub>2</sub> measurements and measured carbonation efficiency from combustion IR analyzer, (B) measured pH and concentrations of dissolved C and Ca in CMFT reactor during carbonation of aqueous cement suspension

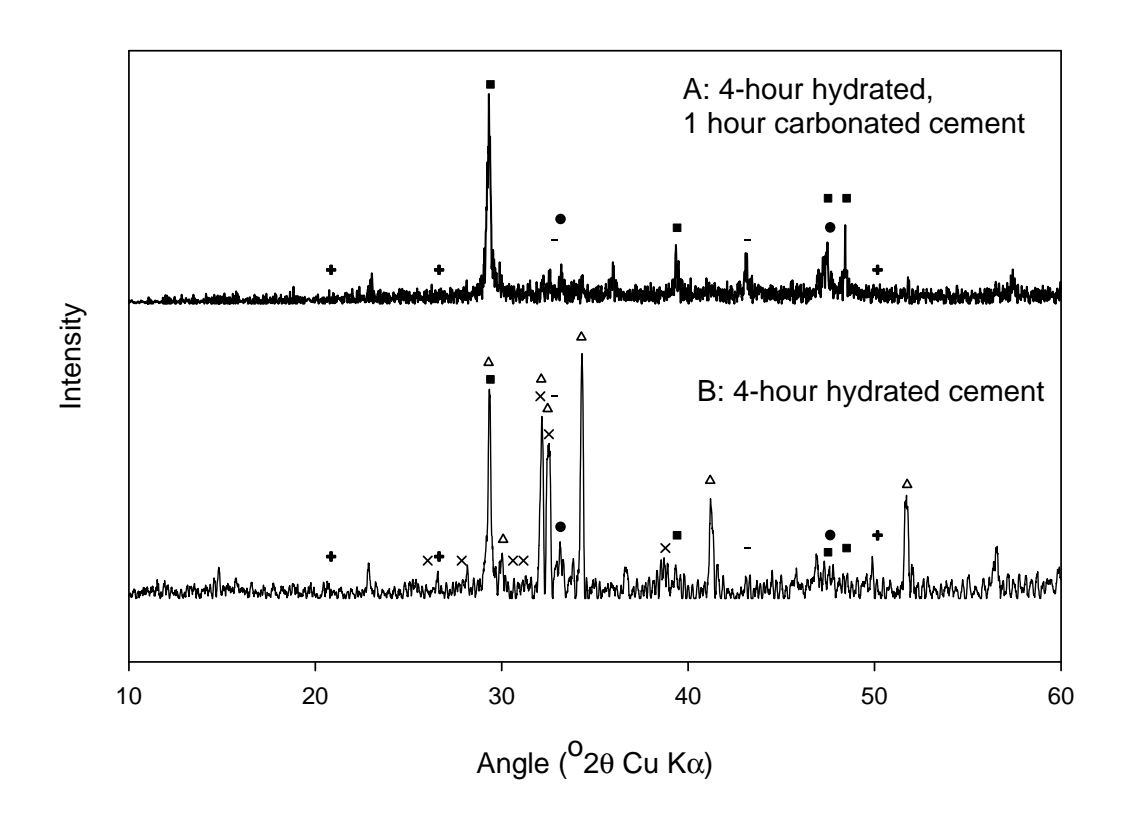


**FIGURE 4.7.** XRD results of (A) 4-hour hydrated and 1-hour carbonated Portland cement, (B) 4-hour hydrated Portland cement ( $\Delta$ ) C<sub>3</sub>S (Ca<sub>3</sub>SiO<sub>5</sub>), (×) C<sub>2</sub>S (Ca<sub>2</sub>SiO<sub>4</sub>), ( $\blacksquare$ ) calcite (CaCO<sub>3</sub>), ( $\bullet$ ) C<sub>3</sub>A (3CaO.Al<sub>2</sub>O<sub>3</sub>), (+) quartz (SiO<sub>2</sub>) and (-) magnesite (MgCO<sub>3</sub>)

**TABLE 4.1.** Composition and particle size of cement

major oxides (percent of dry mass)		cement phases <sup>1</sup> (percent of dry mass)		particle size distribution (percentage)			
CaO	63.1	C <sub>3</sub> S	67.8	0.8-3.3 μm	30.2		
MgO	2.0	$C_2S$	8.7	3.9-7.8 μm	27.6		
$Na_2O$	0.0	$C_3A$	14.3	9.3-19 μm	21.2		
$K_2O$	0.0	$C_4AF$	2.6	22-44 μm	15.1		
$SO_3$	3.8			53-105 μm	5.6		
$SiO_2$	19.8			125-210 μm	0.4		
$Al_2O_3$	5.0			>250 μm	0.0		
$Fe_2O_3$	2.0						
			02.4	mean diameter μm	15.3		
	0.7.7	total	93.4	median diameter	7.4		
total	total 95.7			μm 10			
				total			

<sup>&</sup>lt;sup>1</sup> Cement phase composition estimated with Taylor's procedure (modified Bogue Formula) [34]

The cement phases are reported in standard cement science nomenclature:

C = CaO,  $S = SiO_2$ ,  $A = Al_2O_3$ ,  $F = Fe_2O_3$ ,  $H = H_2O$ .

### 4.8. Supporting Information Section

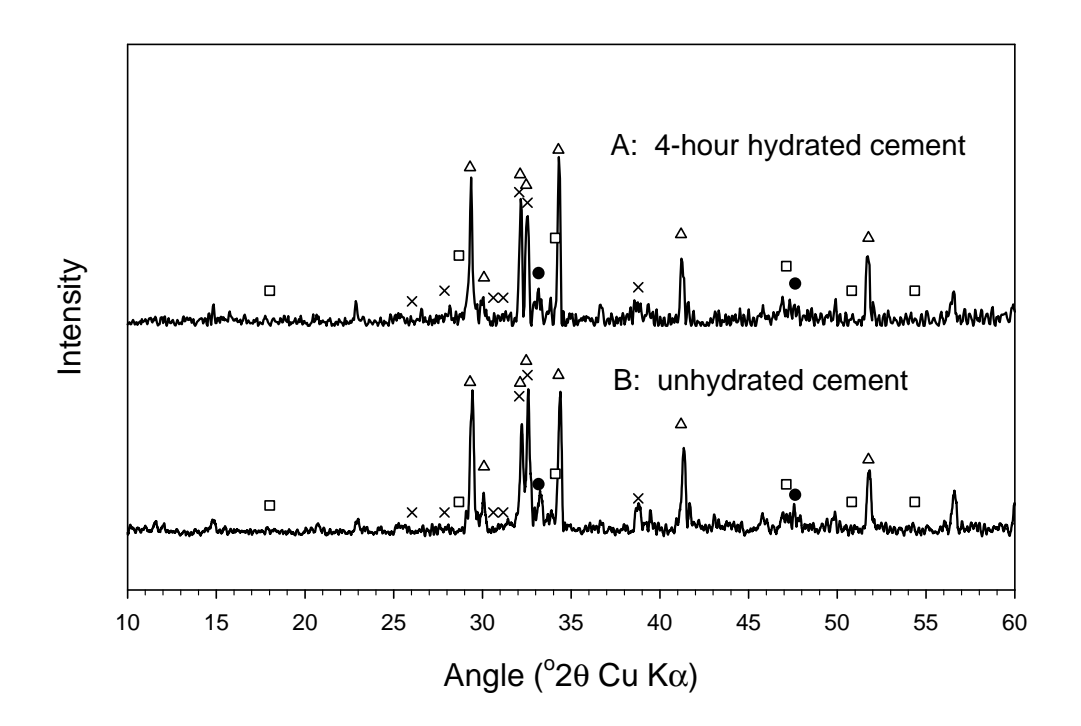


**FIGURE 4S.1.** XRD results of (A) 4-hour hydrated Portland cement, (B) unhydrated Portland cement ( $\Delta$ ) tricalcium silicate (Ca<sub>3</sub>SiO<sub>5</sub>), (×) dicalcium silicate (Ca<sub>2</sub>SiO<sub>4</sub>), ( $\square$ ) portlandite (Ca(OH)<sub>2</sub>), and ( $\bullet$ ) tricalcium aluminate (3CaO.Al<sub>2</sub>O<sub>3</sub>)

TABLE 4S.1. Characteristics of water used in cement slurry

рН	6.9
Temperature (°C)	25
Alkalinity (meq/L )	1.44
Calcium (mmol/L)	$7.7 \times 10^{-1} \pm 0.06$
Magnesium (mmol/L)	$3.0 \times 10^{-1} \pm 0.01$
Potassium (mmol/L)	$5.0 \times 10^{-2} \pm 0.01$
Sodium (mmol/L)	$5.5 \times 10^{-1} \pm 0.01$
Aluminum (mmol/L)	$<4x10^{-4}$
Iron (mmol/L)	$< 8.95 \times 10^{-5}$
Silica (mmol/L)	$3.0 \times 10^{-2} \pm 0.3$

**TABLE 4S.2.** Calibration standards and detection limits for each element analyzed with electron microprobe for carbonated and hydrated concrete

Elements	Standard	<b>Detection limits (wt%)</b>			
Si	Wollastonite	0.04			
Al	Orthoclase	0.03			
Ca	Calcite/Wollastonite	0.04			
K	Orthoclase	0.03			
Fe	Pyrope	0.06			
C	Dolomite	0.08			
Na	Albite	0.04			
S	$CaSO_4$	0.03			
Mg	Dolomite	0.03			

**TABLE 4S.3.** Selected electron microprobe analysis for crystals in Figures 4.4 and 4.5. Values are elemental oxide contents (wt%)

	SiO <sub>2</sub>	$Al_2O_3$	CaO	K <sub>2</sub> O	FeO	$CO_2$	Na <sub>2</sub> O	$SO_3$	MgO	Total
A1-1	24.0	1.4	68.0	0.3	0.2	5.9	0.1	0.2	1.3	101.4
$(C_3S)$										
A1-2	23.3	0.8	68.2	0.2	0.3	9.9	0.4	0.1	1.1	104.2
$(C_3S)$										
A1-3	1.2	1.0	54.2	0.1	0.1	36.9	0.1	0.1	1.0	94.6
(calcite)										
A1-4	0.4	0.5	53.9	0.0	0.1	41.2	0.1	0.1	0.3	96.5
(calcite)										
A2-1	0.2	0.4	53.1	0.1	0.1	42.1	0.0	0.1	0.4	96.5
(calcite)	0.0	0.0	52.5	0.1	0.0	40.7	0.1	0.1	0.0	0.7.6
A2-2	0.3	0.3	53.7	0.1	0.2	42.7	0.1	0.1	0.2	97.6
(calcite)	22.5	1.5	(7.6	0.2	0.2	5.0	0.1	0.1	1.2	100 (
A2-3	23.5	1.5	67.6	0.3	0.3	5.9	0.1	0.1	1.3	100.6
$(C_3S)$	0.7	0.5	50.2	0.1	0.4	40.0	0.0	0.2	0.7	101.0
A2-4	0.7	0.5	50.3	0.1	0.4	48.0	0.0	0.3	0.7	101.0
(calcite)	0.2	0.1	57.4	0.0	0.1	40.9	0.0	0.1	0.5	99.1
A3-1	0.2	0.1	37.4	0.0	0.1	40.8	0.0	0.1	0.3	99.1
(calcite) A3-2	0.0	0.1	57.5	0.0	0.1	37.8	0.0	0.1	0.4	96.1
(calcite)	0.0	0.1	37.3	0.0	0.1	37.0	0.0	0.1	0.4	90.1
A4-1	0.0	0.2	57.4	1.0	0.0	39.9	0.0	0.0	0.4	98.0
(calcite)	0.0	0.2	37.4	1.0	0.0	37.7	0.0	0.0	0.4	70.0
A4-2	0.1	0.1	58.4	0.0	0.0	39.1	0.1	0.2	0.8	98.9
(calcite)	0.1	0.1	20.1	0.0	0.0	57.1	0.1	0.2	0.0	, 0.,
A4-3	0.2	0.3	57.4	0.0	0.1	41.8	0.0	0.1	0.5	100.4
(calcite)										
A4-4	0.1	0.0	57.3	0.1	0.2	39.1	0.0	0.0	0.2	97.7
(calcite)										

The minerals were defined based on the weight percentage of oxides in their composition (e.g. calcite includes CaO (56 wt%) and  $CO_2$  (44 wt%)

The experimental investigation of physico-chemical processes limiting the CO<sub>2</sub> uptake were presented in Chapter 4. A numerical model was also developed for carbonation curing of concrete in the flow-through reactor. Mass balance equations of CO<sub>2</sub> and cement compounds were solved numerically. The numerical model can be used to study the effect of different carbonation processes such as CO<sub>2</sub> gas transport, gas-liquid mass transfer as well as carbonation reaction rates on CO<sub>2</sub> uptake efficiency. The results of numerical model are presented in Chapter 5.

### **Chapter 5**

# MATHEMATICAL MODELING OF ACCELERATED CO<sub>2</sub> CURING OF CONCRETE IN A FLOW-THROUGH REACTOR

Sormeh Kashef-Haghighi, Subhasis Ghoshal

Department of Civil Engineering, McGill University, Montreal, QC, Canada

To be submitted in

Cement & Concrete Research, April 2012

### 5.1. Introduction

Carbon dioxide capture and storage (CCS) technologies are being developed as an option for reduction of CO<sub>2</sub> emissions from fossil fuel-based industries [1]. Potential methods include CO<sub>2</sub> storage in underground geological formations [2, 3] such as oil and gas fields or unmineable coal seams, in deep oceans [4] and in abundant surface minerals such as olivine, serpentinite and wollastonite [5] through exothermal reaction of carbon dioxide with metal oxides which produce stable carbonates [6-9].

Accelerated concrete curing using CO<sub>2</sub> gas is considered as a carbon dioxide mineral sequestration technology in which CO<sub>2</sub> reacts with cement, a material rich in calcium oxide, under ambient temperatures and pressures to form thermodynamically stable calcium carbonate. Moreover, this technology forms a concrete product with enhanced properties compared to conventional hydration curing methods [10]. Among the various cement products which can be used for accelerated CO<sub>2</sub> curing are precast, non-reinforced concrete blocks and bricks or concrete products with non-metallic reinforcements [11, 12].

To date, there have been no attempts at modelling the CO<sub>2</sub> uptake during the accelerated curing process. Much of the effort in modelling is based on CO<sub>2</sub> uptake over time in built concrete structures. The atmospheric CO<sub>2</sub> diffuses into concrete and reacts with calcium hydroxide, the main hydration product of cement, resulting in a decrease of pH which leads to the initiate of corrosion of steel reinforcement bars. This phenomenon, called passive carbonation of concrete, is a major physicochemical process behind deterioration of reinforced

concrete structures [13-15]. Mathematical models of passive carbonation have been performed to estimate the penetration depth of  $CO_2$  in concrete structures under different conditions [16-20]. There are significant differences between the passive carbonation in aged concrete and accelerated carbonation curing.

The composition of cement in accelerated CO<sub>2</sub> curing is different from the passive carbonation of aged concrete. In accelerated CO<sub>2</sub> curing, the cement which is mainly composed of calcium silicates (tricalcium silicate (3CaO.SiO<sub>2</sub> or C<sub>3</sub>S), dicalcium silicate (2CaO.SiO<sub>2</sub> or C<sub>2</sub>S)), tricalcium aluminate (3CaO.Al<sub>2</sub>O<sub>3</sub> or C<sub>3</sub>A) and tetracalcium aluminoferrite (4CaO.Al<sub>2</sub>O<sub>3</sub>.Fe<sub>2</sub>O<sub>3</sub> or C<sub>4</sub>AF), is placed in contact with moisture for an initial hydration period of several hours, to provide some hardening for achieving the required concrete product shape before carbonation. The brief hydration period leads to the formation of small amounts of calcium silicate hydrate gel (3CaO.2SiO<sub>2</sub>.3H<sub>2</sub>O or C-S-H) and calcium hydroxide (Ca(OH)<sub>2</sub>), but the remaining unhydrated cement phases (C<sub>3</sub>S and C<sub>2</sub>S) are more abundant than hydration products [21]. It is this mixture of cement phases that are subjected to carbonation. The composition of concrete in passive carbonation is, however, mainly composed of hydration products (C-S-H and Ca(OH)<sub>2</sub>). Furthermore, the accelerated carbonation curing is carried out in a few hours in order to produce a desirable strength in concrete [10] with partial pressures of CO<sub>2</sub> typically higher than atmospheric CO<sub>2</sub> in order to maintain a high CO<sub>2</sub> diffusion rate in concrete [12, 22], whereas passive carbonation occurs over a long period of time (i.e. several years) and involves only diffusion of atmospheric CO<sub>2</sub> into the concrete matrix. The accelerated carbonation curing of concrete in a 1-D flow-through reactor was investigated in our previous study [23] in which both advection and dispersion are the dominant CO<sub>2</sub> mass transport phenomenon through the concrete matrix.

This study is the first to develop a mathematical model for CO<sub>2</sub> transport and reactivity during accelerated CO<sub>2</sub> curing of concrete. In this study, carbonation curing of concrete in a 1-D flow-through reactor with a CO<sub>2</sub> partial pressure of 0.02 MPa was studied. The carbonation curing of concrete in a flow-through reactor is not the conventional method for accelerated carbonation curing which is conducted in pressurized chambers. However, it would save the energy of CO<sub>2</sub> gas compression required for autoclave curing. Accelerated carbonation in pressurized chambers are retrofitted to current steam curing facilities in order to avoid significant changes in precast concrete plants. The advantages of CO<sub>2</sub> accelerated concrete curing in a flow-through reactor has been discussed in an earlier study [23]. The CO<sub>2</sub> concentration in the outlet gas of the reactor and distribution of calcium carbonate formed during carbonation under different operating conditions were measured experimentally and compared to the results from the mathematical model. The carbonation process in the 1-D flow-through reactor was modeled in order to study the dynamics of CO2 uptake by concrete during carbonation, and to understand the factors limiting the CO<sub>2</sub> uptake efficiency. The carbonation model was a numerical solution of differential equations of CO<sub>2</sub> gas advection and dispersion, gas-liquid mass transfer and carbonation reactions of all active cement species which undergo carbonation. The system of equations was also transformed to dimensionless form by using several dimensionless numbers in order to compare the importance of different

physiochemical processes including the CO<sub>2</sub> gas dispersion, CO<sub>2</sub> gas-liquid mass transfer and carbonation reaction rate on CO<sub>2</sub> uptake efficiency in concrete.

#### 5.2. Experimental materials and methods

Compact concrete specimens were prepared with Type 10 Portland cement (St. Lawrence Cement), kiln dried sand (Bomix) and tap water [23]. Each concrete specimen contained 151 g of cement, 607 g of fine aggregate and 39 or 48 mL of water representing a water/cement ratio of 0.26 or 0.32, respectively. The fresh mixture was compacted in a steel mold by 8 MPa pressure to maintain precise sample dimensions of 12.5 cm diameter and 3.1 cm height. One hour after casting, the samples were mounted in a PVC shell and sealed using 5-minute epoxy. The mounted samples were stored in a sealed 100% humidity chamber at room temperature for hydration for 3 hours, in order to gain an initial strength for handling in the carbonation curing reactor. The compact concrete specimens were carbonated in a 1-D flow-through, stainless steel reactor at constant temperature, inlet gas pressure, gas flow-rate, CO<sub>2</sub> partial pressure and relative humidity. The gas mixture was 20% or 40% high purity CO<sub>2</sub> in nitrogen balance (Praxair Inc). The CO<sub>2</sub> uptake by concrete was measured by an infrared-based CO<sub>2</sub> analyzer (Eltra CS-800). A CO<sub>2</sub> gas sensor (Quantek model 906 NDIR) was also used to monitor the concentration of CO<sub>2</sub> in the effluent gas of the reactor during the carbonation process. Additional details on carbonation curing experiments in the 1-D flow-through reactor can be found in an earlier publication [23].

The porosity and surface area of compact concrete was studied using Mercury Intrusion Porosimetry (MIP) and Brunauer–Emmett–Teller (BET) nitrogen sorption. A Micrometrics 9320 Mercury porosimeter, with a pressure range of sub-ambient to 207 MPa was used for pore size range of 0.006-237 μm. Several samples were cored from different locations of the compact concrete column, dried and then used for porosity measurement [23]. The BET nitrogen sorption method was used for measuring the surface area of concrete in pore size range of 1.7-300 nm using a Micrometrics TriStar 3000 sorptometer at 77.3 K. The total specific surface area, in the pore size range of 0.0017-237 μm, used in the carbonation model was defined based on the two methods.

#### **5.3.** The mathematical model framework

The mathematical model of accelerated carbonation includes the transport and reaction of CO<sub>2</sub> in the compact concrete specimen in a 1-D flow-through reactor (Figure 5.1). The partial differential equation used for calculation of CO<sub>2</sub> concentration in gas phase ([CO<sub>2</sub> (g)]) includes three terms for advection, dispersion and gas-liquid mass transfer to pore aqueous phase.

$$\frac{\partial(\varepsilon \,\varphi^{a}[CO_{2}(g)])}{\partial t} = D_{CO_{2}(g)} \frac{\partial^{2}(\varepsilon \,\varphi^{a}[CO_{2}(g)])}{\partial x^{2}} - v \frac{\partial(\varepsilon \,\varphi^{a}[CO_{2}(g)])}{\partial x} - r_{CO_{2}(aq)} \quad (5.1)$$

The pore space was unsaturated, therefore, the total porosity,  $\varepsilon$ , is divided into two parts:  $\phi^a$  for pore fraction filled with air and  $\phi^w$  for pore fraction filled with liquid water which were calculated based on the water produced or consumed during

hydration and carbonation reactions. In the above equation,  $D_{\text{CO}_2(g)}$  is the dispersion coefficient of CO<sub>2</sub> gas, v is the seepage velocity of CO<sub>2</sub> gas and  $r_{\text{CO}_2(aq)}$  is the rate of CO<sub>2</sub> dissolution to pore water. The dispersion coefficient was measured by passing a tracer gas (N<sub>2</sub>) with the same flow-rate as the CO<sub>2</sub> gas mixture and  $D_{\text{CO}_2(g)}$  was calculated by fitting the breakthrough curve.

The CO<sub>2</sub> concentration in the aqueous phase ([CO<sub>2</sub> (aq)]) is influenced by the rate of CO<sub>2</sub> mass transfer from gas phase ( $r_{\text{CO}_2(\text{aq})}$ ), diffusion of dissolved CO<sub>2</sub> in aqueous phase in a porous matrix ( $D^*_{\text{CO}_2(\text{aq})}$ ) and the rate of CO<sub>2</sub> consumption during carbonation reactions ( $r_{\text{C}}$ ).

$$\frac{\partial(\varepsilon \,\varphi^{w}[CO_{2}(aq)])}{\partial t} = D_{CO_{2}(aq)}^{*} \frac{\partial^{2}(\varepsilon \,\varphi^{w}[CO_{2}(aq)])}{\partial x^{2}} + r_{CO_{2}(aq)} - r_{C}$$
 (5.2)

The diffusion coefficient  $D_{\text{CO}_2(\text{aq})}^*$  was obtained from literature on CO<sub>2</sub> transport in concrete [17].

The rate of CO<sub>2</sub> consumption during carbonation reactions is determined by the reaction rates of all cement phases which participate in carbonation. These cement phases also include the hydration products which are formed during the 4 hours of hydration. The amounts of hydration products formed during this period were obtained from a mathematical model of cement hydration which was developed in this study. The hydration and carbonation chemical reactions are described in Section 5.4.

## 5.3.1. Boundary conditions and initial concentrations for the above PDEs

For the carbonation model, the domain  $\Omega$  represents the concrete specimen which is exposed to the  $CO_2$  gas mixture at the inlet surface (Figure 5.1). The exposed boundary,  $\Gamma^R$  or the first-type (Dirichlet) boundary, has constant  $CO_2$  gas concentration. The  $CO_2$  gas flux is homogenous in the inlet surface and the gas transport is assumed one dimensional. The surrounding of specimen is bounded by  $\Gamma^N$  (second-type (Neumann) boundary) as the specimen is sealed with epoxy to a PVC shell. The domain is bounded by  $\Gamma^N$  in the outlet surface, where the concentration of  $CO_2$  in the gas mixture is measured, and is chosen to represent no-flux condition for all active species.

The initial concentrations of cement phases and porosity for the carbonation model were the simulation results of a 4-hour hydrated concrete. The initial concentration of dissolved CO<sub>2</sub> in the concrete aqueous phase is zero and the CO<sub>2</sub> gas concentration in the inlet is 8.67 (mol.m<sup>-3</sup>), as calculated from the partial pressure of CO<sub>2</sub> in the gas mixture (20% CO<sub>2</sub> in N<sub>2</sub> balance).

# 5.4. Production and consumption rate of reactive compounds during hydration and carbonation curing

During accelerated carbonation curing, dissolved CO<sub>2</sub> reacts with unhydrated cement phases as well as the hydration products. The changes in cement composition during hydration and carbonation are summarized in Figure 5.2.

## 5.4.1. Chemical reactions during hydration period prior to accelerated carbonation curing

Cement compounds react with water and hydration products are formed. Tricalcium silicate dissolves quite rapidly in the first seconds after water is added; however, the dissolution rate decreases rapidly before saturation [24]. The overall hydration of  $C_3S$  as shown in Table 5.1 (Eq. 5.1.1) forms calcium hydroxide and calcium silicate hydrate gel [21]. Dicalcium silicate follows the same hydration mechanism as  $C_3S$  but at a slower rate (Eq. 5.1.2).

In the presence of gypsum (calcium sulfate), which is a component of cement, C<sub>3</sub>A hydrates and forms ettringite (3CaO.Al<sub>2</sub>O<sub>3</sub>.3CaSO<sub>4</sub>.32H<sub>2</sub>O, AFt or trisulfate), as shown in Eq. 5.1.3. Ettringite reacts with additional amounts of C<sub>3</sub>A forming calcium aluminate monosulfate hydrate (3CaO.Al<sub>2</sub>O<sub>3</sub>.CaSO<sub>4</sub>.12H<sub>2</sub>O). The Ca(OH)<sub>2</sub> produced from hydration of C<sub>3</sub>S and C<sub>2</sub>S is consumed in reaction with tetracalcium aluminoferrite (C<sub>4</sub>AF) and gypsum (Eq. 5.1.4). Hydration reactions of C<sub>3</sub>A and C<sub>4</sub>AF after gypsum is consumed are shown in Eqs. 5.1.5 and 5.1.6 [18]. For short hydration periods as in accelerated concrete curing, gypsum is, however, unlikely to be exhausted. Among the hydration products, calcium silicate hydrate, calcium hydroxide and ettringite undergo carbonation, and thus the concentration of these compounds at the end of initial hydration period influences the extent of accelerated carbonation. In the hydration model, the amount of these hydration products formed during the hydration period prior to carbonation were calculated.

#### 5.4.2. Chemical reactions during accelerated carbonation curing

Carbon dioxide gas dissolves in pore water and hydrates to  $H_2CO_3$ , which is a slow and rate-determining process (Eq. 5.3). Following dissolution,  $H_2CO_3$  ionizes to  $HCO_3^-$  and  $CO_3^{2-}$  instantaneously [25].

$$CO_2(aq) + H_2O \xrightarrow{r_{H,C}} H_2CO_3 \to H^+ + HCO_3^- \to 2H^+ + CO_3^{2-}$$
 (5.3)

At pH above 10, the following reaction (Eq. 5.4) is more dominant than the reaction between CO<sub>2</sub> and H<sub>2</sub>O [26].

$$CO_2(aq) + OH^- \xrightarrow{r_{H,C}} HCO_3^- \rightarrow H^+ + CO_3^{2-}$$

$$(5.4)$$

Bicarbonate ions further dissociates and forms carbonate ions. As long as sources contributing to high pH, such as excess Ca(OH)<sub>2</sub>, are present, the pH remains above 12 and the dissolved CO<sub>2</sub> is in the form of CO<sub>3</sub><sup>2-</sup>, but when these sources are no longer available, continuous exposure to a CO<sub>2</sub> (g) rich atmosphere causes a decrease in pH and bicarbonate ions begin to dominate among other dissolved carbonate species [27].

Calcium silicates ( $C_3S$  and  $C_2S$ ) dissolve in water and forms  $Ca^{2+}$  and  $SiO_4^{2-}$  ions. Calcium ions instantaneously react with carbonate ions and form solid calcium carbonate (Eq. 5.5) [28].

$$Ca^{2+} + CO_3^{2-} \longrightarrow CaCO_3(s)$$
 (5.5)

The overall reactions of calcium silicates are reported as Eqs. 5.1.7-5.1.8 [29]. The hydration products, calcium silicate hydrate, ettringite and calcium hydroxide, undergo carbonation as described in Eqs. 5.1.9-5.1.11.

#### **5.4.3.** Rate of formation of hydration products

The hydration reactions were explained in Section 5.4.1. The rate of production of hydration products can be calculated from the rate of hydration reactions described in Eqs. 5.1.1-5.1.6 (Table 5.1):

$$r_{H,CH} = (3/2)r_{H,C_3S} + (1/2)r_{H,C_2S} - 4r_{H,C_4AF} - r_{H,C_3A} - 2r_{H,C_4AF,S}$$
(5.6)

$$r_{\text{H.CSH}} = (1/2)r_{\text{H.C.},\text{S}} + (1/2)r_{\text{H.C.},\text{S}}$$
 (5.7)

$$r_{\mathrm{H,AFt}} = r_{\mathrm{H,C_3A,S}} \tag{5.8}$$

where  $r_{H,i,S}$  is the hydration rate of species i in the presence of gypsum and  $r_{H,i}$  in the absence of gypsum. The initial high hydration reaction rates, which are mostly controlled by surface reaction, decrease with the progress of hydration. One of the hypotheses proposed for this deceleration of  $C_3S$  hydration is that a thin metastable layer of C-S-H forms which restricts the diffusion of reactive ions [24]. Therefore, the overall reaction rates have been formulated as power law empirical equations and as a function of the progress of hydration [14]. The hydration reaction rates (Eq. 5.9) of cement phases ( $C_3S$ ,  $C_2S$ ,  $C_3A$  or  $C_4AF$ ) are expressed as a function of the fraction of each compound which have been hydrated at each time, the reaction constants ( $k_{H,i}$ ) and partial reaction order ( $n_i$ ) as shown in Eq. 5.9.

$$r_{H,i} = (k_{H,i}/[i]_0^{n_i-1})[i]^{n_i}$$
(5.9)

The coefficients and constants for the cement hydration model are listed in Table 5.2. In the equation, [i] and  $[i]_0$  are the current and initial concentration of the specific cement species undergoing hydration.

Water in pores was consumed during the hydration reactions. The rate of water consumption was calculated as shown in Eq. 5.10.

$$\frac{\partial(\varepsilon\,\omega)}{\partial t} = -3r_{H,C_3S} - 2r_{H,C_2S} - 10r_{H,C_3A,S} - 18r_{H,C_4AF,S} - 22r_{H,C_4AF} - 12r_{H,C_3A} \tag{5.10}$$

where  $\omega$  is the moisture concentration in pores. The fraction of pore filled with water ( $\phi^w$ ) was calculated from the moisture concentration.

For the hydration model, the initial concentrations of C<sub>3</sub>S, C<sub>2</sub>S, C<sub>3</sub>A and C<sub>4</sub>AF in terms of moles per unit volume of concrete are listed in Table 5.2. The initial porosity of the compacted concrete mixture was estimated based on the total volume of the compacted mixture and the weight and density of the cement and aggregate used in the mixture. The initial water content was also calculated based on the water/cement ratio in the concrete mixture.

The porosity of concrete is altered during hydration due to the differences in molar volume of products and reactants. Porosity at each time step ( $\epsilon_t$ ) was calculated as shown by Eq. 5.11 during hydration.

$$\varepsilon_{t} = \varepsilon_{t-1} - \sum ([i]_{t} - [i]_{t-1}) \Delta \overline{V}_{H,i}$$

$$(5.11)$$

 $\Delta \overline{V}_{H,i}$  is the change in volume per mole of reactant i during hydration and the values are reported in Table 5.2 and i represents all the cement phases that undergo hydration.

#### 5.4.4. Rate of CO<sub>2</sub> dissolution

The dissolution of CO<sub>2</sub> gas to the aqueous phase is proportional to deviation from the equilibrium and is given by:

$$r_{\text{CO}_2(\text{aq})} = k_t (k_{\text{Henry}} [\text{CO}_2(g)] - [\text{CO}_2(\text{aq})])$$
 (5.12)

In the above equation,  $k_t$  is the interfacial gas-liquid mass transfer coefficient for  $CO_2$  and  $k_{Henry}$  is the dimensionless Henry's constant for equilibrium partitioning of  $CO_2$  gas to water. The values of the constants used in the carbonation model are listed in Table 5.3.

#### 5.4.5. Rate of formation of carbonation products

The carbonation reactions (Eqs. 5.1.7-5.1.11) are aqueous phase reactions and involve both dissolution of solid compounds and reaction with dissolved  $CO_2$ . The kinetics of these carbonation reactions are reported to be first order with dissolved  $CO_2$  concentration as well as the exposed surface area of reactive solid phases such as  $C_3S$  and  $C_2S$  [16]. The kinetics of these carbonation reactions have been formulated in the literature only as empirical equations which lump the dissolution and carbonation processes. Because the dissolution rate of  $C_3S$  decelerates very quickly before reaching saturation, and carbonation might have an effect on dissolution rate by affecting the formation of metastable C-S-H layer, an empirical equation for the overall rate of carbonation of  $C_3S$  as shown in Eq. 5.13 was used. The reaction constants ( $k_i$ ) were obtained from literature as listed in Table 5.3 [16].

$$r_{i} = k_{i} a_{s,i} [CO_{2}(aq)]$$

$$(5.13)$$

Sakai et al. have reported a slower rate of ettringite carbonation compared to C-S-H [30]. In this model, a carbonation rate constant equal to that for C-S-H was selected for ettringite.

Solid calcium hydroxide dissolves in pore water to form hydroxide and calcium ions. The dissolution of solid calcium hydroxide ( $r_{D,CH}$ ) is approximated by Eq. 5.14 [18, 31].

$$r_{\rm D,CH} = (1/2)k_{\rm s}a_{\rm s,CH} \, \epsilon \, \phi^{\rm w}([{\rm OH}^{-}]_{\rm eq} - [{\rm OH}^{-}])$$
 (5.14)

The carbonation rate of dissolved  $Ca(OH)_2$  ( $r_{CH}$ ) is controlled by the rate of formation of carbonate ions ( $r_{CH}=r_{H,C}$ ) as the dissociation of dissolved  $Ca(OH)_2$  to calcium ions and reaction of calcium ions and carbonate ions are relatively much faster. The hydration rate of  $CO_2$  ( $r_{H,C}$ ) which leads to formation of carbonate and bicarbonate ions has been measured by Pinsent et al. [26]. At pH above 10, the  $CO_2$  hydration rate is a function of hydroxide ions in the solution and the reaction rate is calculated as below:

$$r_{H,C} = k[OH^-][CO_2(aq)]$$
(5.15)

At lower pH, the hydration reaction rate is dominated by equation 5.3 and the rate of reaction is first order with concentration of dissolved CO<sub>2</sub>.

$$r_{\mathrm{H,C}} = k'[\mathrm{CO}_2(\mathrm{aq})] \tag{5.16}$$

From the above carbonation reaction rates, the rate of consumption of dissolved  $CO_2$  can be calculated as Eq. 5.17. In this equation, the carbonation reaction rates of solid cement phases were expressed per unit total volume of concrete while for dissolved calcium hydroxide was expressed per unit volume of aqueous phase and the term  $\varepsilon \phi^w$  was used to normalize the rates to per unit volume of concrete. The concentrations of cement phases changed during carbonation reactions and were calculated based on the carbonation reaction rates.

$$r_{\rm C} = (3r_{\rm C_3S} + 2r_{\rm C_2S} + 3r_{\rm CSH} + 3r_{\rm AFt} + \varepsilon \, \phi^{\rm w} r_{\rm CH})$$
(5.17)

# 5.4.6. Changes in porosity and specific surface area of concrete during carbonation

The porosity of concrete was altered during carbonation due to the differences in molar volume of products and reactants and was calculated in a similar way as shown in Eq. 5.11. The changes in volume per mole of reactant during carbonation are reported in Table 5.2 as  $\Delta \overline{V}_i$ .

The exposed surface area of reactants reduces as carbonation proceeds because of the formation and precipitation of solid products. Thus, in this study we introduce a reduction coefficient ( $f_{\rm C}$ ) in order to account for this phenomenon (Eq. 5.18).

$$a_{\rm s} = a_{\rm s_0} - f_{\rm C} \cdot [\text{CaCO}_3] \tag{5.18}$$

where  $a_{\rm s}$  is the specific surface area of concrete per unit volume. In this study,  $f_{\rm C}$  was fitted to one set of experimental data and verified with the experimental results at different conditions. The initial specific surface area  $(a_{\rm s0})$  was estimated from the total pore surface area per unit weight of concrete (S) measured using mercury intrusion porosimetry (MIP) [23] as well as Brunauer–Emmett–Teller (BET) and the density of concrete  $(\rho_{\rm con})$  as listed in Table 5.2 (Eq. 5.19):

$$a_{\rm s0} = S\rho_{\rm con} \tag{5.19}$$

Over time, the surface area of each cement phase was calculated based on the total surface area and the relative volume of each species to total solid volume by assuming that the ratio of surface area for each species to total surface area is the same as volume ratio.

$$a_{s,i} = a_s[i](1/(1-\varepsilon))\overline{V}_i$$
(5.20)

where  $\overline{V}_i$  is molar volume of species *i*, listed in Table 5.2.

#### 5.5. Results and Discussion

#### 5.5.1. Changes in concrete composition during hydration period.

The changes in concentrations of cement phases and hydration products during 4 hours of hydration are shown in Figure 5.3. Among the cement compounds, hydration of C<sub>3</sub>S and C<sub>3</sub>A initiate during the hydration period of 4 hours. The hydration reaction rate constants used in the hydration model for this study were the same used by Papadakis et al. [32].

The concrete porosity calculated by the model decreased during hydration from 26.1% to 24.5% after 4 hours of hydration. The porosity of concrete was measured after 24 hours of hydration as 20.5%. This time was required to gain an initial strength for core sampling for porosity measurement using Mercury Intrusion Porosimetry (MIP) [23]. This measured porosity was comparable with the porosity calculated by the hydration model as 21.5%.

## 5.5.2. Carbonation uptake calculated from the mathematical model for various water/cement ratios and gas flow-rates

The ratio of CO<sub>2</sub> concentration in the outlet to the inlet gas during carbonation is plotted in Figure 5.4. The simulation results for a flow-rate of 1.17 Lpm and water/cement ratio of 0.26 are presented in Figure 5.4-A. Without reducing the surface area of active compounds because of formation of solid calcium carbonate  $(f_{\rm C}=0)$ , the CO<sub>2</sub> concentration in the outlet gas did not match the experimental values. The surface area reduction factor  $(f_C)$  was fitted to the experimental results at 1.17 Lpm and w/c=0.26 and the results from the model and experiment matched at the  $f_{\rm C}$  value of 5.6 m<sup>2</sup>/mol. This value represents the average surface area that a mole of solid calcium carbonate covers after deposition. The average surface area of calcite crystals is approximately 3.55 m<sup>2</sup>/mol for grain sizes of 44-62 µm as reported by Anderson [33]. The CO<sub>2</sub> uptake in concrete at two different gas flow-rates of 0.08 Lpm and 2.00 Lpm are also compared in Figure 5.4-B. The results from the mathematical model, using the same surface area reduction factor, matched the experimental results for gas flow-rate of 0.08 Lpm and 1.17 Lpm, reasonably well. The modeling results for the higher gas flow-rate of 2 Lpm, however, did not match the experimental results for the first 10 minutes of carbonation. The experimental measurements showed channelling of CO<sub>2</sub> at higher flow-rate which decreased the carbonation efficiency to 10.7±0.02. The experimental results are shown with symbols in Figure 5.4, the results for gas flow-rates of 1.17, 0.08 and 2 Lpm and water/cement ratio of 0.26 were reported in an earlier publication [23].

As CO<sub>2</sub> gas flows through the concrete matrix, it dissolves in pore water and reacts with active cement compounds to form CaCO<sub>3</sub>. Therefore, the CO<sub>2</sub> concentration in the outlet of concrete specimen starts to increase much later compared to the concentration in the inlet region. Figure 5.5-A shows the concentration of CO<sub>2</sub> (g) in concrete pores during accelerated carbonation. In those regions where the CO<sub>2</sub> concentration was low, the CO<sub>2</sub> dissolution was also very small and no CaCO<sub>3</sub> was formed. Therefore, an advancing carbonation front was seen in the concrete specimen. Figure 5.5-B shows the distribution of CaCO<sub>3</sub> formed along the length of the concrete specimen during carbonation. The formation of carbonation front was seen both from the mathematical model and the measurements of CO<sub>2</sub> uptake by concrete from combustion CO<sub>2</sub> analysis. Solid samples were taken from the inlet surface, mid-length and outlet surface of carbonated compact concrete specimen after 5, 10 and 30 minutes of carbonation and the CO<sub>2</sub> content was measured using an infrared-based CO<sub>2</sub> analyzer. The data has been presented in an earlier publication [23]. The concentration of solid calcium carbonate formed during carbonation as predicted by the mathematical model correlated with the experimental measurements (Figure 5.5-B).

# 5.5.3. Prediction of carbonation uptake efficiency with changes in concrete parameters

The mathematical model can be used to predict the total carbonation uptake efficiency with changes in the initial concrete composition (e.g. water/cement ratio) or operating parameters (e.g. partial pressure of CO<sub>2</sub> gas or gas flow-rate). Figure 5.6 shows the changes in carbonation efficiency with the percentage of

CO<sub>2</sub> in gas mixture and the initial specific surface area of concrete. By increasing the CO<sub>2</sub> percentage in the gas mixture from 20% to 40%, the CO<sub>2</sub> partial pressure doubled in the gas phase and resulted in a higher concentration of CO<sub>2</sub> in both gas and aqueous phase. The initial carbonation reaction rates increased with the rise in CO<sub>2</sub> (aq) (Eq. 5.13) and, consequently, more calcium carbonate was formed during the initial 20 minutes of carbonation (Figure 5.6-A). Formation of calcium carbonate inhibited further carbonation and CO<sub>2</sub> uptake ceased after 12 minutes which happened earlier compared to carbonation with lower CO<sub>2</sub> percentage of 20% (26 minutes). The model showed that the exposed specific surface area of reacting cement compounds, such as C<sub>3</sub>S and Ca(OH)<sub>2</sub>, reduced significantly within an hour of carbonation. The specific surface area of solid calcium hydroxide reduced to a negligible amount and that of C<sub>3</sub>S reduced to 8.6% of the initial specific surface area. The results from the mathematical model were comparable to the experimental results (shown in symbols in Figure 5.6-A). The extent of carbonation efficiency remained in the same range as the gas mixture with 20% CO<sub>2</sub>. In other words, a higher partial pressure of CO<sub>2</sub> increased the rate of carbonation but when the solid calcium carbonate formed during carbonation reached the same value as the case with 20% CO<sub>2</sub>, carbonation ceased and the efficiency reached a plateau at the same value with lower CO<sub>2</sub> partial pressure. The decrease in CO<sub>2</sub> percentage to 10% delayed the CO<sub>2</sub> uptake and the carbonation efficiency did not reach its maximum value during 30 minutes of carbonation.

An increase in the specific surface area of reactive cement compounds increases the dissolution rate and, therefore, the overall carbonation rate (Eq.

5.13). The specific surface area of concrete can be increased by, for example, using smaller size cement particles. In the model, the specific surface area for each compound was calculated from the total specific surface area  $(a_s)$  and the concentration of that compound (Eq. 5.20). The assumption for these simulation results is that other concrete properties such as mass of cement in the specimen remain constant and the only parameter changing is the specific surface area of concrete resulting in a higher surface area for each compound. A ten times increase in the specific surface area increased the carbonation efficiency from 17% to 32% within 30 minutes. With an increase in the initial specific surface area, more calcium carbonate should deposit in order to decrease the specific surface area to the extent that carbonation ceases. In other words, with an increase in specific surface area of active cement compounds, both the rate and extent of carbonation increased. When the specific surface area was reduced to half, the carbonation ceased at a lower efficiency of 8.4% implying that precipitation of a smaller amount of calcium carbonate stopped the carbonation process.

#### 5.6. Dimensional Analysis

Dimensional analysis was performed in order to study the effect of different mechanisms such as CO<sub>2</sub> gas transport, gas-liquid mass transfer to pore water and carbonation reactions on the carbon dioxide uptake by concrete. The equations were transformed into dimensionless version using maximal concentrations [14, 16, 17, 34, 35]. For cement phases these maximal values are calculated from the hydration model immediately before commencement of carbonation, while for

calcium carbonate, the maximum value was calculated from the initial concentration of reactive cement species (Table 5.4). For porosity, the maximum value was defined as the porosity of 4-hour hydrated concrete as it decreases with carbonation. For gas phase CO<sub>2</sub> concentration, the inflow CO<sub>2</sub> concentration was used as the maximum as shown in Table 5.4.

The dimensionless parameters used in this study were:

(1) Damköhler number (Da) which relates a reaction rate to a convection rate [36]; in this study the Da was defined as the maximum rate of carbonation reaction for compound i (Eq. 5.13) to advection rate of  $CO_2$  gas:

$$Da = L(r_{\text{im}}) / \left[ (\varepsilon \varphi^{a})_{0} [CO_{2}(g)]_{0} v \right]$$
(5.21)

A *Da* number was defined for each cement compound which undergoes carbonation: *Da1* (C<sub>3</sub>S), *Da2* (C<sub>2</sub>S), *Da3* (C-S-H), *Da4* (AFt) and *Da5* (Ca(OH)<sub>2</sub>

- (s)). The carbonation reaction rates were the rate limiting process during accelerated carbonation curing as explained later.
- (2) mass transfer Stanton number (St) indicating the ratio of gas-liquid mass transfer to the advective mass transfer [37] and in this study was defined as the relation of  $CO_2$  gas-liquid mass transfer rate to advection rate of  $CO_2$  (g):

$$St = Lk_{\rm t}/v \tag{5.22}$$

and (3) Inverse Peclet number (IPN) relating the rate of dispersive to advective  $CO_2(g)$  transport. A low IPN means advection dominates gas dispersion and vice versa.

$$IPN = D_{\text{CO}_2(g)}/vL \tag{5.23}$$

Time and space were also defined in dimensionless form as  $\tau = vt/L$  and  $\xi = x/L$  (x represents the distance from the inlet surface of specimen), respectively. The time scale was selected as L/v which is the advection time-scale for  $CO_2$  gas.

Using the non-dimensional parameters, the mass balance equations for CO<sub>2</sub> gas transport and gas-liquid mass transfer can be written as Eq. 5.4.10 in Table 5.4, for dissolved CO<sub>2</sub> transport and carbonation reactions as in Eq. 5.4.11, and for the active cement compounds (such as C<sub>3</sub>S and C<sub>2</sub>S) as in Eq. 5.4.12. The values of dimensionless numbers are listed in Table 5.5.

The dimensionless numbers showed the competition between different carbonation processes. The dimensionless analysis was performed on accelerated concrete curing in flow-through reactor with flow-rate of 1.17 Lpm and water/cement ratio of 0.26. The dimensionless parameter of CO<sub>2</sub> gas-liquid mass transfer (*St*) was 16.45 showing a higher rate of CO<sub>2</sub> gas-liquid mass transfer compared to CO<sub>2</sub> gas advection. The Damköhler number for carbonation reaction of C<sub>3</sub>S and C<sub>2</sub>S was 0.5 and 0.02, respectively, suggesting that the overall CO<sub>2</sub> uptake rate is more dependant on the carbonation reaction rate than the advection rate of CO<sub>2</sub> (g) when the gas flow-rate is 1.17 Lpm. However, at slower flow-rates, the advection term might become rate limiting compared to chemical reaction rates.

The *IPN* number was 2.6x10<sup>-3</sup>, indicating a much higher advection rate for CO<sub>2</sub> gas compared to dispersion. As the Damkohler and Stanton dimensionless numbers suggest, the carbonation reaction rates were the limiting processes during carbonation curing in 1-D flow-through reactor with gas flow-rate of 1.17 Lpm, i.e. the CO<sub>2</sub> gas-liquid mass transfer and advection rate were not the rate limiting

mechanisms at this flow-rate. These parameters were changed in the model in order to monitor the sensitivity of carbonation efficiency on these mechanisms. The changes in 30 minutes carbonation efficiency with changes in these dimensionless parameters are shown in Figure 5.7. The 30-minutes carbonation efficiency changed with dimensionless Damköhler numbers as seen in Figure 5.7-A. The 30-min carbonation efficiency increased from 17% to 19.1% with an increase in the Damköhler number for C<sub>3</sub>S carbonation (Da1) from the initial value of 0.5 to 50. The carbonation efficiency did not increase to that extent with changes in the Damköhler number for  $C_2S$  carbonation (Da2). The reason is that each mole of C<sub>3</sub>S reacts with 3 moles of CO<sub>2</sub> while for C<sub>2</sub>S it takes 2 moles of CO<sub>2</sub> for carbonation. The variation in Damköhler number can happen, for instance, by changing the specific surface area of concrete and, therefore, changing the carbonation rate of active cement species (Eq. 5.13). The increase in carbonation efficiency with an increase in the specific surface area of concrete was also seen in Figure 5.6-B.

The efficiency was stable to the gas-liquid mass transfer dimensionless number (St) at values higher than 10. An increase in St from the initial value of 16.45 to 35, changed the 30-min carbonation efficiency from 17% to 17.5%, which shows that carbon dioxide gas-liquid mass transfer was not the rate controlling process and the carbonation efficiency was rather insensitive to the exact value of gas-liquid mass transfer coefficient ( $k_1$ ). However, at values lower than 1, the gas-liquid mass transfer was rate controlling and, therefore, the carbonation uptake efficiency becomes more sensitive to the exact value of  $k_1$ .

A 50% variation of *IPN*, changed the 30-min carbonation efficiency by only 0.1% which shows negligible effect of gas dispersion on carbonation efficiency. Therefore, at the gas flow-rate of 1.17 Lpm, CO<sub>2</sub> dispersion coefficient played a negligible role in carbonation efficiency (plug flow condition) while the uptake increased slightly at higher *IPN* numbers (more dispersion).

#### 5.7. Conclusions

The accelerated carbonation curing was performed on 4 hour-hydrated concrete specimens in a 1-D flow-through reactor. The mathematical model developed in this study for accelerated carbonation curing was verified by the experimental results for different gas flow-rates (0.08, 1.17 and 2 Lpm), water/cement ratios (0.26 and 0.32 with flow-rate of 1.17 Lpm) and percentage of CO<sub>2</sub> in gas mixture (20% and 40% with flow-rate of 1.17 Lpm and w/c ratio of 0.26). Our experimental set-up ensures constant temperature and inlet CO<sub>2</sub> pressure during carbonation curing and thus allows the chemical and CO<sub>2</sub> transport modeling without accounting for temperature and pressure changes. A surface area reduction term was used in order to model the effect of formation and deposition of solid calcium carbonate on exposed surface area of active cement compounds. The model can be used in order to predict the CO<sub>2</sub> uptake efficiency under different operating conditions. An increase in the partial pressure of CO<sub>2</sub> gas increased the rate of CO<sub>2</sub> uptake by concrete but the extent of carbonation did not change significantly (i.e. remained as 17%). The mathematical model suggests that the extent of carbonation efficiency can increase with an increase in specific

surface area of concrete. The 30 minute carbonation efficiency increased from 17% to 32% with a ten times increase in the initial specific surface area of concrete. With an increase in specific surface area of active cement compounds, both the rate and extent of carbonation increased.

Several dimensionless numbers were used to study the sensitivity of carbonation to different carbonation processes such as CO<sub>2</sub> gas dispersion, gasliquid mass transfer and carbonation rate. The carbonation efficiency during 30 minutes of carbonation was not limited by the rate of CO<sub>2</sub> gas-liquid mass transfer as the Stanton number suggests. The carbonation reaction rates of unhydrated cement compounds were the rate controlling processes during this period as the Damköhler numbers suggest, i.e. higher CO<sub>2</sub> uptake could be achieved by improving the dissolution and carbonation rates of unhydrated cement. The rates can be improved by increasing the exposed surface area of these active cement compounds. The efficiency increased from 17% to 19% when carbonation rate of C<sub>3</sub>S was increased two orders of magnitude but did not increase to that extent with changes in carbonation rate of C<sub>2</sub>S.

#### 5.8. Acknowledgments

The authors would like to acknowledge the National Science and Engineering Research Council of Canada, St. Lawrence Cement and CJS Technology for funding of this project and le fonds québécois de la recherche sur la nature et les technologies for providing a doctorate fellowship to SK.

## 5.9. Notation

$R_{ m agg/c}$	aggregate/cement weight ratio (dimensionless)
$R_{ m w/c}$	water/cement weight ratio (dimensionless)
$ ho_{ m c}$	density of cement (kg.m <sup>-3</sup> )
$ ho_{ m agg}$	density of aggregate (kg.m <sup>-3</sup> )
$ ho_{ m w}$	density of water (kg.m <sup>-3</sup> )
$ ho_{ m con}$	density of concrete (kg.m <sup>-3</sup> )
$a_{\rm s}$	specific surface area of concrete per unit volume (m <sup>2</sup> .m <sup>-3</sup> of concrete)
$a_{\rm s0}$	initial surface area of concrete per unit volume (m <sup>2</sup> .m <sup>-3</sup> of concrete)
$a_{\mathrm{s,i}}$	surface area of species $i$ per unit volume of concrete (m <sup>2</sup> .m <sup>-3</sup> )
$\epsilon, \epsilon_0$	concrete current and initial porosity (dimensionless)
$\Delta \overline{V}_{ m H,i} \ \Delta \overline{V}_{ m i}$	change in volume per mole of species $i$ reacting during hydration and carbonation (m <sup>3</sup> .mol <sup>-1</sup> )
$\phi^{\rm w}$	fraction of pores filled with water (dimensionless)
$\phi^{a}$	fraction of pores filled with air (dimensionless)
<u>S</u>	concrete specific surface area (m <sup>2</sup> .kg <sup>-1</sup> )
$\overline{V_{ m i}}$	molar volume of species $i$ (m <sup>3</sup> .mol <sup>-1</sup> )
$MW_{\rm i}$	molar weight of species $i$ (kg.mol <sup>-1</sup> )
$k_{\mathrm{H,i}}, n_{\mathrm{i}}$	rate constant and hydration power-law coefficient of species $i$ (s <sup>-1</sup> ,
$[i],[i]_0$	dimensionless) current and initial molar concentrations of species $i$ , for $CO_2$ (g),
[,1,[,1]]	CO <sub>2</sub> (aq) and Ca(OH) <sub>2</sub> (aq) intrinsic concentration (mol.m <sup>-3</sup> of pore air/water) and for solid compounds (mol.m <sup>-3</sup> of concrete)
$r_{ m H,i}$	hydration rate of species $i$ in the absence of gypsum (mol.m <sup>-3</sup> .s <sup>-1</sup> )
$r_{\mathrm{H,i,S}}$	hydration rate of species $i$ in the presence of gypsum (mol.m <sup>-3</sup> .s <sup>-1</sup> )
$k_{t}$	overall gas-liquid mass transfer coefficient for CO <sub>2</sub> (s <sup>-1</sup> )
$k_{\mathrm{Henry}}$	Henry's constant for CO <sub>2</sub> (aqueous phase concentration/gas phase
$k \ k' \ k_{ m i}$	concentration) (dimensionless) CO <sub>2</sub> hydration reaction constant of Eq. 5.4 (high pH) (mol.m <sup>-3</sup> .s <sup>-1</sup> ) CO <sub>2</sub> hydration reaction constant of Eq. 5.3 (low pH) (s <sup>-1</sup> ) rate constants of carbonation reaction for species <i>i</i> (m.s <sup>-1</sup> )
$k_{\rm s}$	mass transfer coefficient for the dissolution of Ca(OH) <sub>2</sub> (s) (m.s <sup>-1</sup> )

 $f_{\rm C}$  specific surface area reduction per mole of CaCO<sub>3</sub> formed due to

carbonation (m<sup>2</sup>.mol<sup>-1</sup>)

v gas seepage velocity (m.s<sup>-1</sup>)

 $D_{\text{CO}_2(g)}$  dispersion coefficient of CO<sub>2</sub> gas (m<sup>3</sup>.s<sup>-1</sup>)

 $D_{\text{CO}_{2}(\text{aq})}^{*}$  effective diffusivity of dissolved CO<sub>2</sub> (m<sup>3</sup>.s<sup>-1</sup>)

 $r_{\rm CO_2(aq)}$  CO<sub>2</sub> dissolution term (mol.m<sup>-3</sup>.s<sup>-1</sup>)

 $r_i$  carbonation rate of species i (mol.m<sup>-3</sup>.s<sup>-1</sup>)

 $r_{\rm H.C}$  CO<sub>2</sub> hydration term (mol.m<sup>-3</sup>.s<sup>-1</sup>)

 $r_{\rm D.CH}$  dissolution rate of solid calcium hydroxide (mol.m<sup>-3</sup>.s<sup>-1</sup>)

 $r_{\rm CH}$  carbonation rate of dissolved Ca(OH)<sub>2</sub> (mol.m<sup>-3</sup> pore water.s<sup>-1</sup>)

ω moisture concentration in pores (mol.m<sup>-3</sup> pore)

#### **Dimensional Analysis:**

Stanton gas-liquid mass transfer number (dimensionless)

Damköhler number (dimensionless)

IPN Inverse Peclet number (dimensionless)

 $\begin{array}{ll} \tau & \text{dimensionless time} \\ \xi & \text{dimensionless space} \end{array}$ 

L depth of the concrete specimen (m)

#### 5.10. References

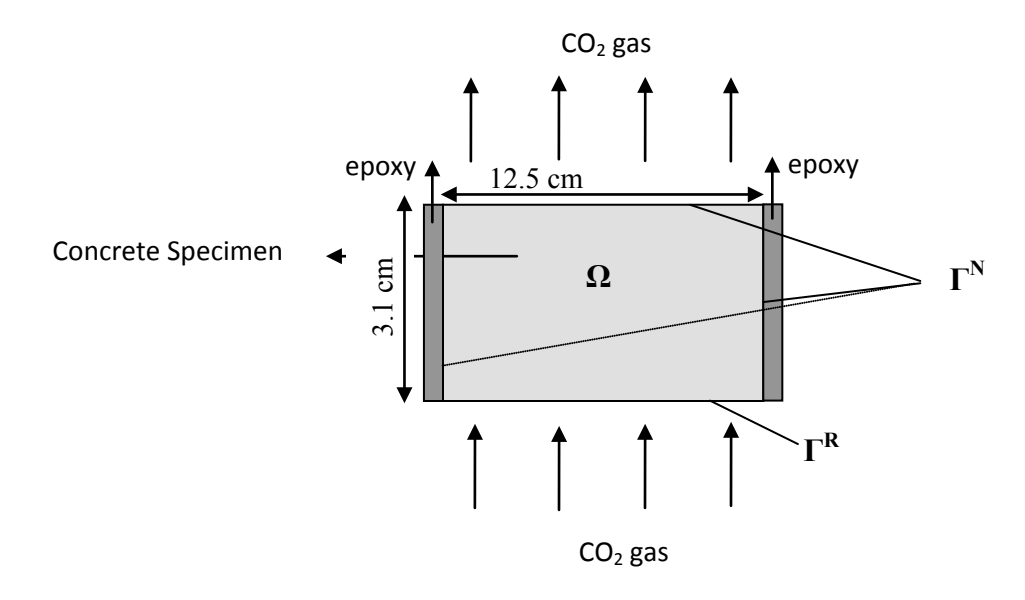
- [1] IPCC, Special report on carbon dioxide capture and storage. **2005**: Cambridge University Press.
- [2] Wilson, E.J., M.G. Morgan, J. Apt, M. Bonner, C. Bunting, J. Gode, R.S. Haszeldine, C.C. Jaeger, D.W. Keith, S.T. McCoy, M.F. Pollak, D.M. Reiner, E.S. Rubin, A. Torvanger, C. Ulardic, S.P. Vajjhala, D.G. Victor, and I.W. Wright, Regulating the geological sequestration of CO<sub>2</sub>. *Environ. Sci. Technol.*, **2008**, 42 (8), 2718-22.
- [3] White, C.M., B.R. Strazisar, E.J. Granite, J.S. Hoffman, and H.W. Pennline, Separation and capture of CO<sub>2</sub> from large stationary sources and sequestration in geological formations--coalbeds and deep saline aquifers. *J. Air Waste Manag. Assoc.*, **2003**, 53 (6), 645-715.
- [4] Riestenberg, D.E., C. Tsouris, P.G. Brewer, E.T. Peltzer, P. Walz, A.C. Chow, and E.E. Adams, Field studies on the formation of sinking CO<sub>2</sub> particles for ocean carbon sequestration: effects of injector geometry on particle density and dissolution rate and model simulation of plume behavior. *Environ. Sci. Technol.*, **2005**, 39 (18), 7287-7293.
- [5] Maroto-Valer, M.M., D.J. Fauth, M.E. Kuchta, Y. Zhang, and J.M. Andresen, Activation of magnesium rich minerals as carbonation feedstock materials for CO<sub>2</sub> sequestration. *Fuel Process. Technol.*, **2005**, 86 (14-15), 1627.
- [6] Huijgen, W.J.J., G.J. Witkamp, and R.N.J. Comans, Mineral CO<sub>2</sub> sequestration by steel slag carbonation. *Environ. Sci. Technol.*, **2005**, 39 (24), 9676-9682.
- [7] Huntzinger, D.N., J.S. Gierke, S.K. Kawatra, T.C. Eisele, and L.L. Sutter, Carbon dioxide sequestration in cement kiln dust through mineral carbonation. *Environ. Sci. Technol.*, **2009**, 43 (6), 1986-1992.
- [8] Huijgen, W.J.J. and R.N.J. Comans, Carbon dioxide storage by mineral carbonation. IEA GHG report 2005/11. **2005**, Cheltenham, UK: Energy Research Centre of the Netherlands
- [9] Jarvis, K., R.W. Carpenter, T. Windman, Y. Kim, R. Nunez, and F. Alawneh, Reaction mechanisms for enhancing mineral sequestration of CO<sub>2</sub>. *Environ. Sci. Technol.*, **2009**, 43 (16), 6314-6319.
- [10] Monkman, S. and Y. Shao, Carbonation curing of slag-cement concrete for binding CO<sub>2</sub> and improving performance. *J. Mater. Civ. Eng.*, **2010**, 22 (4).
- [11] Shao, Y., M.S. Mirza, and X. Wu, CO<sub>2</sub> sequestration using calcium-silicate concrete. *Can. J. Civ. Eng.*, **2006**, 33 (6), 776-784.
- [12] Monkman, S., Maximizing carbon uptake and performance gain in slagcontaining concretes through early carbonation. 2008, McGill University: Montreal, QC, Canada.

- [13] Papadakis, V.G., C.G. Vayenas, and M.N. Fardis, Experimental investigation and mathematical modeling of the concrete carbonation problem. *Chem. Eng. Sci.*, **1991c**, 46 (5-6), 1333.
- [14] Papadakis, V.G., C.G. Vayenas, and M.N. Fardis, A reaction engineering approach to the problem of concrete carbonation. *AlChE J.*, **1989**, 35 (10), 1639-1650.
- [15] Saetta, A.V., B.A. Schrefler, and R.V. Vitaliani, The carbonation of concrete and the mechanism of moisture, heat and carbon dioxide flow through porous materials. *Cem. Concr. Res.*, **1993**, 23 (4), 761.
- [16] Peter, M.A., A. Muntean, S.A. Meier, and M. Böhm, Competition of several carbonation reactions in concrete: a parametric study. *Cem. Concr. Res.*, **2008**, 38 (12), 1385-1393.
- [17] Meier, S.A., M.A. Peter, A. Muntean, and M. Böhm, Dynamics of the internal reaction layer arising during carbonation of concrete. *Chem. Eng. Sci.*, **2007**, 62 (4), 1125-1137.
- [18] Papadakis, V.G., C.G. Vayenas, and M.N. Fardis, Fundamental modeling and experimental investigation of concrete carbonation. *ACI Mater. J.*, **1991b**, 88 (4), 363-373.
- [19] Burkan Isgor, O. and A.G. Razaqpur, Finite element modeling of coupled heat transfer, moisture transport and carbonation processes in concrete structures. *Cem. Concr. Compos.*, **2004**, 26 (1), 57.
- [20] Bary, B. and A. Sellier, Coupled moisture--carbon dioxide-calcium transfer model for carbonation of concrete. *Cem. Concr. Res.*, **2004**, 34 (10), 1859.
- [21] Lea, F.M., The Chemistry of Cement and Concrete. **1970**, London: Edward Arnold.
- [22] Monkman, S. and Y. Shao, Assessing the carbonation behavior of cementitious materials. *J. Mater. Civ. Eng.*, **2006**, 18 (6), 768.
- [23] Kashef-Haghighi, S. and S. Ghoshal., CO<sub>2</sub> sequestration in concrete through accelerated carbonation curing in a flow-through reactor. *Ind. Eng. Chem. Res.*, **2010**, 49, 1143-1149.
- [24] Bullard, J.W., H.M. Jennings, R.A. Livingston, A. Nonat, G.W. Scherer, J.S. Schweitzer, K.L. Scrivener, and J.J. Thomas, Mechanisms of cement hydration. *Cem. Concr. Res.*, **2010**, In Press.
- [25] Fernandez Bertos, M., S.J.R. Simons, C.D. Hills, and P.J. Carey, A review of accelerated carbonation technology in the treatment of cement-based materials and sequestration of CO<sub>2</sub>. *J. Hazard. Mater.*, **2004**, 112 (3), 193.
- [26] Pinsent, B.R.W., L. Pearson, and F.J.W. Roughton, The kinetics of combination of carbon dioxide with hydroxide ions. *Trans. Faraday Soc.*, **1956**, 52, 1512-1520.
- [27] Kutchko, B.G., B.R. Strazisar, D.A. Dzombak, G.V. Lowry, and N. Thaulow, Degradation of well cement by CO<sub>2</sub> under geologic sequestration conditions. *Environ. Sci. Technol.*, **2007**, 41 (13), 4787-4792.
- [28] Teir, S., S. Eloneva, and R. Zevenhoven, Production of precipitated calcium carbonate from calcium silicates and carbon dioxide. *ENERG CONVERS MANAGE*, **2005**, 46 (18-19), 2954-2979.

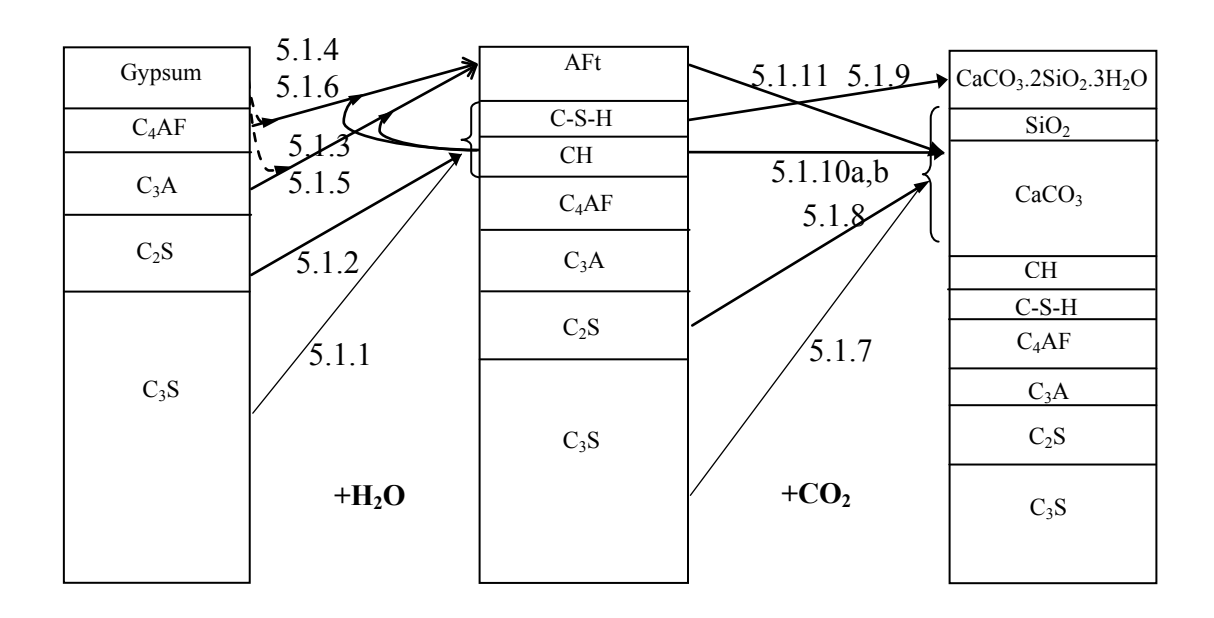
- [29] Goodbrake, C.J., J.F. Young, and R.L. Berger, Reaction of hydraulic calcium silicates with carbon dioxide and water. *J. Am. Ceram. Soc.*, **1979**, 62 (9-10), 488-491.
- [30] Lamond, J. and J. Pielert, Significance of tests and properties of concrete and concrete-making materials. **2006**: ASTM International. 645.
- [31] Ramachandran, P.A. and M.M. Sharma, Absorption with fast reaction in a slurry containing sparingly soluble fine particles. *Chem. Eng. Sci.*, **1969**, 24 (11), 1681.
- [32] Papadakis, V.G., C.G. Vayenas, and M.N. Fardis, Physical and chemical characteristics affecting the durability of concrete. *ACI Mater. J.*, **1991a**, 8 (2), 186-196.
- [33] Anderson, T.F., Surface area measurement in calcite grains by isotopic exchange with C14-labeled carbon dioxide

Geochim. Cosmochim. Ac., 1968, 32, 1177-1186.

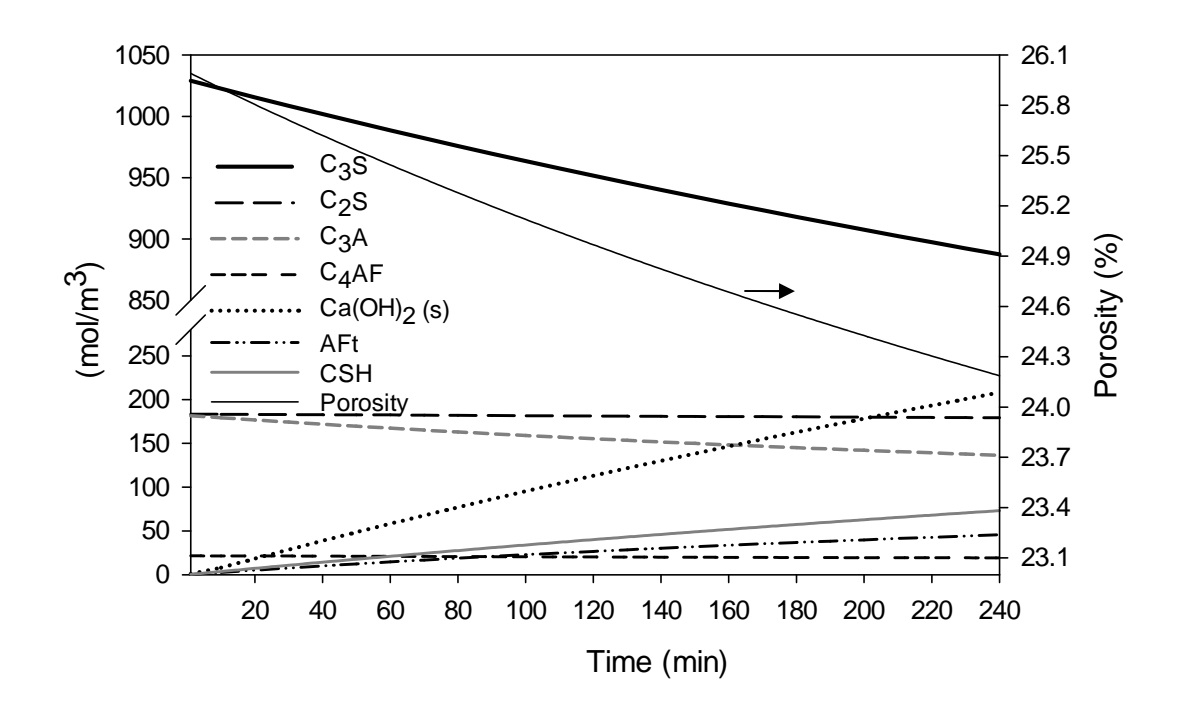
- [34] Logan, J.D., Transport Modeling in Hydrogeochemical Systems. Interdisciplinary Applied Mathematics. **2001**, New York: Springer-Verlag.
- [35] Yang, J., D.W. Hand, J.C. Crittenden, D.R. Hokanson, E.J. Oman, and D. Audeves, Dynamic mathematical modeling of an isothermal three-phase reactor: model development and validation. *J. Environ. Eng.*, **2003**, 129 (7), 586.
- [36] Fogler, H.S., Elements of chemical reaction engineering. Fourth ed, ed. Editor, P.H. **2006**.
- [37] Deckwer, W.D., R. Burckhart, and G. Zoll, Mixing and mass transfer in tall bubble columns. *Chem. Eng. Sci.*, **1974**, 29 (11), 2177-2188.
- [38] Pichler, C., R. Lackner, and H.A. Mang, A multiscale micromechanics model for the autogenous-shrinkage deformation of early-age cement-based materials. *Eng. Fract. Mech.*, **2007**, 74 (1-2), 34.
- [39] Sarkar, S., S. Mahadevan, J.C.L. Meeussen, H. van der Sloot, and D.S. Kosson, Numerical simulation of cementitious materials degradation under external sulfate attack. *Cem. Concr. Compos.*, **2010**, 32, 241–252.



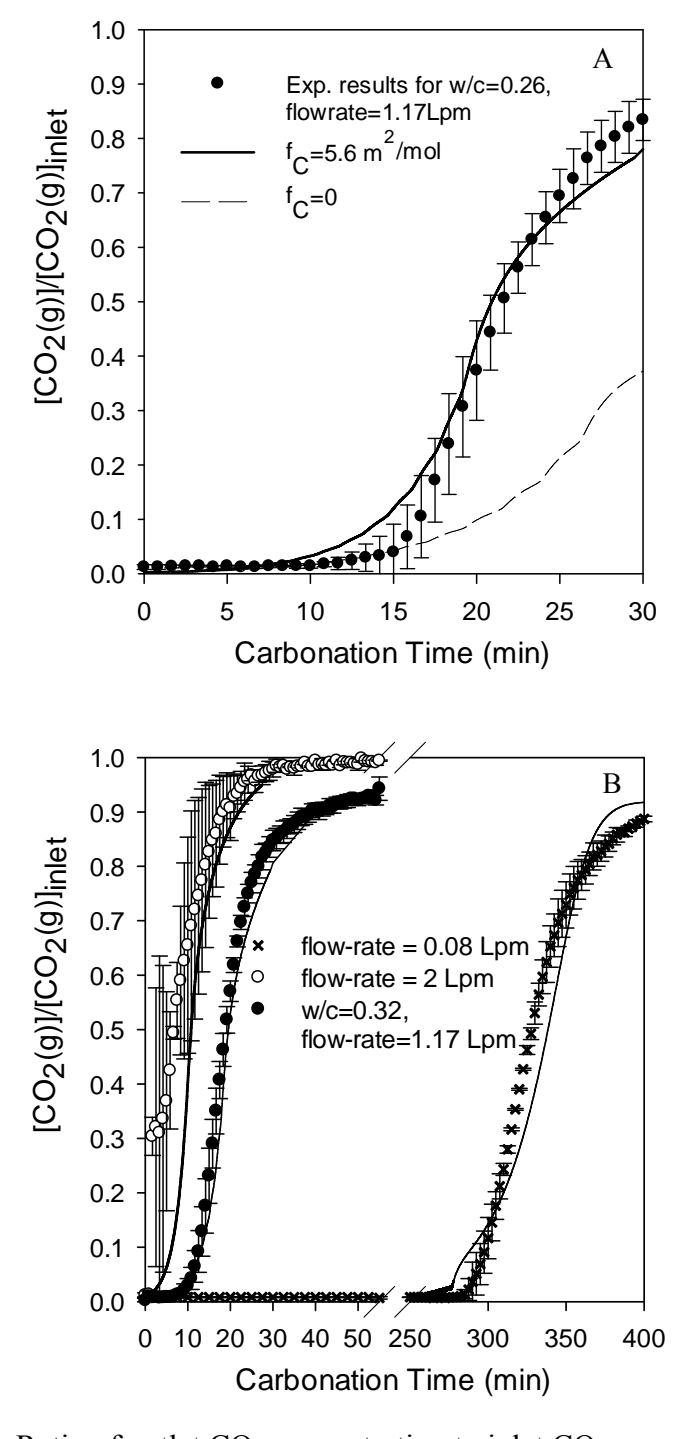
**FIGURE 5.1.** Schematic view of concrete carbonation in the 1-D flow-through reactor



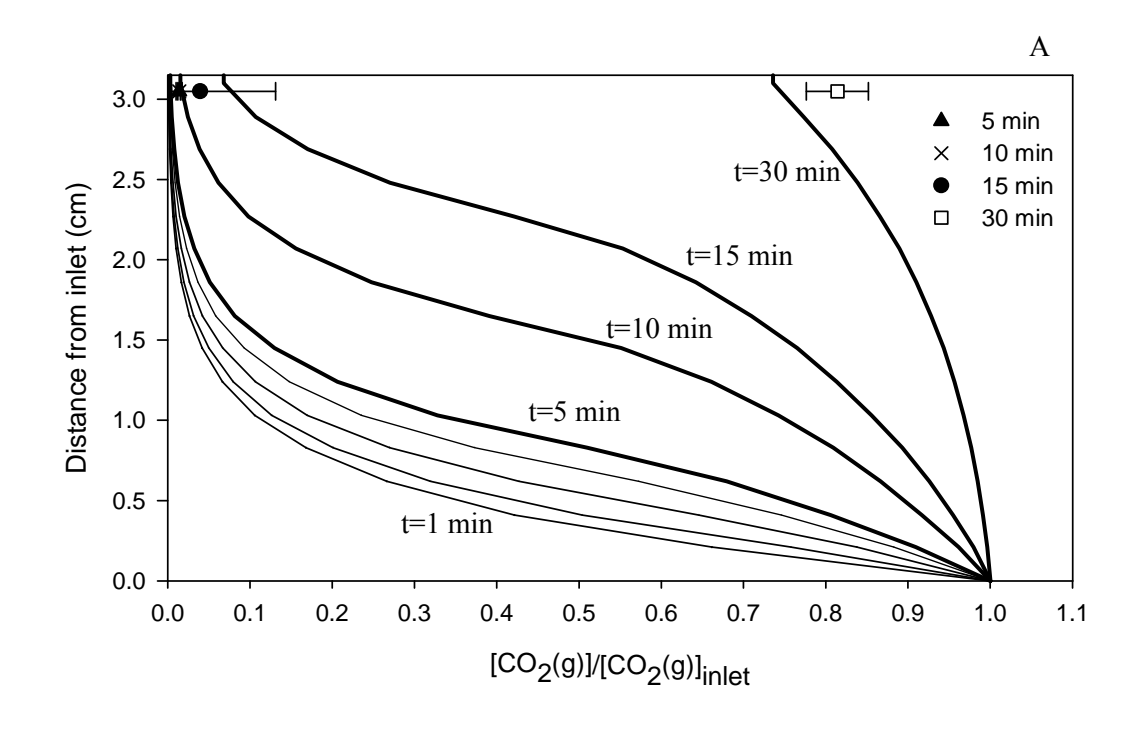
**FIGURE 5.2.** Changes in cement composition during hydration and carbonation, the numbers on arrows are related to equation numbers in Table 5.1.

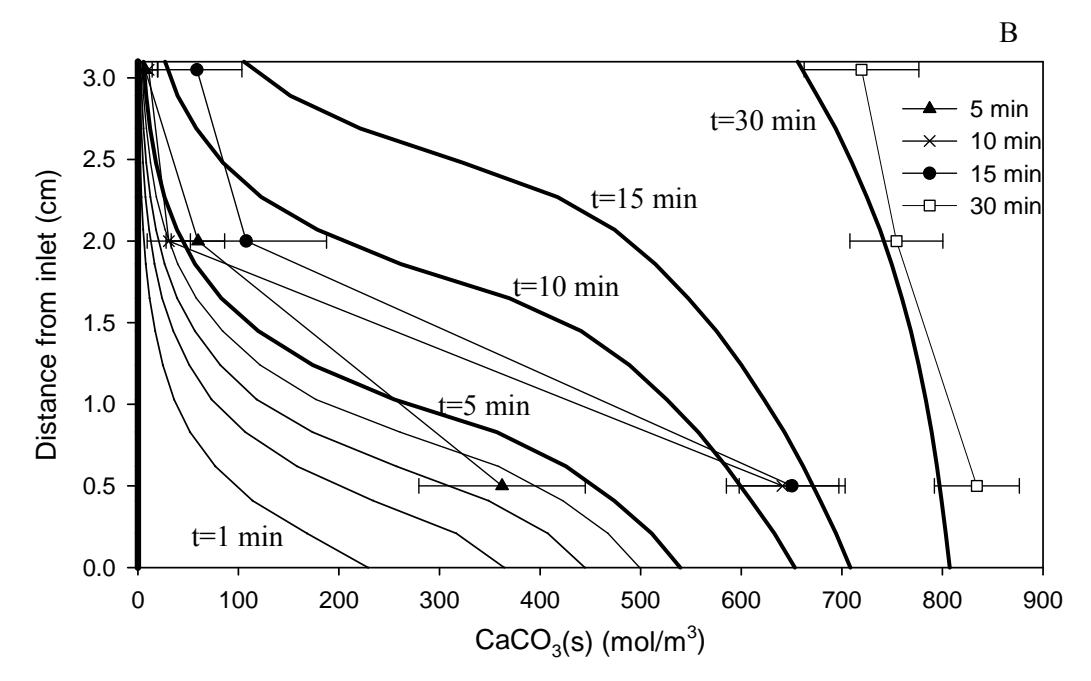


**FIGURE 5.3.** Concentration of cement phases during 4 hours of hydration calculated from the hydration model developed in this study

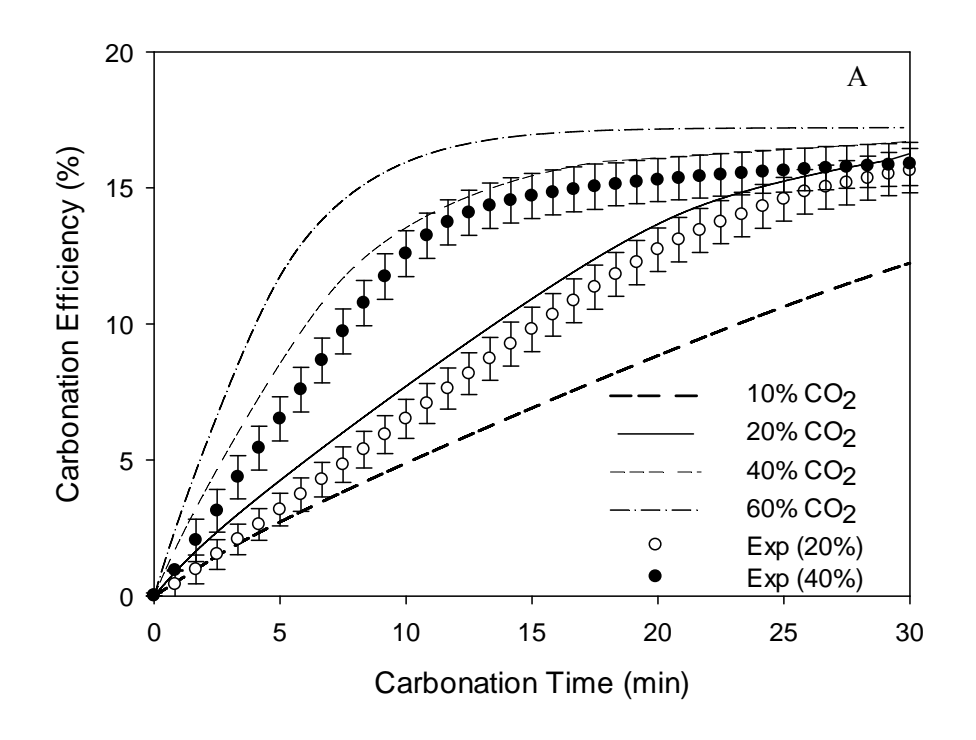


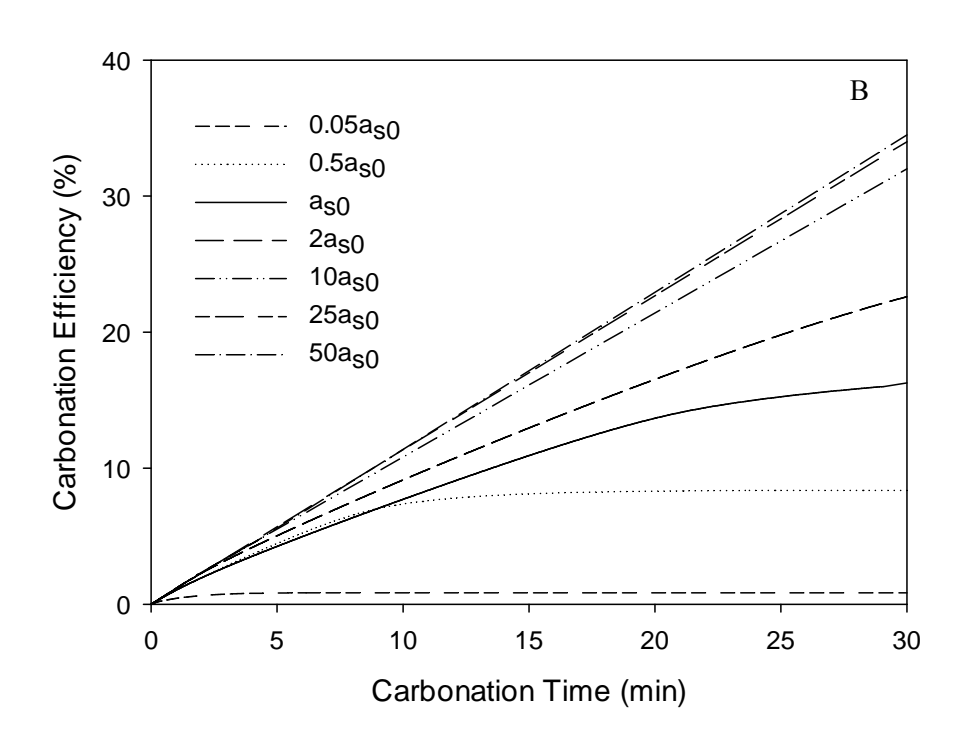
**FIGURE 5.4.** Ratio of outlet  $CO_2$  concentration to inlet  $CO_2$  concentration vs. carbonation time, symbols refer to experimental results and solid lines refer to the mathematical model (A) flow-rate: 1.17 Lpm, w/c: 0.26 (B) flow-rates: 0.08 and 2 Lpm, w/c: 0.26 and flow-rate: 1.17 Lpm, w/c: 0.32 (experimental results have been published in an earlier publication [23]).



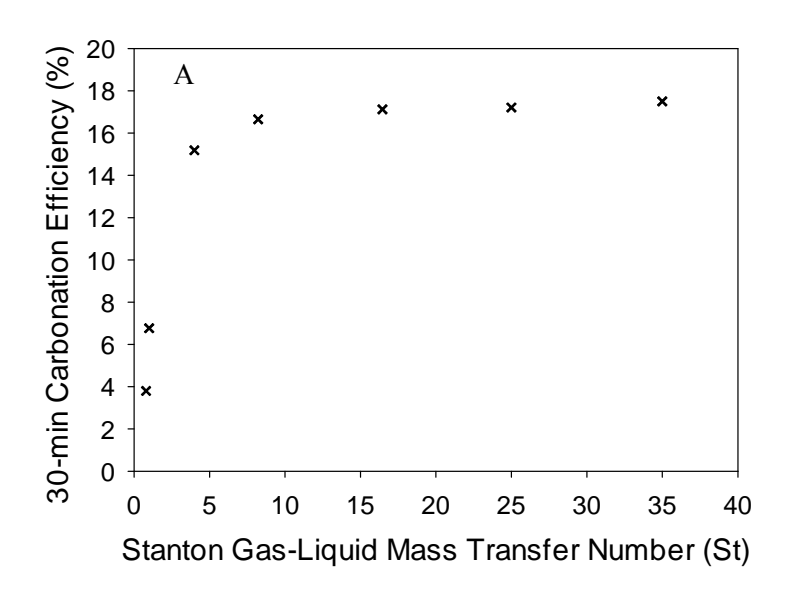


**FIGURE 5.5.** (A) Ratio of  $CO_2(g)$  concentration in pores to inlet  $CO_2(g)$  concentration along the length of concrete specimen during carbonation, the measured values at the outlet are shown by symbols (B) production of solid  $CaCO_3$  along the length of the compact concrete with carbonation time, experimental measurements are shown by symbols





**FIGURE 5.6.** Prediction of 30-minute carbonation efficiency by the mathematical model with changes in (A) percentage of  $CO_2$  in the gas mixture, the experimental results for 20% and 40%  $CO_2$  in  $N_2$  balance are shown by symbols and (B) the specific surface area of concrete.



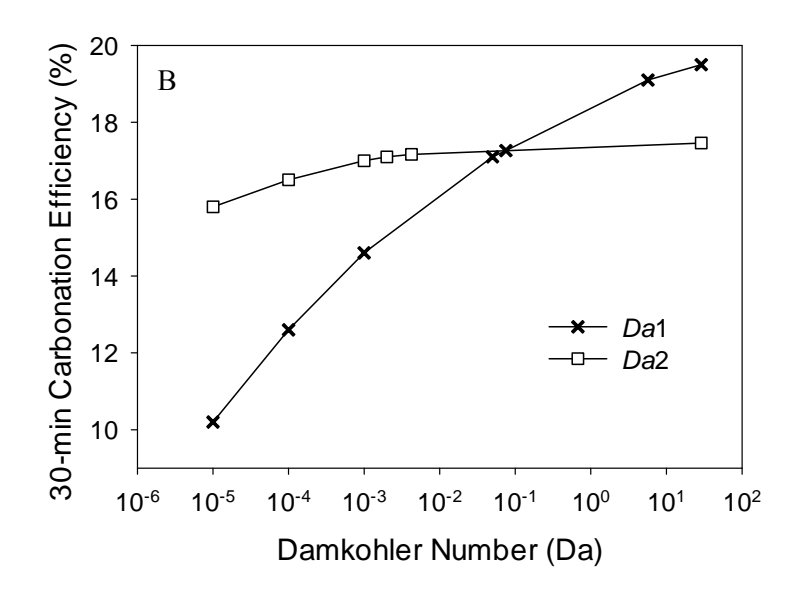


**FIGURE 5.7.** Sensitivity analysis with respect to (A) Damköhler number and (B) Stanton number.

**TABLE 5.1.** Chemical reactions during hydration and carbonation of cement

#### **Hydration Reactions**

$$2(3\text{CaO.SiO}_2) + 6\text{H}_2\text{O} \xrightarrow{\text{r}_{\text{H,C}_3\text{S}}} (3\text{CaO.2SiO}_2.3\text{H}_2\text{O}) + 3\text{Ca}(\text{OH})_2$$
 (5.1.1)

$$2(2\text{CaO.SiO}_2) + 4\text{H}_2\text{O} \xrightarrow{\text{r}_{H,C_2S}} (3\text{CaO.2SiO}_2.3\text{H}_2\text{O}) + \text{Ca(OH)}_2$$
 (5.1.2)

$$(3\text{CaO.Al}_2\text{O}_3) + 3\text{CaSO}_4.2\text{H}_2\text{O} + 26\text{H}_2\text{O} \xrightarrow{r_{\text{H,C}_3\text{A,S}}}$$

$$(3\text{CaO.Al}_2\text{O}_3.3\text{CaSO}_4.32\text{H}_2\text{O})$$
(5.1.3)

$$(4\text{CaO.Al}_2\text{O}_3.\text{Fe}_2\text{O}_3) + 2\text{Ca}(\text{OH})_2 + 2(\text{CaSO}_4.2\text{H}_2\text{O}) + 18\text{H}_2\text{O} \xrightarrow{r_{\text{H,C}_4\text{AF,S}}}$$

$$(6\text{CaO.Al}_2\text{O}_3.\text{Fe}_2\text{O}_3.2\text{CaSO}_4.24\text{H}_2\text{O})$$

$$(5.1.4)$$

$$(3\text{CaO.Al}_2\text{O}_3) + \text{Ca(OH)}_2 + 12\text{H}_2\text{O} \xrightarrow{\text{r}_{\text{H,C}_3\text{A}}}$$

$$(5.1.5)$$
 $(3\text{CaO.Al}_2\text{O}_3.\text{Ca(OH)}_2.12\text{H}_2\text{O})$ 

$$(4\text{CaO.Al}_2\text{O}_3.\text{Fe}_2\text{O}_3) + 4\text{Ca(OH)}_2 + 22\text{H}_2\text{O} \xrightarrow{\text{r}_{\text{H,C}_4\text{AF}}}$$

$$(6\text{CaO.Al}_2\text{O}_3.\text{Fe}_2\text{O}_3.2\text{Ca(OH)}_2.24\text{H}_2\text{O})$$
(5.1.6)

#### **Carbonation Reactions**

$$3\text{CaO.SiO}_2(s) + 3\text{CO}_2(aq) + n\text{H}_2\text{O} \xrightarrow{\text{r}_{\text{C}_3\text{S}}} \text{SiO}_2.n\text{H}_2\text{O} + 3\text{CaCO}_3$$
 (5.1.7)

$$2\text{CaO.SiO}_2(s) + 2\text{CO}_2(aq) + n\text{H}_2\text{O} \xrightarrow{\text{r}_{\text{C}_2\text{S}}} \text{SiO}_2.n\text{H}_2\text{O} + 2\text{CaCO}_3$$
 (5.1.8)

$$3\text{CaO.2SiO}_2.3\text{H}_2\text{O}(\text{s}) + 3\text{CO}_2(\text{aq}) \xrightarrow{r_{\text{CSH}}} 3\text{CaCO}_3.2\text{SiO}_2.3\text{H}_2\text{O}$$
 (5.1.9)

$$Ca(OH)_2(s) \xrightarrow{r_{D,CH}} Ca(OH)_2(aq)$$
 (5.1.10a)

$$Ca(OH)_2(aq) + CO_2(aq) \xrightarrow{r_{CH}} CaCO_3 + H_2O$$
(5.1.10b)

$$3\text{CaO.Al}_2\text{O}_3.3\text{CaSO}_4.32\text{H}_2\text{O}(\text{s}) + 3\text{CO}_2(\text{aq}) \xrightarrow{\text{r}_{AFt}} 3\text{CaCO}_3 + 3\text{CaSO}_4.2\text{H}_2\text{O} + 2\text{Al}(\text{OH})_3(\text{s}) + 9\text{H}_2\text{O}$$
 (5.1.11)

**TABLE 5.2.** Coefficients and constants for the cement hydration model

	C <sub>3</sub> S	C <sub>2</sub> S	C <sub>3</sub> A	C <sub>4</sub> AF
$k_{\rm H,i}  \text{x} 10^5  (\text{s}^{-1})  (20^{\rm o} \text{C})$	1.17	0.16	2.46	1.00
$n_{\rm i}$ (dimensionless)	2.65	3.10	2.41	3.81
$MW_i \times 10^3 (\text{kg.mol}^{-1})$	228.30	172.22	270.18	485.96
$m_i$ (dimensionless)	0.678	0.087	0.143	0.026
$\Delta \overline{V}_{\mathrm{H,i}} \times 10^5  (\mathrm{m}^3.\mathrm{mol}^{-1})$	5.33	3.94	14.98	11.28
$[i]_0  (\text{mol.m}^{-3})^{(a)}$	1042.00	177.25	185.71	18.77

(a) The initial concentrations were calculated as: 
$$[iJ_0 = \frac{m_i \rho_c (1 - \varepsilon \varphi^a)}{MW_i (R_{w/c} \frac{\rho_c}{\rho_w} + R_{agg/c} \frac{\rho_c}{\rho_{agg}} + 1)}$$

In the above equation,  $m_i$  is the weight fraction of species i per dry mass of cement,  $MW_i$  is the molar weight of species i,  $\varepsilon$  and  $\varphi^a$  are the initial porosity and fraction of pore filled with air, respectively.

**TABLE 5.3.** Constants used in the carbonation model

$D_{CO_2(g)}$	$D^*_{CO_2(aq)}$	[OH <sup>-</sup> ] <sub>eq</sub>	S	v	
5.19x10 <sup>-7 (a)</sup> (m <sup>2</sup> .s <sup>-1</sup> )	1.16x10 <sup>-13 (b)</sup> (m <sup>2</sup> .s <sup>-1</sup> )	43.2 (c,d) (mol.m <sup>-3</sup> )	1.69x10 <sup>3 (e)</sup> (m <sup>2</sup> .kg <sup>-1</sup> )	1.16x10 <sup>-2</sup> (m.s <sup>-1</sup> )	
k'	$k_{ m t}$	$k_{\rm Henry}$ at 25°C	k at 25°C	$k_{ m s}$	$k_{ m C2S} = k_{ m CSH}$
$3.58x10^{-2 \text{ (f)}} \\ \text{(s}^{-1})$	1.91 <sup>(g)</sup> (s <sup>-1</sup> )	8.317x10 <sup>-1</sup>	8.3 <sup>(f,h)</sup> (m <sup>3</sup> .mol <sup>-1</sup> .s)	5x10 <sup>-5 (h)</sup> (m.s <sup>-1</sup> )	1x10 <sup>-9 (c)</sup> (m.s <sup>-1</sup> )
$\Delta V_{\mathrm{C_3S}}$	$\Delta V_{ m C_2S}$	$\Delta V_{ m CSH}$	$\Delta V_{ m CH}$	$[CO_2(g)]_0$	$k_{\mathrm{C3S}}$
6.73x10 <sup>-5 (i)</sup> (m <sup>3</sup> .mol <sup>-1</sup> )	6.73x10 <sup>-4 (i)</sup> (m <sup>3</sup> .mol <sup>-1</sup> )	15.39x10 <sup>-6 (h)</sup> (m <sup>3</sup> .mol <sup>-1</sup> )	3.85x10 <sup>-6 (h)</sup> (m <sup>3</sup> .mol <sup>-1</sup> )	8.67 (mol.m <sup>-3</sup> )	9x10 <sup>-8 (c)</sup> (m.s <sup>-1</sup> )
$V_{\mathrm{C_3S}}$	$V_{\mathrm{C_2S}}$	$V_{\mathrm{CSH}}$	$V_{\text{Ca(OH}_{2}(s)}$		
7.24x10 <sup>-5 (j)</sup> (m <sup>3</sup> .mol <sup>-1</sup> )	5.24x10 <sup>-5 (j)</sup> (m <sup>3</sup> .mol <sup>-1</sup> )	2.28x10 <sup>-4 (j)</sup> (m <sup>3</sup> .mol <sup>-1</sup> )	3.30x10 <sup>-5 (j)</sup> (m <sup>3</sup> .mol <sup>-1</sup> )		
$R_{ m agg/c}$	$R_{ m w/c}$	$ ho_{ m con}$	$ ho_{ m c}$	$ ho_{ m agg}$	$ ho_{ m w}$
4	0.26 or 0.32	$2.10 \times 10^{3}$ (kg.m <sup>-3</sup> )	$3.16x10^3$ (kg.m <sup>-3</sup> )	$2.61 \times 10^3$ (kg.m <sup>-3</sup> )	997.05 (kg.m <sup>-3</sup> )

<sup>(</sup>a) Measured by passing a tracer gas (N<sub>2</sub>) through the compact concrete specimen and fitting the breakthrough curve
(b) Meier et al. [17]
(c) Papadakis et al. [18]
(d) Initial pH measurement

<sup>(</sup>e) Mercury intrusion porosimetry (MIP) measurement [23] (f) Pinsent et al. [26]

<sup>(</sup>g) Fitted to the first 5 minutes of carbonation, a value was selected based on outlet CO2 concentration and product CaCO<sub>3</sub> formed

<sup>(</sup>h) Papadakis et al. [14]
(i) Calculated from molar volume of species obtained from Pichler et al. [38] and Sarkar et al. [39]

<sup>(</sup>j) Pichler et al. [38]

**TABLE 5.4.** Dimensionless parameters used in this study. In these equations, [i] is the concentration of cement phase i in concrete.

$ui = [i]/[i]_0$	(5.4.1)
$uCaCO_3 = [CaCO_3]/(3[C_3S]_0 + 2[C_2S]_0 + [Ca(OH_2(s)]_0 + 3[AFt]_0)$	(5.4.2)
$uCO_{2}(g) = \varepsilon \phi^{a} [CO_{2}(g)] / (\varepsilon \phi^{a})_{0} [CO_{2}(g)]_{0}$	(5.4.3)
$\begin{split} uCO_2(aq) &= \epsilon  \phi^w \big[ CO_2(aq) \big] \big/ (\epsilon  \phi^w )_0 \big[ CO_2(aq) \big]_{max} \ where \\ \big[ CO_2(aq) \big]_{max} &= k_{Henry} \big[ CO_2(g) \big]_0 \end{split}$	(5.4.4)
$uCa(OH)_{2}(aq) = \epsilon \phi^{w} [Ca(OH)_{2}(aq)]/(\epsilon \phi^{w})_{0} [Ca(OH)_{2}(aq)]_{max}$	(5.4.5)
$\beta_i = [i]_0 / (\epsilon  \phi^a)_0 [CO_2(g)]_0$	(5.4.6)
$\beta_{\mathrm{CO}_2(\mathrm{aq})} = (\epsilon  \phi^{\mathrm{w}})_0 [\mathrm{CO}_2(\mathrm{aq})]_{\mathrm{max}} \big/ (\epsilon  \phi^{\mathrm{a}})_0 [\mathrm{CO}_2(\mathrm{g})]_0$	(5.4.7)
$\delta = D_{CO_2(aq)}^* / (vL)$	(5.4.8)
$Dr_i = r_i / r_{im}$	(5.4.9)
$\begin{split} &\frac{\partial (uCO_{2}(g))}{\partial \tau} = (IPN) \frac{\partial^{2}(uCO_{2}(g))}{\partial \xi^{2}} - \frac{\partial (uCO_{2}(g))}{\partial \xi} \\ &- (St)(k_{Henry} \cdot uCO_{2}(g) \cdot (\epsilon  \phi^{a})^{-1} - \beta_{CO_{2}(aq)} \cdot uCO_{2}(aq) \cdot (\epsilon  \phi^{w})^{-1}) \end{split}$	(5.4.10)
$\begin{split} &\beta_{CO_2(aq)} \cdot \frac{\partial (uCO_2(aq))}{\partial \tau} = \beta_{CO_2(aq)} \cdot \delta \cdot \frac{\partial^2 (uCO_2(aq))}{\partial \xi^2} \\ &+ (St)(k_{Henry} \cdot uCO_2(g) \cdot (\epsilon  \phi^a)^{-1} - \beta_{CO_2(aq)} \cdot uCO_2(aq) \cdot (\epsilon  \phi^w)^{-1}) \\ &- (3D_{\tilde{C}_3S}.Da1 + 2D_{\tilde{C}_2S}.Da2 + 3D_{\tilde{C}_{SH}}.Da3 + 3Dr_{AFt}.Da4 + Dr_{D,CH}.Da5) \end{split}$	(5.4.11)
$\frac{\partial(ui)}{\partial \tau} = +(-Dai/\beta_i)(Dr_i)$ where: $Da1$ (C <sub>3</sub> S), $Da2$ (C <sub>2</sub> S), $Da3$ (C-S-H), $Da4$ (AFt) and $Da5$ (CH(s))	(5.4.12)

**TABLE 5.5.** Dimensionless parameters for gas flow-rate=1.17 Lpm and w/c=0.26

St	IPN	δ		
16.45	$2.6 \times 10^{-3}$	$2.23 \times 10^{-7}$		
Dal (C <sub>3</sub> S)	Da2 (C <sub>2</sub> S)	Da3 (CSH)	Da4 (AFt)	Da5 (CH (s))
50.28x10 <sup>-2</sup>	2.79x10 <sup>-2</sup>	12.83x10 <sup>-2</sup>	2.83x10 <sup>-2</sup>	6.4732
$\beta_{CO_2(aq)}$	$\beta_{C_3S}$	$\beta_{C_2S}$	$\beta_{CSH}$	β <sub>CH (s)</sub>
4.44x10 <sup>-1</sup>	774.96	59.52	62.83	176.92

### Chapter 6

### **Contributions and Limitations of this Study**

#### 6.1. Contributions to New Knowledge

Accelerated CO<sub>2</sub> curing of concrete has been suggested as a carbon dioxide mitigation technology in which CO<sub>2</sub> reacts with cement and is stored as thermodynamically stable calcium carbonate in concrete products. In this method, a value added product is also formed: CO<sub>2</sub>-cured concrete. Pressure chambers have been used for accelerated CO<sub>2</sub> curing of concrete which require high pressure of CO2 in order to provide sufficient diffusion through the pores and a homogeneous carbonated product. In this research, the rate and extent of CO<sub>2</sub> uptake by concrete was assessed in a flow-through reactor which requires a lower pressure compared to pressure chambers. Compacted fresh concrete and aqueous cement suspension were carbonated with a model, synthetic flue gas composed of 20% or 40% CO<sub>2</sub> in N<sub>2</sub> balance. The synthetic flue gas was passed through the sample at ambient temperature and at low inlet pressure (0.11 MPa) in a 1-D flow-through reactor and the CO<sub>2</sub> uptake was monitored during carbonation. The effect of carbonation on the microstructure of concrete was studied using a scanning electron microscopy imaging technique. Carbonation of aqueous cement suspension in a completely mixed flow-through carbonation reactor eliminated the effect of pore blockage and increased the exposed surface area of reactive

compounds and increased the carbonation efficiency. A mathematical model of concrete carbonation in the 1-D flow-through reactor was also developed and the effect of carbonation processes on CO<sub>2</sub> uptake efficiency was studied. The major findings and contributions are listed as below:

# 6.1.1 This study is the first to assess the CO<sub>2</sub> uptake kinetics and extent in concrete during accelerated CO<sub>2</sub> curing in a flow-through carbonation reactor.

The CO<sub>2</sub> uptake by compact concrete was rapid and the carbonation efficiency of 16-20% was achieved within an hour of carbonation with a gas flow-rate of 1.17 Lpm and CO<sub>2</sub> partial pressure of 0.021 MPa. The carbonation efficiency attained in the flow-through reactor was comparable to the carbonation efficiencies achieved in pressure chambers in previous studies (approximately 17-28%). However, the energy required for carbonation curing of 1 m<sup>3</sup> of concrete with flue gas compressed to 0.11 MPa is less than 0.013 GJ and is negligible compared to energy required for steam and autoclave curing (0.59 and 0.71 GJ) or the energy required for carbonation curing in a pressure chamber. A high degree of carbonation was achieved in the inlet surface of compact concrete at the early period of carbonation and this carbonation 'front' advanced over time towards the outlet and resulted in a homogeneous carbonated concrete.

Additional CO<sub>2</sub> uptake by concrete following gas shut off periods in intermittent carbonation experiments showed that the carbonation efficiency was

limited in part by slow dissolution and/or diffusion of dissolved reactive components in the concrete matrix. The CO<sub>2</sub> uptake efficiency increased to approximately 24% after a few cycles of carbonation and gas shut off periods.

# 6.1.2. Formation of solid product during carbonation curing, mainly calcite, restricted CO<sub>2</sub> transport to the cement matrix microstructure and decreased the porosity of concrete.

Calcite was the main product formed in carbonated cement as detected by X-ray diffraction (XRD). Formation of calcium carbonate was also visualized in carbonated compact concrete specimens using an electron microprobe imaging technique. Pores smaller than approximately 4 µm in diameter, were not seen in carbonated samples as abundantly as in non-carbonated samples. Calcium carbonate formed in the carbonated concrete not only filled the narrow pores among solid matrix in scattered areas, but also deposited adjacent to larger pores. Deposition of CaCO<sub>3</sub> in large pores was either as a layer of calcium carbonate along the edge or as large crystals formed close to the pore. These deposits limit the complete carbonation of the cement active phases because of mass transport limitations of the dissolve CO<sub>2</sub> species to the active cement phases.

The porosity of carbonated sample decreased to 16% in carbonated concrete from an initial porosity of at least 20% (related to 24-hour hydrated concrete) measured by Mercury Intrusion Porosimetry (MIP). This porosity decrease can be due to the differences in molar volume of cement compounds carbonated and

carbonation products or pore clogging because of deposition of solid calcium carbonate.

6.1.3. Carbonation of an aqueous cement suspension in a completely mixed flow-through reactor increased the  $CO_2$  uptake efficiency. However, the maximum theoretical efficiency was not achieved as the solution reached a chemical equilibrium.

In order to eliminate the effect of pore clogging by deposition of calcium carbonate, cement was carbonated in an aqueous suspension form in a completely mixed flow-through reactor. The carbonation efficiency of cement in aqueous suspension was approximately 68% and the maximum theoretical efficiency calculated from Steinour formula was not achieved. The CO<sub>2</sub> uptake by cement ceased within 30 minutes and the concentrations of calcium, dissolved carbon and pH in the aqueous solution reached a plateau. The aqueous cement suspension reached a chemical equilibrium with calcium carbonate, silica gel and CO<sub>2</sub> gas and the carbonation ceased.

When carbonation starts, each mole of CO<sub>2</sub> gas dissolves in water and forms one mole of CO<sub>3</sub><sup>2+</sup> and two moles of H<sup>+</sup> which decreases the pH of aqueous cement suspension. The pH is initially buffered because of the presence of alkali minerals (calcium silicates and a small amount of calcium hydroxide) but decreased as these sources of buffer capacity diminished or were no longer exposed to the aqueous solution. The concentration of calcium and dissolved

carbon decreased rapidly in the solution because of the carbonation reaction and formation of solid calcium carbonate.

6.1.4. A mathematical model of accelerated CO<sub>2</sub> curing of concrete in the flow-through reactor was developed. The mathematical model predictions of CO<sub>2</sub> uptake by concrete at different operating conditions (gas flow-rates and water/cement ratios) matched the experimental measurements. This mathematical model can be used to study the effect of different parameters (e.g. CO<sub>2</sub> percentage in the gas mixture or specific surface area of concrete) on carbonation efficiency.

The partial differential equations describing the mass balance of CO<sub>2</sub> gas, dissolved CO<sub>2</sub> and active cement species were solved mathematically. The results from the mathematical model for carbonation curing matched the experimental results for different gas flow-rates (0.08, 1.17 and 2 Lpm) and water/cement ratios (0.26 and 0.32 with flow-rate of 1.17 Lpm). A surface area reduction term was used in order to model the effect of formation and deposition of calcium carbonate on the exposed surface area of reactive cement compounds which was a function of the molar concentration of calcium carbonate formed during carbonation. An increase in the partial pressure of CO<sub>2</sub> gas increased the rate of CO<sub>2</sub> uptake by concrete but the extent of carbonation remained at 17%. The mathematical model suggests that the extent of carbonation efficiency can increase with an increase in specific surface area of concrete. The 30 minute carbonation efficiency increased

from 17% to 32% with a 10 times increase in the initial specific surface area of concrete. With an increase in specific surface area of active cement compounds, both the rate and extent of carbonation increased.

Several dimensionless numbers were used to study the sensitivity of carbonation to different carbonation processes such as CO<sub>2</sub> gas dispersion, gasliquid mass transfer and carbonation rates. The carbonation efficiency during 30 minutes of carbonation was not limited by the rate of CO<sub>2</sub> gas-liquid mass transfer as the Stanton number suggests. Higher CO<sub>2</sub> uptake could be achieved by improving the carbonation rates of unhydrated cement. The carbonation reaction rates of unhydrated cement compounds (mainly C<sub>3</sub>S) were the rate controlling processes during this period as the Damköhler number suggests (*D1*<1). The carbonation rates can be improved by increasing the exposed surface area of these active cement compounds. The efficiency increased from 17% to 19% when the carbonation rate of C<sub>3</sub>S was increased two orders of magnitude but did not increase to that extent with changes in carbonation rate of C<sub>2</sub>S.

#### **6.2.** Limitations of this study

## 6.2.1. The mathematical model developed in this study is for 1-D flowthrough carbonation curing with isothermal condition.

The carbonation reactions are exothermic and the produced heat may affect the heat balance of concrete, increase the temperature and affect the carbonation reaction rates. However, since the carbonation reactor was kept in water bath for

minimal temperature change, the temperature was assumed to remain constant during carbonation of the compacted concrete. Modeling of certain industrial scale carbonation manufacturing processes will likely require incorporation of heat transfer equations and modification of carbonation rates for temperature.

## 6.2.2. The mechanical properties of concrete cured in the 1-D flowthrough accelerated carbonation curing reactor were not studied.

The purpose of this study was to assess the CO<sub>2</sub> uptake rate and extent in concrete during accelerated carbonation curing. For this purpose, concrete specimens were prepared with different water/cement ratios in concrete mix and cured at various operating conditions such as CO<sub>2</sub> percentage in gas mixture, gas flow-rate, or at several cycles of carbonation (intermittent carbonation) and the carbonation efficiency under these conditions were measured. However, the mechanical properties of cured concrete such as compressive strength and also durability of concrete products was not studied. As outlined in Chapters 3, 4 and 5, several other studies have investigated the mechanical and durability performance of concrete produced by accelerated carbon dioxide curing.